# Variability of carbon dioxide fluxes in heterogeneous urban environments

## From street canyon to neighborhood scale

**Inauguraldissertation**
zur
Erlangung der Würde eines Doktors der Philosophie
vorgelegt der
Philosophisch-Naturwissenschaftlichen Fakultät
der Universität Basel

von

Björn Lietzke
aus Deutschland

Basel, 2015

Genehmigt von der Philosophisch-Naturwissenschaftlichen Fakultät
auf Antrag von:

Prof. Dr. Eberhard Parlow
Meteorologie, Klimatologie und Fernerkundung
Departement Umweltwissenschaften
Universität Basel
Schweiz

Univ.-Prof. Dr.rer.nat. Dr.rer.silv.habil. Helmut Mayer
Professur für Meteorologie und Klimatologie
Albert-Ludwigs-Universität Freiburg
Deutschland

Basel, den 10.12.2013

Prof. Dr. Jörg Schibler
Dekan

# Acknowledgements

Many people earn my thanks for supporting me in the efforts leading to this thesis. Working in the research group of Prof. Dr. Eberhard Parlow was always motivating and I would like to thank him for giving me the opportunity of being part of it. All team members contributed in their own way to the success of this thesis, but I would like to address special thanks to Dr. Roland Vogt who accompanied my work throughout the whole project. Without his support in preparing, planning and installing the measurement sites, the experimental part of the project would not have been possible. His ample knowledge and interest in the field of micrometeorolgy made discussions extremely fruitful and expanded my understanding of micrometeorological processes in the urban atmosphere.

I have to thank each member of the team of scientists and students in the research group for their support and contributions and for making work agreeable. The experience of Dr. Christian Feigenwinter in $CO_2$ measurements and urban climatology was basis for many motivating conversations. Working in the same bureau with Dominik Michel was always a pleasure and lead to a lot of spontaneous discussions on scientific and technical questions. He was also a fellow sufferer in harder times. Besides the previously named, many other supported the installation, maintenance or data analysis of the measurements, namely Sara Koller, Ambros Werner, Thomas Meuli, Patrick Koller, Samuel Diethelm, Michael Schmutz and Serafin Bieder. Hans-Rudolf Rüegg earns thanks for contributing his technical knowledge. I gained interesting insights into CFD modeling by working with Dr. Andres Gartmann. Günter Bing always provided a reliable IT environment. Josette Pfefferli-Stocky did excellent administrative work.

In its first phase, the experiment needed a lot of support by the city authorities, to which I would like to express my thanks in general. Measurements at the Turmhaus were generously supported by the companies Turmhaus Consulting and Basler Versicherungen.

By the effort of Prof. Parlow and Dr. Vogt, the participation in the BRIDGE project became possible which funded a great part of the work leading to this thesis. Besides, BRIDGE gave me the opportunity of participating in an international project and of collaborating with urban planners and scientists from different fields. In this scope I would like to thank all participants of the project, especially Dr. Nektarios Chrysoulakis for organizing and driving the whole project and Dr. Judith Klostermann for inviting me to Wageningen University for a short stay to prepare a meeting together. Her encouraging and supporting nature also motivated me while organizing the final project meeting in Brussels. I would also like to thank Prof. Sue Grimmond and all other authors and reviewers of the book chapter and the project reports to which I contributed.

Finally, greatest thanks go to Jasmin for her patience and loving encouragement. And to my parents, on whose support I could always count.

Basel, November 2013

# Abstract

High carbon dioxide ($CO_2$) emissions in cities are a consequence of high energy consumption by a dense population. Fossil fuel related emissions from urban areas contribute to the increase in average atmospheric concentrations of $CO_2$. Typically, the size of the emissions has been estimated through indirect approaches on the base of energy consumption data, but the number of direct atmospheric measurements of the effective $CO_2$ exchange over cities is increasing since about a decade. Results so far show a lot of uncertainties concerning the processes that control the exchange rates to the atmosphere, i.e. the vertical $CO_2$ flux ($F_C$). The wide range of $F_C$ reported for cities reflects the variety and complexity of urban areas. It shows that the urban structure around an observational site has a great influence on the measured flux and that additional controlling factors need to be taken into account when addressing urban flux patterns.

In this thesis, the main controlling factors for the variability of $F_C$ on different scales in time and space are identified. Long term $CO_2$ concentrations and fluxes are observed at two urban observational sites to account for spatial differences within a city. Micro to local scale exchange processes and spatial distribution patterns between individual urban structure elements are addressed by additional measurements inside a street canyon.

The key factors that control $F_C$ in heterogeneous urban areas are the major emitters of $CO_2$ and their typical cycles on different time scales. Traffic emissions account for average diurnal courses of measured fluxes, while heating related emissions explain seasonality. Sink effects related to photosynthesis are found to be negligible in most cases. The spatial proximity of major roads at both sites is of greater importance than the source area extent and traffic induced $F_C$ is estimated to account on average for 70% of the total flux at one of the sites. Wind direction is – in combination with the spatial distribution of sources – the third and most crucial controlling factor due to its typical cycles and its occasional variability. Diurnal patterns interact with the course of traffic and seasonal characteristics with heating emissions. Both account for typical site specific $F_C$ patterns, whereas deviations from usually prevailing wind directions can lead to flux variance of noticeable size.

Wind directions are also responsible for micro scale distribution and exchange patterns in and above the street canyon. High horizontal concentration differences inside the canyon are a result of in-canyon flows in the form of a helical vortex. Depending on the prevailing wind direction, vertical exchange of $CO_2$ with the layers above is restricted or enhanced.

Annual carbon exchange rate is a typical unit used for comparisons between sites and cities. The spatial heterogeneity of emissions induces a bias into these exchange rates that is related to an unequal reflection by wind direction frequencies. Up-scaling of spatially segregated fluxes leads to a comprehensive and more representative total carbon exchange rate of the average source area than $F_C$ does.

The identified controlling factors explain the patterns of measured $F_C$ and the presented results improve the understanding of the variability of carbon dioxide exchange rates in urban areas. City scale differences and the strong relation on the interdependency of the controlling factors and their typical cycles suggest that the reasons for varying $F_C$ in cities worldwide are related to similarly complex local effects.

# Contents

# List of Figures

# List of Tables

# List of Symbols

| | |
|---|---|
| $s$ | Scalar |
| $\overline{s}$ | Temporal average |
| $s'$ | Turbulent departure from the temporal average |
| | |
| $\Delta A$ | Net moisture advection |
| $\Delta Q_A$ | Net advected flux of heat |
| $\Delta Q_S$ | Net storage change of heat |
| $\Delta W$ | Net storage change of water |
| $\Delta W_a$ | Anthropogenic water storage |
| $\Delta W_g$ | Net change in ground water storage |
| $\Delta W_m$ | Net change in soil moisture storage |
| $\Delta W_n$ | Net change in snowpack storage |
| $\Delta W_w$ | Surface water storage |
| $\Delta x$ | Thickness of an Element |
| $\gamma$ | Vertical inclination angle of the 3D wind vector to the horizontal plane |
| $\lambda E$ | Turbulent latent heat flux |
| $\lambda_b$ | Surface fraction covered by buildings |
| $\lambda_g$ | Surface fraction covered by impervious ground |
| $\lambda_p$ | Plan area index |
| $\lambda_v$ | Surface fraction covered by vegetation |
| $\rho C$ | Volumetric heat capacity |
| $\rho$ | Air density |
| $\rho_v$ | Fluctuating part of water vapor density |
| $\sigma$ | Standard deviation |
| $\theta$ | Virtual acoustic air temperature |
| $\upsilon$ | Traffic density |
| $\upsilon_A$ | Traffic density at Basel Aeschenplatz |
| $\upsilon_J$ | Traffic density at Basel Johanniterbrücke |
| $\upsilon_K$ | Traffic density at Basel Klingelbergstrasse |
| $\zeta$ | Atmospheric stability index |
| $c$ | Measured $CO_2$ concentration |
| $C$ | Combustion |
| $C_B$ | Combustion from buildings |
| $c_p$ | Specific heat capacity of air |
| $C_V$ | Combustion from vehicular traffic |
| $E$ | Evapotranspiration |
| $E_T$ | Transpiration |
| $E_V$ | Evaporation |
| $eF_C$ | Expected $F_C$, up-scaled |
| $F$ | Anthropogenic water release due to combustion |
| $F_C$, $F_C^{EC}$ | Turbulent carbon dioxide flux |
| $F_{C1}$ | $\mathrm{F}_C$ before quality control |
| $F_{C2}$ | $\mathrm{F}_C$ after despiking |
| $F_{C3}$ | $\mathrm{F}_C$ after streamline rotation |
| $F_{C4}$ | $\mathrm{F}_C$ after detrending |
| $F_C^{HA}$ | Net horizontal advection of $F_C$ |

| | |
|---|---|
| $F_C^{STO}$ | Net storage change of $F_C$ in the air |
| $F_I$ | Moisture released from industry |
| $F_M$ | Moisture release from air conditioning, heating and cooling applications |
| $F_V$ | Moisture release from vehicular combustion |
| $F_W$ | Consumption of bottled water |
| eNEE | Expected NEE |
| $GEP$ | Gross ecosystem productivity |
| $H$ | Turbulent sensible heat flux |
| HDD | Heating Degree Days |
| $I$ | Piped water supply |
| $I_G$ | Grey or other reused water |
| $I_R$ | Water used for irrigation |
| $I_S$ | Leakage to/from the piped network |
| $I_U$ | Internal residential/industrial water use |
| $L$ | Obukhov-Length |
| $L_v$ | Latent heat of vaporization |
| LW | Long-wave radiation |
| $N$ | Number of data |
| NEE | Net Ecosystem Exchange |
| NuEE | Net urban Ecosystem Exchange |
| $P$ | Precipitation |
| $P_h$ | Hail |
| $P_m$ | Atmospheric moisture |
| $P_r$ | Rainfall |
| $P_s$ | Snow |
| $Q_A^{in}$ | Advected heat flux into a control volume |
| $Q_A^{out}$ | Advected heat flux out of a control volume |
| $Q_F$ | Anthropogenic heat flux |
| $r$ | Radius |
| $r$ | Runoff (used in Section P1) |
| $R_{SV}$ | Respiration of soils and vegetation |
| $R_{ue}$ | Urban ecosystem respiration |
| $r_F$ | Surface infiltration |
| $r_L$ | Surface runoff |
| $R_M$ | Human respiration activity |
| $R_n$ | Net all-wave radiation |
| $r_O$ | Runoff released by snow melt |
| $r_S$ | Storm water runoff |
| $r_W$ | Waste water flow |
| $R_W$ | Waste decomposition related respiration |
| SW | Short-wave radiation |
| $T$, $T_A$ | Air temperature |
| $T_d$ | Average daily air temperature |
| $T_r$ | Indoor room temperature |
| $u$ | Longitudinal wind velocity component |
| $v$ | Lateral wind velocity component |
| $w$ | Vertical wind velocity component |
| $x_h$ | Set of values for each hour of the day over a set of days |
| $z$ | Measurement height |

| | |
|---|---|
| $z_*$ | Blending height between the RSL and ISL |
| $z_{h(t)}$ | Average height of roughness elements relative to measurement base height |
| $z_d$ | Zero-plane displacement height |
| $z_h$ | Average height of roughness elements |

# List of Abbreviations

| | |
|---|---|
| BAES | Basel Aeschenplatz (observational site) |
| BKLI | Basel Klingelbergstrasse (observational site) |
| BKLIC | Basel Klingelbergstrasse (observational site, street canyon measurements) |
| BRIDGE | SustainaBle uRban plannIng Decision support accountinG for urban mEtabolism |
| BUBBLE | Basel Urban Boundary Layer Experiment |
| CEST | Central European Summer Time |
| CET | Central European Time |
| CFD | Computational Fluid Dynamics |
| CoP | Communities of Practice |
| DSS | Decision Support System |
| EU FP7 | European Community's Seventh Framework Programme |
| GHG | Greenhouse Gases |
| GIS | Geographical Information System |
| IQR | Interquartile Range |
| ISL | Inertial Sublayer |
| LAD | Leaf Area Density |
| LCZ | Local Climate Zones |
| LULC | Land Use/Land Cover |
| MCR Lab | Meteorology, Climatology and Remote Sensing Laboratories |
| MDC | Median Diurnal Cycles |
| PBL | Planetary Boundary Layer |
| QC | Quality Control |
| RSL | Roughness Sublayer |
| ST | Summer Time (Period when CEST is active) |
| UBL | Urban Boundary Layer |
| UCB | Urban Carbon Balance |
| UCL | Urban Canopy Layer |
| UCZ | Urban Climate Zones |
| UEB | Urban Energy Balance |
| UTZ | Urban Terrain Zones |
| UWB | Urban Water Balance |
| UZE | Urban Zones for Energy partitioning |
| WD | Working days (Mo-Fr) |
| WE | Weekend days (Sa, So and public holidays) |
| WGS 84 | World Geodetic System 1984 |
| WPL | Webb, Pearman and Leuning correction |
| WT | Winter Time (Period when CEST is not active) |

# List of publications

This thesis consists of this introductory part and three publications (P1–3) that are incorporated into its structure: a book chapter and two research articles. The chapter (Section P1) is part of a book on the BRIDGE project (Section 1.5). The articles are published in *Atmospheric Environment* (Section P2) and in the *International Journal of Climatology* (Section P3) and are reproduced with the permission of the journals.

P1 **Lietzke, B.**, Vogt, R., Young, D.T. and Grimmond, C.S.B. (2015): Physical fluxes in the urban environment. In: Chrysoulakis, N., de Castro, E.A. and Moors, E.J. (Eds.): Understanding urban metabolism – A tool for urban planning. Routledge, Oxford.

P2 **Lietzke, B.** and Vogt, R. (2013): Variability of $CO_2$ concentrations and fluxes in and above an urban street canyon. *Atmospheric Environment*, 74, p. 60–72.

P3 **Lietzke, B.**, Vogt, R., Feigenwinter, C. and Parlow, E. (2015): On the controlling factors for the variability of carbon dioxide flux in a heterogeneous urban environment. *International Journal of Climatology*, Article published online: 24 January 2015.

Not part of this final thesis are the following publications (not peer reviewed) to which contributions were made as part of the thesis work:

**Lietzke, B.** and Vogt, R. (2009). Part I: Energy in the urban system. In: Grimmond, C.S.B., Lietzke, B., Vogt, R., Young, D., Marras, S. and Spano, D. (2009): BRIDGE Deliverable 2.1 – Inventory of current state of empirical and modeling knowledge of energy, water and carbon sinks, sources and fluxes.

Klostermann, J., **Lietzke, B.**, Moors, E. and González del Campo, A. (2010): BRIDGE Deliverable 8.1 – DSS demonstration report. Evaluation of the applicability of the first BRIDGE DSS prototype; Report of Umbrella Workshop I (5 May 2010).

**Lietzke, B.** (2011): Dynamik der urbanen $CO_2$-Verteilung – Teil 1: Messungen in einer Strassenschlucht. Regio Basiliensis 52(1): pp. 37–44.

Conference talks on the thesis work were held as follows:

**Lietzke, B.** and Vogt, R. (2011): Variability of $CO_2$ in an urban environment: from street canyon to neighbourhood scale, European Geosciences Union General Assembly, Vienna, Austria, April 3–8.

**Lietzke, B.** (2012): Variability of $CO_2$ fluxes and concentrations in and above a street canyon. 8th International Conference on Urban Climate, Dublin, Ireland, August 6–10.

# 1 Introduction

## 1.1 Preface

Cities, regarded from an airplane at night, emerge from their dark rural surroundings as pulsating bodies of lights. Some of them moving around and into and out of the glowing mass, in a way that they convey the impression that the whole system is alive. Somehow, the image that appears from the sky is true. Urban areas can be considered as metabolisms, complex systems of interdependent pathways and flows of materials and energy. They consume goods, fossil fuels, power, water or construction materials, transform it in several ways, store it in their built up structure or biomass and produce outputs like waste, pollutants and manufactured goods. This system-based concept of an 'urban metabolism' (Boyden et al., 1981; Newman, 1999; Wolman, 1965) is of great interest for developing present and future sustainable cities.

In processes toward sustainability, energy input, use and transformation are major points of concern. Challenges that are faced are to increase the energy efficiency of urban structure, to minimize the energy demand and to reduce the environmental burden by increasing the share of renewable energy and reducing carbon emissions into the atmosphere. To address these challenges, information on the flows of energy in typical urban systems is needed. Estimations on the energy consumption of cities are complex due to several physical states and forms (fuels, electricity, heat, radiation) in which energy enters, passes and leaves a system or is stored within. Indicators and measures are as diverse as energy is and vary with the needs and the climates of cities around the globe. Hence, numbers vary as well but likely go up to three-quarters of the World's energy consumption – which is not surprising if we consider that in the year 2011, 52.1% of the World's population and 77.7% of the people in the more developed regions (73.7% in Switzerland) lived in urbanized areas (UNEP, 2012). This high request in energy is largely covered by fossil fuels (like oil, coal or natural gas) which dominate the energy input into urban systems. They are usually transformed through combustion into usable energy or heat and products of the burning processes, emitted as pollutants or greenhouse gases (GHG) into the urban atmosphere.

Through their metabolism and their built-up structure, cities generate their own climate which is different from that of the rural surroundings. It can be assessed using measuring or modeling approaches on different scales. Changed patterns of energy flows in the form of radiation and heat constitute the urban energy balance (UEB), sealed surfaces and little vegetation cover lead to increased rainwater runoff and lower evapotranspiration and affect the urban water balance (UWB) while little vegetation in combination with combustion processes transforming fossil fuels into carbon dioxide lead to increased $CO_2$ emissions in terms of the urban carbon balance (UCB).

The consequences of locally altered climate conditions through urban-induced changes in the energy, water and carbon balances are diverse and range from direct local effects on the inhabitants (e.g. thermal discomfort and increased mortality due to heat waves and air pollution, increased flash floods) to global effects (contribution to the greenhouse effect through $CO_2$ emissions).

Addressing these various effects from a combined planning and science perspective was a main goal of the BRIDGE project. An introduction to BRIDGE is given in Section 1.5. As a contribution to this project, Section P1 was written. It is incorporated in Chrysoulakis et al. (2015) 'Understanding Urban Metabolism: A tool for urban planning', the final book-publication of the project, as an introduction to physical fluxes in the urban environment, viewed from a meteorological perspective. Due to its introductory nature, it is kept as generally understandable as possible, within the scope of the project. Besides an introduction to urban metabolism and the structure of the urban atmosphere, a short general methodical section is contained. In its main part it gives an overview of the urban balances of energy, water and carbon. Each term of the three balances is presented and measurement methods are explained. A more comprehensive description including a literature review for each term can be found in the BRIDGE deliverable D.2.1, on which this book chapter is based.

While, for scientists and planners, the role of energy in the urban system is often of more relevance than the role of water or carbon, the latter has through combustion generated $CO_2$ emissions a strong relation to the energy consumption in urban areas. Emissions into the urban atmosphere increase the level of $CO_2$ and are transported into the higher atmospheric parts through turbulent and advective transport processes. Measuring the vertical part of this $CO_2$ transport and using it as an indicator for combustion activities can give an impression of the use of fossil fuel related energy in the source area of the observation. It also shows how much $CO_2$ a certain urban area injects into the atmosphere and how it contributes to the global carbon cycle. As already mentioned, urban areas likely do account for three-quarters of the World's energy consumption. It can thus also be considered as likely that urban areas are directly and indirectly responsible for a great part of the anthropogenic contribution of $CO_2$ into the atmosphere: Directly, as through emissions inside the city borders; indirectly, as through remote emissions related to the city's activities.

## 1.2 Objectives

The main goal of the field study leading to the principal part of this thesis (Section P2 and Section P3) was to gain increased knowledge on the controlling factors for the variability of $CO_2$ fluxes in a heterogeneous urban environment in the city of Basel, Switzerland.

Knowing the size of the contribution of cities to the global carbon cycle is of importance for e.g. modeling studies which are often based on estimations of city-average fossil fuel consumption (Grimmond et al., 2002). A better understanding of the interaction of processes – both anthropogenic and natural – that control the role of cities in carbon budgets leads to better emission estimates and less uncertainty in model inputs or comparisons between cities. Deriving per city quantification through direct measurements is difficult, mainly because of the heterogeneous urban surface leading to highly variable source distribution and methodological uncertainties. Results from measurement studies on carbon dioxide flux in various cities around the globe are as diverse as the cities and study sites are (Table P3-1), but each of the increasing number of studies substantially contributes to the knowledge of the scientific community.

Uncertainties in urban measurements of $CO_2$-concentrations and fluxes arise mainly from limitations of single-point measurements in the complex urban environment, which is characterized by the rough and heterogeneous surface and spatio-temporally variable anthropogenic sources. Combustion processes in vehicles and heating units are considered to be the major local $CO_2$ emitters in most urban areas, while vegetation activity is usually reduced the more urban and thus sealed an area is.

In order to investigate the local to neighborhood scale variability of $CO_2$-concentrations and fluxes, data from two measurement sites in Basel is analyzed. At the first, a long-term micrometeorological observation site, an extensive field campaign was conducted from October 2009 to February 2011 to additionally address micro- to local scale $CO_2$ transport processes in and above a street canyon. In-canyon $CO_2$ distributions and canyon-top fluxes at 19 m were sampled. Fluxes were also registered at the existing rooftop-tower at 39 m above ground. The second long term site was installed in June 2009 only 1.6 km away on top of a building, sampling $CO_2$ fluxes at 41 m above street level.

The street canyon experiment and its main results are presented in Section P2. A comprehensive analysis of the controlling factors for the flux variability at the second site is found in Section P3.

## 1.3 State of research

Research on urban carbon dioxide surface-atmosphere exchange is a relatively young field with an increasing number of $CO_2$ flux measurement studies since the 1990ies. While in the early stages short-term studies like the pioneering 1995 experiment by Grimmond et al. (2002) in Chicago, USA, or 2000 by Nemitz et al. (2002) in Edinburgh, Scotland, were common, an increasing amount of long-term studies emerged during the last decade. Soegaard and Möller-Jensen (2003) were the first to measure flux data for a whole year (2001) in Copenhagen, Denmark. By combining the results with mobile flux measurements and remote sensing derived spatial emission estimates based on land-use classifications, they calculated an average $CO_2$ emission rate of $35\,\mathrm{g\,m^{-2}\,day^{-1}}$ (or $9.21\,\mu\mathrm{mol\,m^{-2}s^{-1}}$) for the whole city. Moriwaki and Kanda (2004) also measured flux data for one year in Tokyo, Japan, from 2001 to 2002. As part of their investigations, they calculated emissions from traffic based on a traffic volume database, from heating as a function of house density and energy consumption and from human body exhalation on the basis of an assumed average breathing volume and population density. In the same years, between Summer 2001 and 2002, the Basel Urban Boundary Layer Experiment (BUBBLE, Rotach et al. (2005)) was conducted, focusing also on $CO_2$ exchange characteristics in and above a street canyon through sampling a 10-level concentration profile and fluxes at two heights (Christen, 2005; Vogt et al., 2006) over one month. This extensive experiment led to a better understanding of the correlation between the diurnal course of $CO_2$ concentration and atmospheric mixing layer height (which can be considered as substitute for the urban boundary layer height (Rotach et al., 2005)) and the dependence of fluxes on traffic density in the canyon. The first observations lasting longer than one year (2002–2006) were presented by Crawford et al. (2011) for a suburban neighborhood in Baltimore, USA, showing that despite the high surface vegetation fraction of 67% the area was on average a small but net source of $CO_2$. At a comparable suburban site in the Salt Lake Valley, USA, Ramamurthy and Pardyjak (2011) measured fluxes of the same size in Summer 2005. They also reported for a set of eight cities an exponential dependence of $CO_2$ fluxes on surface vegetation fraction ($\lambda_v$). Nordbo et al. (2012) extended the comparison to data from 17 measurements of different sampling periods and concluded that urbanized areas are net local sinks of atmospheric $CO_2$ if their natural fraction exceeds about 80% of the total surface – a rather high fraction. An important point they state in their article is that daytime sequestration of carbon via photosynthesis is only one component expressed by $\lambda_v$. Vegetated surface fraction should rather be considered as a holistic proxy for measured $CO_2$ fluxes, coupled by indirect links to other factors determining $CO_2$ release (e.g. road and population density which trigger fossil fuel combustion). A fact that is supported by the results presented in Section P3.

A comprehensive list of papers on $CO_2$ flux studies is given in Table P3-1. Additional review sections on the state of the art in this field of research can be found in Section P3-2 and Section P2-1, whereas the latter also includes a short introduction to $CO_2$ concentration measurements in cities as well as to typical flow patterns and concentration dispersion effects in urban street canyons.

## 1.4 $CO_2$ measurements in Basel

Urban climatological studies have a long tradition at the Meteorology, Climatology and Remote Sensing Lab (MCR Lab) of the University of Basel. The first 32 m tower equipped with micrometeorological instruments was installed at Basel Spalenring for the BUBBLE experiment (Section 1.3). The aim of BUBBLE (2001/02) was to increase the knowledge on mass ($CO_2$), momentum and energy exchange over urban surfaces (Christen, 2005; Rotach et al., 2005; Vogt et al., 2006). It can be considered as the starting point for intensified research on urban $CO_2$ at the MCR Lab. In 2003, measurements from Basel Spalenring were relocated to the present location at Basel Klingelbergstrasse (BKLI), where in March 2004 ongoing continuous $CO_2$ observations started.

Observed variability of $CO_2$ flux over the years and distinct differences in the diurnal courses led to questions concerning the representativeness of the flux for the surrounding urbanized area and the linking to the controlling factors for this variability. Yearly sums of $F_C$ from 2004-2008, presented by Roland Vogt 2009 at the 7th International Conference on Urban Climate in Yokohama, depicted an average annual emission of $14.5 \pm 1\,\mathrm{kg\,m^{-2}}$. Monthly averages showed clear annual courses anti-cyclical to average air temperatures, but also a high inter-annual variability that is prone to – but not singularly explained with – varying heating emissions as a function of air temperature. Going one step deeper in the temporal resolution reveals a fairly similar morning increase for all average monthly diurnal courses and very diverse afternoon evolutions (Fig. 1.1). The typical wind field over Basel is characterized by a domination of east winds at night and west winds during the day, suggesting a spatial dependence of $F_C$. This topic was assessed at BKLI by a first experiment in 2004/05. $CO_2$ concentration profiles were sampled on both sides of

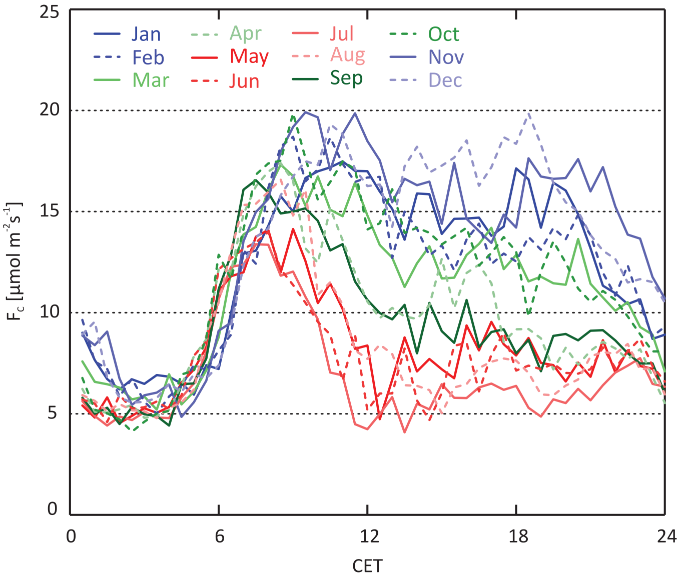


Figure 1.1: Average monthly diurnal courses of $F_C$ at Basel, Klingelbergstrasse for the years 2004–2012 (as presented by the author at the ICUC8, Dublin, 2012).

the building on which the tower is located. Results showed high values at the street-facing facade and lower concentrations in the backyard of the building block, confirming the assumption that spatial emission differences are distinct in this heterogeneous environment. And that they have undoubtedly an effect on measured $F_C$ – and need more comprehensive investigations.

Consequently, in 2009, an observational experiment started, supported by the participation of the MCR Lab in the international project BRIDGE (Chrysoulakis et al. (2013), Section 1.5), through which this thesis was primarily funded. Main objective of the experiment was to investigate the reasons for the spatio-temporal variability of urban $CO_2$ concentrations and fluxes. The aim was to assess this goal on different scales in the spatial and temporal dimension: From street canyon (micro scale) via block/neighborhood level (local scale) to city districts (city scale) and from hourly to inter-annual time scales.

## 1.5 The BRIDGE project

The European Community's Seventh Framework Programme project BRIDGE (SustainaBle uRban plannIng Decision support accountinG for urban mEtabolism, grant agreement no. 211345, 2009–2012) was a joint effort of 14 organizations from 11 countries with the goal to enhance communication and bridge gaps between science and urban planning. A Decision Support System (DSS) was developed to illustrate the advantage of considering environmental issues in urban planning processes and propose sustainability-oriented modifications on the urban metabolism. End-users were incorporated in the developing process by helping to define indicators and objectives in relation to environmental and socioeconomic factors of urban sustainability. Five case study cities across Europe were selected for measuring and modeling the atmospheric components relevant for fluxes of energy, water, carbon and pollutants in the framework of the urban metabolism. With the final DSS, planning alternatives in the five case study cities could be tested with respect to their effects on various sustainability indicators defined by the end-users. A detailed project description is found in Chrysoulakis et al. (2013). Within BRIDGE, the MCR Lab participated in three out of nine work packages (WP): WP2 (Methodology specification), WP3 (Data collection and analysis) and WP8 (Demonstration).

In **WP2**, the MCR Lab contributed to identifying the current understanding of urban metabolism by providing a comprehensive review on energy flows in the urban system, assessed from a meteorological point of view. The focus was laid on the urban energy balance (UEB), the respective methods and models and a literature review on recent research efforts, published as 'Part I: Energy in the urban system' in the project deliverable D.2.1 'Inventory of current state of empirical and modeling knowledge of energy, water and carbon sinks, sources and fluxes'. Presentations in this WP were held at progress meetings in Helsinki and Florence and the mid-term meeting in Brussels.

In the form of a shortened version of D.2.1, the chapter 'Physical fluxes in the urban environment' is contributed to 'PART II: Measurements and modelling of physical flows' of the final book on the BRIDGE project 'Understanding Urban Metabolism: A tool for urban planning' (Chrysoulakis et al., 2015). This book chapter is part of this thesis and incorporated as Section P1.

**WP3** was on data collection and analysis and had to provide datasets of the physical flows in the five case study cities Athens, Helsinki, Florence, London and Gliwice. Micrometeorological in-situ data collection and analysis for Gliwice, Poland, were in our responsibility. Consequently, this data was presented at several BRIDGE meetings.

Key instruments in the BRIDGE methodology were periodical gatherings of local planners and scientists, known as Communities of Practice (CoP). Demonstration of the DSS at two umbrella CoPs (Athens and Brussels) and organizing the final demonstration event (Brussels) were the tasks we were responsible for in **WP8**. To D.8.1 'DSS demonstration report' a fundamental analysis of the first umbrella CoP and the outcomes of the local CoPs was contributed, illustrating the core issues and challenges for sustainable urban planning in the BRIDGE case study cities. Minor inputs were made to D.8.2 'BRIDGE demonstration event – Sustainable urban planning', the proceedings of the 2nd umbrella CoP.

A great share of the thesis work was covered by BRIDGE related activities, thus personal project contributions of the author are listed in Section 6.

# 2 Methodological and conceptual background

## 2.1 Scales

In the context of meteorological observations, quite a range of scales in different dimensions have to be considered. Vertically, the atmosphere can be separated into layers according to the height of influence of effects related to the earth's surface. Horizontally, the scales of atmospheric processes determine the spatial extent – and so do they in the time dimension (Fig. 2.1). In practice, the different scales are actually linked and interrelated over all levels and all three dimensions.

> *"Big whirls have little whirls*
> *that feed on their velocity,*
> *and little whirls have lesser whirls*
> *and so on to viscosity."*
> *— L. F. Richardson, Weather Prediction by Numerical Process, 1922*

### 2.1.1 Vertical scales

*2.1.1.1 Planetary boundary layer*

The lowest part of the atmosphere (as sketched in Fig. P1-1) is considered the atmospheric or planetary boundary layer (PBL). Here, surface-atmosphere interactions have a relevant influence on thermodynamic processes and flow properties on time scales less than a day (Garratt, 1993). The vertical extent of the PBL ranges typically between 100–3000 m, is variable in the horizontal and the time-domain and dependent on atmospheric stratification and the roughness influences of the underlying surface. The PBL can be separated into a mixed layer and an underlying surface layer. In the mixed layer or Ekman layer, turbulence is assumed to be independent of the roughness of single surface elements and fluxes are decreasing with height. During daytime the mixed layer is growing as a consequence of surface heating and strong convection. At night, radiative cooling of the surface typically leads to stable stratification, less turbulent mixing and the development of a shallower nocturnal boundary layer replacing the daytime mixed layer. Over urban areas this nocturnal boundary layer usually stays unstable due to the release of stored heat from the urban structure. The surface layer between the mixed layer and the surface has a typical height of 10% of the PBL.

*2.1.1.2 Urban boundary layer*

The roughness of cities leads to the development of an urban variation of the PBL, the urban boundary layer (UBL, see also Fig. P1-1). A roughness sublayer (RSL) develops up to the height where effects of individual surface features are discernable (Oke, 2004). Between the RSL and the top of the surface layer, signatures from individual surface

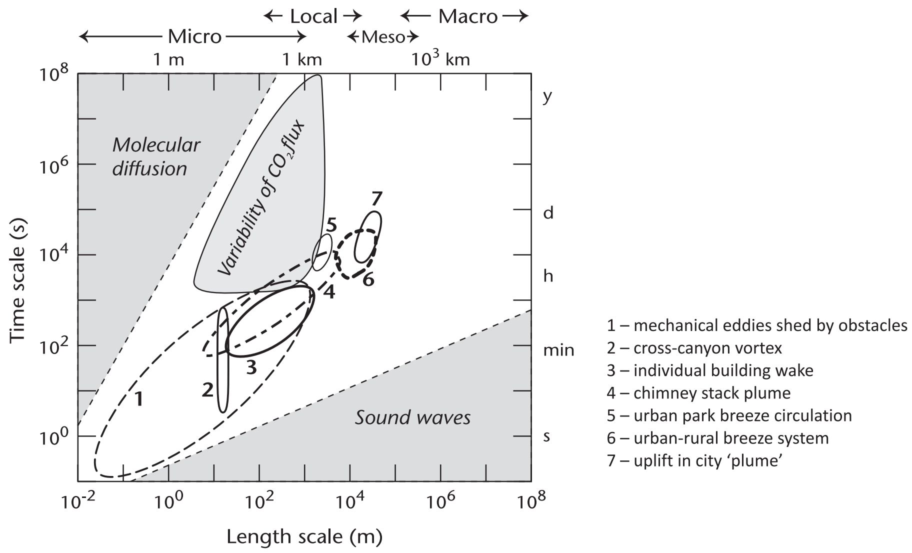


Figure 2.1: Scales of time and space in the field of urban climate with examples of motion phenomena. Additionally depicted are the scales that are focused on in this thesis in relation to the variability of carbon dioxide fluxes. Adapted from Oke (2006).

elements are blended into a mean signal and vertical variations of shear stress and fluxes are usually less than 10%. This inertial sublayer (ISL) is also referred to as constant flux layer where Monin-Obukhov similarity theory often applies. The ISL is dependent on the height of the RSL and hence reduced or even not existent over cities (Rotach, 1999).

The definition of the blending height $z_*$ between the RSL and ISL is not straightforward and is in practice often assumed to be around two times the average height of roughness elements ($z_h$) like buildings or trees, even if ranges from $1.5z_h$ over densely built-up areas to $5z_h$ in low density areas are reported (Grimmond and Oke, 1999; Raupach et al., 1991). Similar to the diurnal dynamic of the height of the UBL (Rotach et al., 2005; Vogt et al., 2006) $z_*$ has a temporal dynamic primarily depending on atmospheric stability and thus often shows diurnal variations. Of importance for flux measurements is that they take part above $z_*$ where, under ideal conditions, vertical fluxes of energy and matter are expected to be constant with height and sampling of a signal that is representative for the local scale can be assumed (Feigenwinter et al., 2012). Due to the often high extent of the RSL, this is in practice not always achieved.

In analogy to plant canopies, the lowest part of the RSL where surface elements like buildings and trees are located, is referred to as the urban canopy layer (UCL). It extends up to the average height of the roughness elements $z_h$ and is the layer in which most of our daily live in urban areas happens. Opposed to natural canopies, urban built-up structures are usually non-permeable for atmospheric transport processes, channel the flow and lead to fairly inhomogeneous turbulence distribution. Distinct microclimates can establish and affect the complete vertical extent of the UCL. Exchange processes of energy and matter are strongly dependent on the three-dimensionality of the urban structure and the source/sink distribution. Within the UBL, these processes are not only governed by enhanced mechanical mixing and reduced atmospheric stability, they also depend on local advection, organized motions, a highly turbulent shear layer at the top of the UCL, wake diffusion behind buildings and stationary vortices leading to significant dispersive fluxes (Feigenwinter et al. (2012); Roth (2000)).

Such vortices can occur in the free spaces between the urban roughness elements, e.g. in street canyons. Their structure and orientation is strongly dependent on the orientation of the roughness elements (usually buildings) to the wind direction and on their dimensions and roof geometries. Vortices often have a highly three-dimensional structure and do e.g. elongate along the canyon axis, forming corkscrew-like flows that lead to distinct distribution patterns of locally emitted pollutants or $CO_2$ inside street canyons (Section P1).

### 2.1.2 Horizontal scales

All atmospheric processes are linked to typical scales. As depicted in Fig. P1-1, horizontal scales interact with the vertical separation of the PBL into layers and are usually categorized into Macro-, Meso-, Local- and Microscale (Fig. 2.1). For urban purposes the latter three are of relevance and a more detailed classification, e.g. according to elements of the UCL as in Table P1-1 is necessary. A useful urban adaption of horizontal length scales is suggested by Britter and Hanna (2003) including the following scale definitions: regional (up to 100 or 200 km), city (up to 10 or 20 km), neighborhood (up to 1 or 2 km) and street (less than 100 to 200 m). The street or 'street canyon' scale addresses the features mentioned above for the UCL. At neighborhood scale, the inhomogeneities from the street canyon scale get less important and a more homogeneous image evolves. This spatial homogeneity of the urban structure (which, after Oke (2006), is a term used to describe the typical dimension of buildings and streets and the respective open spaces in an area) allows for the assumption of statistical homogeneity of atmospheric processes over the neighborhood scale and the forming of an inertial sublayer. Consequently, flux measurements above $z_*$ are related to the neighborhood scale. In this work the application of horizontal scales is adapted to the experimental setup (Section 3): *Micro scale* addresses the measurements inside and above the street canyon; the two individual flux observations in the ISL represent through the extent of their footprints the *local scale*; and the two sites together, despite that they are only 1.6 km apart from each other, are expected to account for differences on the *city scale* as their source areas do not overlap.

### 2.1.3 Time scales

Similar to the range of horizontal scales, the field of urban meteorology and climatology deals with a wide range of time scales from parts of seconds to centuries Oke (2006). A good illustration of the energy cascade in atmospheric turbulence is given by the famous statement of Lewis Fry Richardson shown at the beginning of this Chapter which he made in his 1922 book *Weather Prediction by Numerical Process*. Kinetic Energy is passed down from large scale motions via eddies of different sizes and rotational frequency to its final dissipation into heat. In the other direction, larger structures can be induced by the sum of small scale processes. Atmospheric flux measurements are typically based on high frequency motions in the order of fractions of seconds and are aggregated to longer averages, up to years. The time scales of typical processes related to the field of urban climate and the relation to respective length scales is depicted in Fig. 2.1.

### 2.1.4 Scales of interest

Each study has its own typical framework of scales. Fluxes measured with the eddy-covariance method (Section 2.2) are based on small scale turbulence but are typically calculated for half-hourly data sets and hence define, together with the spatial resolution of the observations inside the street canyon (Fig. 3.2), the lower boundary of the scales of interest in this study (Fig. 2.1). Observed carbon dioxide fluxes are related to seasonal source/sink characteristics on the neighborhood scale, making the yearly or inter-annual time scale the upper boundary. Macro scale processes as e.g. synoptical winds have as well an influence which blends with orographical effects to wind patterns typical for the local scale.

The depicted range for the scales of interest in Fig. 2.1 lies above the time scales of the individual atmospheric motion phenomena, indicating that the focus of the analyses in this study lies on urban climate phenomena on coarser time scales.

## 2.2 Eddy-covariance method

The conventional technique to calculate surface-atmosphere exchange of heat, mass (e.g. $CO_2$) or momentum is the eddy-covariance (EC) method. This statistical approach relies on the observation of simultaneous fluctuations of the three-dimensional velocity components of air ($u$, $v$, $w$) and a scalar of interest ($s$). By following Reynolds decomposition (e.g. Aubinet et al. (2012); Lee et al. (2004)) measured time series of these parameters, like the vertical wind component $w$, can be split into an average part $\overline{w}$ and a fluctuating part $w'$. The vertical turbulent scalar flux can then be expressed through the covariance of $w'$ and $s'$ measured at high frequency (e.g. 10–20 Hz) over a certain averaging time (usually 30 or 60 min), represented by the amount of data $N$ included:

$$\overline{w's'} = \frac{1}{N}\sum_{i=1}^{N} w'_i s'_i, \tag{1}$$

where $w$ and $s$ are split into a fluctuating part $i$ and a time-average part represented by the overbars (Lee et al., 2004). Next to the necessity of the flow to be turbulent, the EC method relies on some theoretical assumptions that should be fulfilled, like stationarity of the fluctuations over $N$ and a horizontally homogeneous flow. While the EC method is well established and has proven to deliver good results over flat and homogeneous surface types (Baldocchi, 2008), the mentioned assumptions lead to restrictions over very rough surfaces like cities (Feigenwinter et al., 2012). Stationary conditions are, for example, usually rare in urban areas, thus non-stationarity filters are often applied (Foken and Wichura, 1996). The highly diversified surface structure and non-uniform sources lead to spatially heterogeneous flows. Fluxes are valid for the point in space where they are measured. If in the ISL, they can be linked to a certain source area, but storage change in the control volume or horizontal advection may alter the flux signal (Fig. P1-2). Some systematic errors connected to the EC method and the challenging measurement environment make proper sensor placement and comprehensive quality control during data processing an important task (see e.g. Foken et al. (2012); Mauder and Foken (2006); Mauder et al. (2008); Rebmann et al. (2012)).

## 2.3 Source areas

By getting closer to the ground, the flow structure is stronger affected by surface objects and the measured flux signals by single sources. Inside the RSL and UCL, fluxes are strongly affected by the three-dimensionality of the flow caused by distortions (wake turbulence) through urban canopy objects (buildings, trees). Opposed to the ISL, a height dependency exists (Rotach, 2001) and attribution to a source area is not possible.

Even in the ISL a proper relation of measured fluxes or concentrations to a certain source area or footprint is challenging (see e.g. Bergeron and Strachan (2011); Järvi et al. (2012); Kordowski and Kuttler (2010)) and can only be achieved through modeling approaches, i.e. analytical (Hsieh et al., 2000; Kormann and Meixner, 2001) or numerical (Kljun et al., 2002; Schmid, 1994; Sogachev and Lloyd, 2004). Analytical models are usually simpler in their application and thus more widely used. In this thesis the model by Kormann and Meixner (2001) is applied, which is valid under all atmospheric stability conditions and describes the crosswind-integrated and crosswind-distributed footprint of scalar fluxes.

Footprints are usually depicted in the form of different relative contribution levels. The size of the footprint is depending on the height of the observation, the surface roughness length (the urban structure), turbulence intensity, atmospheric stability, wind speed and – important in heterogeneous urban areas – direction (Vesala et al., 2008). Instantaneous flux footprints can be averaged to flux weighted long term source areas (see Fig. P3-2).

In urban areas, emission sources like roads or chimneys are extremely variable in their strength and distribution. If the spatial emission patterns are not exactly known, flux footprints are only of restricted help. Without e.g. weighting with spatially modeled emission distribution data as e.g. in Christen et al. (2011), urban footprints only give an unweighted impression of the 'area' that contributes to the measured fluxes and not of the actual 'source' distribution.

# P1 Physical fluxes in the urban environment

**Lietzke, B.**, Vogt, R., Young, D.T. and Grimmond, C.S.B. (2015):
Physical fluxes in the urban environment. In: Chrysoulakis, N., de Castro, E.A. and Moors, E.J. (Eds.): Understanding urban metabolism – A tool for urban planning. Routledge, Oxford.

# 4

# PHYSICAL FLUXES IN THE URBAN ENVIRONMENT

*Björn Lietzke[1], Roland Vogt[1], Duick T. Young[2] and C.S.B. Grimmond[2]*

[1]*UNIVERSITY OF BASEL,* [2]*UNIVERSITY OF READING*

## Urban metabolism: the meteorological view

Meteorologists are most interested in understanding how energy in the form of radiation and heat influences the urban climate and how this energy is transported, transformed and stored (e.g. in urban building structures). They also are interested in the effects of precipitation on cities, how storm water runoff is changed and how much water is emitted into the atmosphere through evapotranspiration. In addition, they want to know how much cities worldwide contribute to climate change through their emissions to the global carbon cycle. For meteorologists to address the challenges of sustainable cities and urban planning, information on the distribution and flows of energy, water and carbon in typical urban systems have to be known.

From a meteorological perspective, the urban metabolism of a city is strongly dependent on the prevailing regional and local climate and its built-up structure. Together these define the microclimate within the street canyons, on the roads, in the buildings, and at any other place in an urban area. In this context, the urban energy, water and carbon balances are presented in this chapter.

## Urban atmosphere

### *Layers and scales*

A key issue of importance for urban investigations is the definition of the appropriate scale of a study area. A classification of urban canopy layer (UCL) elements according to scale considerations is given in Table 4.1. Vertically, the urban atmosphere can be divided into layers as illustrated in Figure 4.1. The lower atmosphere that is influenced by the urban structure is called the urban boundary layer (UBL). From the ground up to roughly the average height of roughness elements like buildings or trees ($z_h$) is the UCL. It is produced by micro-scale processes in their immediate surroundings. The UCL is part of the roughness sublayer (RSL) which is dependent on the height and density of roughness elements and extends to the height $z_* = a \cdot z_h$ where $a$ ranges between 2 and 5 (Raupach et al. 1991). Above this is the inertial sublayer (ISL) where under ideal conditions vertical fluxes of energy or matter can be expected to be constant with height. The upper part of the UBL, which is to a large extent determined by meso-scale advective processes, is referred to as the outer UBL (Rotach et al. 2005).

Table 4.1: Classification of elements of the urban canopy layer (UCL) and their scales (adapted from Oke 2006).

| *UCL units* | *Built features* | *Meteorological scale* | *Typical horizontal length scales* |
|---|---|---|---|
| 1. Element | Individual surface element (pavement, trees etc.) | Micro | $< 10$ m $\times$ 10 m |
| 2. Building | Building | Micro | 10 m $\times$ 10 m |
| 3. Canyon | Street, canyon, property | Micro | 30 m $\times$ 40 m |
| 4. Block | Block, neighbourhood, factory | Micro/Local | 0.5 km $\times$ 0.5 km |
| 5. Land-use class (UTZ, UCZ, LCZ, UZE)* | City centre, residential, or industrial zone | Local | 5 km $\times$ 5 km |
| 6. City | Urban area | Local/Meso | 25 km $\times$ 25 km |
| 7. Urban region | City plus its environs | Meso | 100 km $\times$ 100 km |

*A number of different classifications at this scale exist including: UTZ: Urban Terrain Zones (Ellefsen 1990/91), UCZ: Urban Climate Zones (Oke 2006), LCZ: Local Climate Zone (Stewart & Oke 2012), UZE: Urban Zones for Energy partitioning (Loridan & Grimmond 2012).

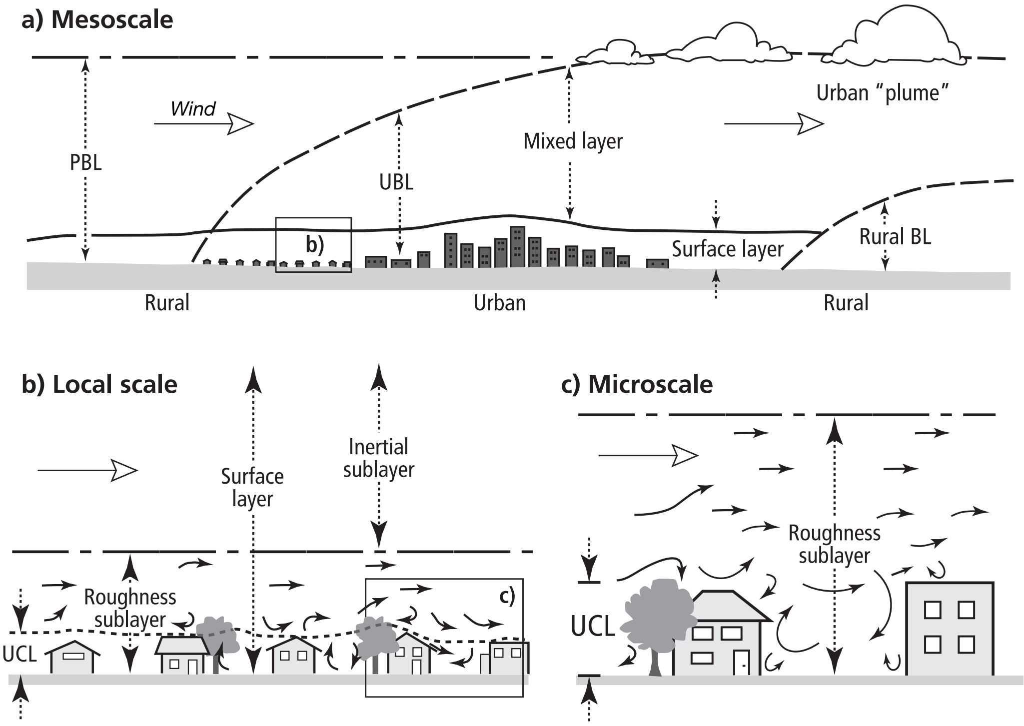


Figure 4.1: Scales and layers (planetary boundary layer: PBL; urban boundary layer: UBL; urban canopy layer: UCL) in the urban atmosphere (Feigenwinter et al. 2012; adapted from Oke 2006).

### *Processes and variability*

The exchange of mass and scalars in the urban atmosphere is governed by several processes linked to the heterogeneity of the 3D urban structure. These have a direct influence on the emission and distribution of energy, water and carbon and their transport to the atmosphere. Enhanced mechanical and thermal turbulence in cities change the wind field and induce perturbed streamlines which have an influence on micro- to local-scale transport processes.

Given urban areas are not spatially homogeneous, atmospheric measurements in the UBL are strongly dependent on the spatial and temporal source/sink distribution. This leads to strict requirements for the siting of measurement instruments (Feigenwinter et al. 2012; Oke 2006) as vertical turbulent fluxes, for example, are extremely sensitive to strong local sources in combination with prevailing wind directions (Lietzke & Vogt 2013). Ideal sites are hard to find and it is thus of great importance to know the source area of atmospheric measurements, i.e. the urban area for which observations are representative.

## Methods

The energy, water and carbon balances of an urban system can be determined by considering their physical flows in and out of a control volume, which, considering mass conservation, leads to a volume balance approach as depicted in Figure 4.2.

The measurement of the fluxes is achieved with different, often very specific methods. These methods are discussed in the subsequent sections together with the respective processes they measure. One elementary and widely used method to derive the vertical exchange of energy and mass as part of an air volume, the Eddy Covariance (EC) method, is presented here, since this method was mainly used in the BRIDGE project (Chrysoulakis et al. 2013), as described in Chapter 5.

The EC method relies on the fact that atmospheric turbulence is usually the main vertical transport mechanism in the ISL of the UBL. High frequency variations (typically 10-20 Hz) of the vertical wind component $w$ and the scalar $s$ of interest (e.g. $H_2O$ or $CO_2$) are measured and, after decomposing into mean and turbulent parts by applying Reynolds averaging, their covariance $\overline{w's'}$ gives the vertical turbulent exchange rate of the respective scalar. The primes denote the deviations from the mean and the overbar the average.

Measurements have to be situated at the top of the control volume (Figure 4.2), which is ideally inside the ISL, to capture the vertical transport in and out of the volume. The instrument of choice is usually an ultrasonic anemometer-thermometer in combination

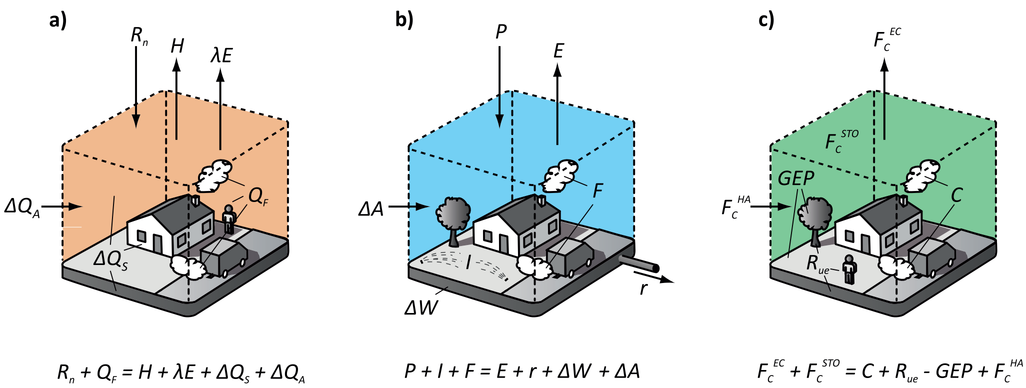


Figure 4.2: Schematic depiction of the (a) Urban Energy Balance; (b) Urban Water Balance; and (c) Urban Carbon Balance from a micrometeorological perspective. The directions of the arrows represent positive fluxes. For an explanation of variables see the text (adapted from Feigenwinter et al. 2012).

with a gas analyzer that measures the scalars of interest (see Chapter 5 for details). An extensive overview on the EC method is given in Aubinet et al. (2012).

For inhomogeneous urban areas, the EC method is more suitable than other approaches, such as the flux-gradient relations, which normally fail in the RSL (Christen 2005; Piringer et al. 2002; Roth & Oke 1995). Measurements higher up in the ISL are difficult in urban areas due to a lack of higher towers and because of fetch considerations. Therefore, care needs to be taken when using micrometeorological techniques to consider averaging time, the flux source area and sensor placement to ensure representativeness of the flux in an urban context (Foken 2008; Grimmond 2006).

## Physical fluxes

### *Energy fluxes – Urban Energy Balance*

#### *Introduction*

Following the volume balance approach, the energy balance of an urban system (Urban Energy Balance - UEB) can be determined by considering the energy flows in and out of the control volume:

$$R_n + Q_F = H + \lambda E + \Delta Q_S + \Delta Q_A$$

where $R_n$ is the net all-wave radiation, $Q_F$ is the anthropogenic heat flux, $H$ is the turbulent sensible heat flux, $\lambda E$ is the turbulent latent heat flux, $\Delta Q_S$ is the net storage change within the control volume and $\Delta Q_A$ is the net advected flux. All terms are usually expressed as energy flux density per horizontal or vertical area (typically W m$^{-2}$, also MJ m$^{-2}$ d$^{-1}$ for temporal sums). In the following sections each of the UEB terms are discussed.

Theoretical knowledge of the processes forming the UEB and the resultant effects on the UBL is well developed based on numerous observational studies. For typical urban areas, the daytime energy balance is characterized by a significant storage heat flux term, a strong sensible heat flux away from the surface and weak evapotranspiration. As a consequence of strong nocturnal release of stored heat, both turbulent heat fluxes remain directed upward on average at night, a notable difference to the rural environment. This has consequences for the stability of the urban ISL and the RSL which are thermally unstable most of the time (Christen 2005).

#### *Net all-wave radiation $R_n$*

Net all-wave radiation ($R_n$) is the balance between the incoming (↓) and outgoing (↑) short- (SW) and long-wave (LW) radiation fluxes and represents the primary source of energy in the UEB:

$$R_n = SW\downarrow - SW\uparrow + LW\downarrow - LW\uparrow$$

Measurements can be made using pyranometers for the short-wave fluxes and pyrgeometers for the long-wave fluxes, or by using net radiometers. In a typical urban atmosphere radiative fluxes are, if compared to their rural counterparts, altered by pollutants. Whereas SW↓ will be reduced, LW↓ is greater. In typical mid-latitude cities, these changes are normally opposed by a lower short-wave albedo due to darker surface materials (whereas in low-latitude cities, walls and roofs are generally brighter) and a higher surface temperature at night, which augments the long-wave emission (Oke 1987). The net effect on urban/rural radiation differences therefore remains small (Oke 1987, Rotach et al. 2005).

### *Anthropogenic heat flux $Q_F$*

The anthropogenic heat flux ($Q_F$) derives mainly from combustion exhausts by stationary and mobile sources (Grimmond 1992; Sailor 2010). Thus, its contribution to the UEB tends to be highest in cold climates in the wintertime when the energy input from human sources is comparatively large (primarily due to domestic heating). But even in summertime it may become significant for cities with high air conditioning usage. QF is difficult to determine because of its strongly varying patterns in space and time and because it cannot be measured directly. It is therefore not surprising that many different approaches to estimate this term can be found in literature.

A common approach is to estimate ($Q_F$) based on inventories of existing socio-economic data, e.g. from energy use data (Sailor 2010). These kinds of data have been analysed as part of the BRIDGE project (Allen et al. 2010; Iamarino et al. 2012; Lindberg et al. 2013; Chapter 5). A second approach, if daily or yearly totals of the energy balance equation are considered, and $\Delta Q_S$ can be assumed to be zero, allows calculation of $Q_F$ as the residual term (Christen & Vogt 2004; Pigeon et al. 2007a), or with storage heat flux measurements at a monthly diurnal timescale (Offerle et al. 2005). A third approach explored as part of the BRIDGE project, uses micro-scale analysis of the EC data (Kotthaus & Grimmond 2012) to determine the amount of energy released from buildings. This uses the spikes of heat, water and carbon dioxide ($CO_2$) 10 Hz data, which impact the departure of the mean used in the EC calculation.

The spatial and temporal patterns of $Q_F$, have large impacts on the urban climate and is impacted by many of the urban planning alternatives (Chapter 3), therefore understanding the role and size of this term is important.

### *Turbulent sensible heat flux $H$*

The vertical transport of energy by the sensible heat flux ($H$) as measured by the EC method is expressed:

$$H = \rho c_p \overline{w'T'}$$

where $\rho$ is the air density (kg m$^{-3}$), $c_p$ is the specific heat capacity of air (J kg$^{-1}$ K$^{-1}$) and $\overline{w'T'}$ (K m s$^{-1}$) is the average of the product of the turbulent fluctuations of air temperature $T$ and the vertical wind speed $w$. During daytime this term is primarily driven through energy input by $Rn$, while at night storage release from the urban structure keeps $H$ at a higher level compared to rural areas.

### *Turbulent latent heat flux $\lambda E$*

The turbulent latent heat flux $\lambda E$ transports moisture away from the surface because of a change of state (e.g. condensation, evaporation). This depends primarily on the availability of water, particularly the presence of vegetated areas (transpiration) or wet surfaces (evaporation). Similar to the sensible heat flux it can be written as:

$$\lambda E = L_v \overline{w'\rho_v'}$$

with $L_v$ the latent heat of vaporization (J kg$^{-1}$) and $\rho_v'$ the fluctuating water vapor density (kg m$^{-3}$). $\lambda E$ can be measured directly using the EC method (e.g. a sonic anemometer coupled with an open-path infrared gas analyzer). The quantification of $\lambda E$ is complicated by the extremely heterogeneous sources of moisture. This term is discussed further in the next section, when evapotranspiration (its water equivalent) is considered.

### *Net storage change* $\Delta Q_S$

The rate of change of heat storage ($\Delta Q_S$) consists of the uptake or release of energy by the ground, buildings and vegetation and in the volume. It includes the changes of latent and sensible heat content in the air of the considered control volume. The latter changes are often neglected as they are small compared to the heat storage changes in urban materials.

$\Delta Q_S$ within an urban control volume can be theoretically expressed as the sum of storage fluxes for single surface elements (Offerle et al. 2005):

$$\Delta Q_S = \sum_i \frac{\Delta T_i}{\Delta t} (\rho C)_i \Delta x_i \lambda_{pi}$$

where $\Delta T / \Delta t$ is the rate of temperature change, $\rho C$ (J m$^{-3}$ K$^{-1}$) is the volumetric heat capacity, $\Delta x$ (m) is the element thickness and $\lambda_p$ (m$^2$) is the plan area index for each element $i$ (Offerle et al. 2005).

As cities are not expected to cool down, or heat up during a year, the annual total of $\Delta Q_S$ has to be zero by definition (Christen 2005; Offerle et al. 2005). This is helpful in calculating annual surface energy balances and in assigning annual residuals to other terms as, for example, the anthropogenic heat flux. $\Delta Q_S$ is a spatially and temporally variable term of the energy balance, depending on differences in surface type and radiant loading. It is of particular relevance in the urban energy balance as it can account for more than half of the daytime net radiation at highly urbanized sites (Roberts et al. 2006).

Direct measurements in urban areas are practically unattainable due to the complexity of urban structures and materials. $\Delta Q_S$ therefore has to be determined by indirect methods or models. As for most fluxes that are not directly measureable, there is a lack of standard for the determination of urban heat storage and quite a range of methods exist. A commonly used method is to consider the storage flux term as the residual of the energy balance (e.g. Christen & Vogt 2004; Grimmond & Oke 1995, 1999; Roth & Oke 1994; Spronken-Smith et al. 2006):

$$\Delta Q_S = R_n - H - \lambda E$$

$\Delta Q_A$ and $Q_F$ are here considered as negligible. Another widely used parameterization approach is based on relations between the net all-wave radiation $Rn$ and the storage heat flux $\Delta Q_S$ for typical surface materials (Camuffo & Bernardi 1982; Grimmond & Oke 1991; Oke et al. 1981).

### *Net advected flux* $\Delta Q_A$

Storage change in a control volume due to advection can be expressed as a result of the flow in and out of the volume:

$$\Delta Q_A = Q_A^{in} - Q_A^{out}$$

The scale of the advection is critical relative to the scale of interest. Local-scale advection has largely been neglected for a long time in urban measurement studies based on assuming that the fetch conditions were similar so the term could be considered to be small and the theoretical assumption of horizontal homogeneity was adopted. However, the fetch is rarely sufficiently extensive and consistent, so the latter is often questionable.

To date $\Delta Q_A$ has only been investigated at the local scale in urban environments in cities with meso-scale circulations, such as diurnal sea-breeze circulations (e.g. Pigeon et al. 2007b), or drainage flows (e.g. Spronken-Smith et al. 2006) where it has been shown to be important. The circulations between the city and the surroundings (e.g. Lemonsu & Masson 2002) and because of local-scale features (e.g. urban parks; Spronken-Smith et al. 2000) are thought to be important influences in urban areas. However, these processes remain under-studied in urban areas because of the vast array of instrumentation needed and the need to couple the observations with 3D modelling (e.g. Pigeon et al. 2007b). In the BRIDGE project, the role of advection has been considered at the local scale in London (Kotthaus & Grimmond 2013a, 2013b; Loridan et al. 2013).

## *Water Fluxes – Urban Water Balance*

### *Introduction*

The urban environment is significantly different to natural hydrological watersheds in terms of land use, water flows and surface cover leading to the modification of the hydrological cycle. In addition, the transport and removal of water through the piped water system adds an anthropogenic component. Artificial surfaces found in urban areas enhance the surface runoff leading to an enhanced risk of flooding and the transport of pollutants (Burian et al. 2002), along with a reduction in infiltration leading to lower replenishment of groundwater (Stephenson 1994).

The Urban Water Balance (UWB) applies the principle of mass conservation to the transfer of water through a specific domain, or catchment (Grimmond et al. 1986), allowing the study of both spatial and temporal patterns of water supply and usage (Mitchell et al. 2001). It can be written as (Grimmond & Oke 1991):

$$P + I + F = E + r + \Delta W + \Delta A$$

where $P$ is precipitation, $I$ is the urban piped water supply, $F$ is water release due to human activity, $E$ is evapotranspiration, $r$ is runoff, $\Delta W$ is net change in water storage and $\Delta A$ is the net advection of moisture in and out of the control volume. Each of the terms is usually expressed as a depth of water, or as a volume per unit time. It is also common to express individual terms as a percentage of the annual precipitation (often assumed to be the main input into the system) especially in the study of individual components such as runoff and evapotranspiration (e.g. Berthier et al. 2006; Xiao et al. 2007).

### *Precipitation $P$*

Precipitation is a key input into the UWB as the amount and intensity directly impact the potential magnitude of evapotranspiration, runoff and infiltration and the amount of recharge to surface and groundwater stores. The components of total precipitation ($P$) are:

$$P = P_r + P_h + P_s + P_m$$

where $P_r$ is rainfall, $P_h$ is hail, $P_s$ is snow and $P_m$ is atmospheric moisture which condenses on contact with the surface in the form of fog, mist or dew. The form of precipitation dictates the timing of the availability of water for runoff, infiltration and evapotranspiration. Snow and hail, which fall in a solid/semi-solid state, have to undergo a change of state to liquid or gaseous form and thus for a time period may be recorded as an increase in storage in the UWB. Depending on the climate, this can last for many months and affect the UWB at a later date through runoff or evaporation (e.g. Järvi et al. 2014, for Helsinki).

Precipitation measurement within urban areas has traditionally used tipping bucket rain gauges. Radar can provide spatial information, but cannot be used alone due to uncertainty in its accuracy (Berne et al. 2004; Vieux & Bedient 2004).

*Piped water supply $I$*

The total piped water supply ($I$) consists of:

$$I = I_U + I_R + I_G + I_S$$

where $I_U$ is the internal residential/commercial/industrial water use, $I_R$ is water used for irrigation, I$I_G$G is grey or other reused water and $I_S$ is the leakage to/from the piped network.

The magnitude of the water supplied is driven by a combination of demand from urban inhabitants and supply by the water utility companies or agencies, which is determined by availability of surface and groundwater supplies. Measurement of the supplied water is often from water utility company water meters (e.g. Morris et al. 2007).

Irrigation is a major component of piped water use in urban areas, where seasonal precipitation and weather patterns are particularly variable (Mitchell et al. 2001), with variability in irrigation related to specific weather events (Grimmond & Oke 1986). However, determining the actual amount of irrigation (as with other water usage) is a much more complex problem as it is related to human perception and behaviour (e.g. Arnfield 2003; Grimmond & Oke 1986).

*Anthropogenic water release due to combustion $F$*

Anthropogenic water release due to combustion of fuels and from industry consists of:

$$F = F_M + F_I + F_V + F_W$$

where $F_M$ is the release of moisture from air conditioning, heating and cooling applications, $F_I$ is the moisture released from industry, $F_V$ is the moisture released due to combustion of from vehicles and $F_W$ is consumption of bottled water. This term has not been neither widely investigated, nor often considered in UWB models (e.g. Grimmond et al. 1986; Mitchell et al. 2001), but in large cities this term can become more important (Moriwaki & Kanda 2004). In Tokyo, Japan local-scale EC observations over a heavily urbanized area (very little vegetation) displayed significantly large latent heat fluxes ($> 100$ W m$^{-2}$ and at times greater than observed sensible heat flux) in the summer months, as a result of anthropogenic moisture release from building cooling systems (Moriwaki et al. 2008).

*Evapotranspiration $E$*

Evapotranspiration includes evaporation of surface water and transpiration through vegetation of water from the sub-surface vadose zone (Xiao et al. 2007). The term is used interchangeably with evaporation in many studies where it is impractical to separate the two components (Brutsaert 1982):

$$E = E_V + E_T$$

where $E_V$ is evaporation and $E_T$ is transpiration. Its energy equivalent is the latent heat flux $\lambda E$..

Given that water is typically limited at the surface within cities due to high areal fractions of unvegetated and impervious surfaces, actual evaporation rates are limited by surface controls and energy availability. When water availability is unlimited the theoretical maximum evaporation is typically referred to as potential evaporation which is usually greater than the actual evaporation (Aston 1977). Despite these limiting factors, $E$ can be one of the most important terms in the UWB as a result of complex microclimates, surface storage and irrigation (Berthier et al. 2006; Grimmond & Oke 1986, 1991, 1999; Mitchell et al. 2001).

Urban parks and open water bodies are of particular interest due to the relatively high vegetation cover and greater amount of available moisture resulting in distinct microclimates (the former akin to that of a desert oasis) in comparison to surrounding more built up areas (Hathway & Sharples 2012; Spronken-Smith et al. 2000; Steeneveld et al. 2014). Spronken-Smith et al. (2000) observed that daily total evapotranspiration in a park in Sacramento, USA, was greater than 300 per cent of the total from the surrounding irrigated suburban area.

Observation of evapotranspiration has been undertaken using mini-lysimeters at the micro scale (Oke 1979), while at the local scale, micrometeorological techniques are often applied (e.g. EC). Alternatively when direct measurement is unavailable it can be determined as a residual term of the UWB equation or using the Bowen ratio energy balance (Nouri et al. 2012). Goldbach & Kuttler (2013) found in Oberhausen, Germany, using EC, that absolute daily maximum evapotranspiration varied by up to 90 per cent between urban and suburban areas where vegetated surface fractions were 0.18 and 0.58, respectively. Data sets from 19 EC sites located in urban and suburban areas of 15 cities worldwide indicated a positive relation between the active vegetated index (indices based on vegetated fraction and seasonal leaf-area index (Loridan et al. 2011) and mean midday evapotranspiration, with a stronger linear dependence on observed $E$ rates prevalent when active vegetated index was $< 0.43$ (Loridan & Grimmond 2012).

### *Runoff* $r$

Runoff is the flow over the surface and through drainage pipes. It represents water that has not been captured by some intermediate store (e.g. tree canopy, roof or surface storage) or has not infiltrated into sub-surface stores within a particular time period. A greater fraction of impervious surfaces in cities in comparison to rural areas leads to more rapid surface flows often enhanced by drainage networks (Semadeni-Davies & Bengtsson 1999). The increase in runoff can lead to a higher probability of flooding and the transport of pollutants (Burian et al. 2002; Xiao et al. 2007). Urban runoff consists of:

$$r = r_S + r_W + r_O + r_L + r_F$$

where $r_S$ is storm water runoff (through storm drains), $r_W$ is waste water flow (sewer system), $r_O$ is runoff released by snow melt, $r_L$ is surface runoff (e.g. overland flow and roof runoff) and $r_F$ is surface infiltration. The rate and magnitude of runoff are regulated by the rate of precipitation, soil moisture content (influences infiltration), land surface properties (e.g. fraction of vegetation cover and permeability), local topography and the design of the drainage system infrastructure.

Runoff is often either modelled in the UWB due to a lack of measured data or the size of the study catchment (Branger et al. 2013; Wang et al. 2008), parameterized using infiltration/runoff coefficients (Hollis & Ovenden 1988) or as a residual (Jia et al. 2001). However, runoff measurement is possible directly using flow meters to determine discharge through a drainage system (Ragab et al. 2003b) or controlled study area (Stephenson 1994; Xiao et al. 2007), water capture to collect and measure roof runoff (Hollis & Ovenden 1988; Ragab et al. 2003a), and indirectly using water balance techniques to determine available water for potential runoff (Inkiläinen et al. 2013). In the BRIDGE case studies, the runoff in two small catchments was observed in Helsinki (see Chapter 10 for details).

#### *Net storage change $\Delta W$*

The net change in storage term ($\Delta W$) refers to the change in water storage within the study catchment. Its magnitude is determined by

$$\Delta W = \Delta W_g + \Delta W_m + \Delta W_w + \Delta W_a + \Delta W_n$$

where $\Delta W_g$ is the net change in ground water storage, $\Delta W_m$ is the net change in soil moisture storage, $\Delta W_w$ is surface water storage (e.g. ponds and lakes), $\Delta W_a$ is anthropogenic storage (e.g. storm water holding and water butts) and $\Delta W_n$ is the net change in snowpack storage.

For large catchments, groundwater within the soil and deeper aquifer(s) can be significant. Techniques to measure soil moisture include tensionmeters (Berthier et al. 2004), gravimetric sampling (Grimmond & Oke 1986) and time domain reflectometry and groundwater levels can be observed through boreholes (Stephenson 1994).

#### *Net moisture advection $\Delta A$*

The net moisture advection is the horizontal transport of moisture by atmospheric flow. It is driven by flows at a number of atmospheric scales ranging from micro- and local-scale turbulence to meso-scale circulations (e.g. sea breezes and valley flow). In many UWB studies the net moisture advection is not considered (e.g. Grimmond et al. 1986; Lemonsu et al. 2007).

## *Carbon fluxes – Urban Carbon Balance*

#### *Introduction*

Compared to energy and water, the urban balance of carbon - in the form of $CO_2$ - shows greater deviations from its rural counterpart. Anthropogenic $CO_2$ emissions, derived from the burning of fossil fuels, are the major net source for global atmospheric carbon (Denman et al. 2007) and cities contribute a great share. Thus, knowledge of the spatiotemporal distribution of sources and sinks in urban environments and the processes that determine atmospheric transport in the UBL is of great importance.

Using a volume budget approach that focuses on surfaceatmosphere processes, the Urban Carbon Balance (UCB) can be written as:

$$F_C^{EC} + F_C^{STO} = C + R_{ue} - GEP + F_C^{HA}$$

where $F_C^{EC}$ is the integrative turbulent mass flux density of $CO_2$, $F_C^{STO}$ is the storage change between the surface and the measurement level, $C$ represents emissions through anthropogenic combustion processes, $R_{ue}$ is the respiration of the urban ecosystem (including from humans), $GEP$ stands for the sink effects due to photosynthesis and $F_C^{HA}$ is the horizontal advection contribution. Terms are usually expressed as $CO_2$ flux density per horizontal or vertical area (typically $\mu$mol m$^{-2}$ s$^{-1}$ or kg m$^{-2}$ a$^{-1}$).

#### *Turbulent $CO_2$ flux $F_C^{EC}$*

A common way to determine the turbulent vertical mass flux density of $CO_2$ ($F_C^{EC}$) is by the use of the EC method, combining sonic with infrared gas analyzer measurements (a list of urban studies can be found in Lietzke et al. (2014). Two types of gas analyzers are widely used: open path analyzers where $CO_2$ concentrations are measured instantaneously in the probed air volume (e.g. Moriwaki & Kanda 2004; Vogt et al. 2006) and closed path analyzers where air is sucked through a tube into an enclosed measurement system (e.g. Grimmond et al. 2002; Järvi et al. 2012). The first has the advantage of measuring *in situ* but is sensitive to disturbances of the measurement path, e.g. through rain, dew or dust. The latter measurements are subject to a time lag and an attenuation of the signal, dependent on the length of the tube, but are not influenced by meteorological disturbances (Grimmond et al. 2002; Järvi et al. 2009).

Summing $F_C^{EC}$ over a defined timescale yields the net urban ecosystem exchange ($NuEE$) rate analogous to the net ecosystem exchange ($NEE$) rates of rural ecosystems. The main contrast to non-urban ecosystems is that the urban surfaces generally act as a $CO_2$ source; consequently $F_C^{EC}$ is nearly always positive. This results in positive $NuEE$ values which are usually higher the more urbanized an area is.

#### *Net storage change in the air $F_C^{STO}$*

Fluxes in the RSL are not constant with height (Rotach 2001) and thus a vertical flux divergence over time has to be assumed in the air volume between the urban surface and the measurement level. This is considered in the term $F_C^{STO}$, which can be determined using representative measurements of the concentration change within the air volume over time (Feigenwinter et al. 2012). In an urban environment, this would need several vertical profile measurements to account for the spatial variability within the EC source area - which is rarely feasible. Similar to $\Delta Q_S$, $F_C^{STO}$ can assumed to be zero over a longer time period. On a diurnal scale it becomes relevant as, for example, nocturnally accumulated $CO_2$ in the shallow UBL and the street canyons is flushed in the morning, when thermal mixing starts, leading to an overestimation of $F_C^{EC}$ compared to the actual emissions (Feigenwinter et al. 2012).

#### *Combustion $C$*

Anthropogenic emissions through combustion of fossil fuels are the main contributors to the UCB, consisting of:

$$C = C_B + C_V$$

The combustion from buildings ($C_B$) and vehicular traffic ($C_V$) can be distinguished by the type of fuel they burn (natural gas, oil or wood for heating versus gasoline or diesel for driving) and the spatiotemporal emission patterns. Source distribution is, as for $Q_F$, very heterogeneous. While $C_V$ can be considered as a line source on the bottom of the control volume that is primarily dependent on the diurnal/weekly traffic use behavior, $C_B$ generated by heating depends on climate related human activity (heating in winter, air conditioning in summer), has a distinct seasonal cycle (Lietzke et al. 2014) and consists of point sources at certain heights (e.g. chimneys) (Kotthaus & Grimmond 2012). Industry emissions as a part of $C_B$ follow their own patterns that need to be taken into account as appropriate.

Through isotopic analyses of air samples (Clark-Thorne & Yapp 2003; Pataki et al. 2003), the fraction of atmospheric $CO_2$ generated by either $C_B$ or $C_V$ can be derived. Inventory based approaches using fossil fuel consumption data and traffic density analyses (e.g. Helfter et al. 2011; Ward et al. 2013) can give an estimate of $C_B$ and $C_V$, or are used as input to model their contributions. Spatiotemporal adequately resolved data is rarely available so that e.g. fuel consumption often has to be scaled down from city to neighbourhood or building scale (e.g. Christen et al. 2011). An indicator of fuel burned for heating purposes can be heating degree days based on outside air temperature and the desired inside air temperature (Lietzke et al. 2014).

### *Urban ecosystem respiration* $R_{ue}$

Urban ecosystem respiration ($R_{ue}$) can be separated into respiration of soils and vegetation ($R_{SV}$), waste decomposition ($R_W$) and human respiration ($R_M$):

$$R_{ue} = R_{SV} + R_W + R_M$$

Compared to natural ecosystems, urban $R_{SV}$ is influenced by irrigation and fertilization. $R_M$ depends on the density of people that live or work in an area and, on the basis of an individual, the physiological level of activity (active, resting, sleeping etc.). Moriwaki & Kanda (2004) estimated human body respiration emissions at rest to be 8.87 mg $CO_2$ $s^{-1}$.

### *Gross ecosystem productivity* $GEP$

Gross ecosystem productivity ($GEP$) is a measure of the uptake of $CO_2$ through photosynthesis from the air. In cities, both $GEP$ and $R_{SV}$ are primarily dependent on the surface fraction of vegetation (parks, lawns and trees), its density and type and the local climate which determines the seasonal photosynthesis rate. Productivity of urban vegetation is usually high due to irrigation, higher temperatures, less frost damage (urban heat island) and fertilization (e.g. nitrogen oxides ($NO_x$) deposition) (Trusilova & Churkina 2008), but physiological stress due to air pollution may lead to reduced $GEP$. Chamber measurements (Christen et al. 2011) help in estimating soil and lawn activity. In urban areas, photosynthesis is typically not able to compensate for the high $CO_2$ emissions by combustion (Kotthaus & Grimmond 2012; Lietzke & Vogt 2013), but may have a limiting effect on measured fluxes (Coutts et al. 2007; Kordowski & Kuttler 2010; Ward et al. 2013). Depending on the extent of urbanization, particularly vegetation effects, temporary sink effects can be observed (e.g. Crawford et al. 2011; Ramamurthy & Pardyjak 2011).

### *Net advection* $F_C^{HA}$

Similar to advection in the UEB and UWB, net horizontal advection of $CO_2$ ($F_C^{HA}$) in urban areas is rarely addressed in studies. Results from a number of field experiments in forests (Aubinet et al. 2010) show that there is a large uncertainty in quantifying horizontal and vertical advection fluxes. Both terms are large, are coupled and seem not to cancel each other. To date, it is not known how relevant this is for the urban environment.

## References


Allen, L., Lindberg, F. & Grimmond, C. (2010). Global to city scale model for anthropogenic heat flux. *International Journal of Climatology*, 31, 19902005.

Arnfield, A. (2003). Two decades of urban climate research: a review of turbulence, exchanges of energy and water, and the urban heat island. *International Journal of Climatology*, 23, 126.

Aston, A. (1977). Water-resources and consumption in Hong Kong. *Urban Ecology*, 2, 327351.

Aubinet, M., Feigenwinter, C., Heinesch, B., Bernhofer, C., Canepa, E., Lindroth, A., Montagnani, L., Rebmann, C., Sedlak, P. & Van Gorsel, E. (2010). Direct advection measurements do not help to solve the night-time $CO_2$ closure problem: evidence from three different forests. *Agricultural and Forest Meteorology*, 150, 655664.

Aubinet, M., Vesala, T. & Papale, D., eds (2012). *Eddy Covariance – a Practical Guide to Measurement and Data Analysis*. Dordrecht, The Netherlands, Springer Atmospheric Sciences.

Berne, A., Delrieu, G., Creutin, J. & Obled, C. (2004). Temporal and spatial resolution of rainfall measurements required for urban hydrology, *Journal of Hydrology*, 299, 166179.

Berthier, E., Andrieu, H. & Creutin, J. (2004). The role of soil in the generation of urban runoff: development and evaluation of a 2D model. *Journal of Hydrology*, 299, 252266.

Berthier, E., Dupont, S., Mestayer, P. & Andrieu, H. (2006). Comparison of two evapotranspiration schemes on a sub-urban site, *Journal of Hydrology*, 328, 635646.

Branger, F., Kermadi, S., Jacqueminet, C., Michel, K., Labbas, M., Krause, P., Kralisch, S. & Braud, I. (2013). Assessment of the influence of land use data on the water balance components of a peri-urban catchment using a distributed modelling approach. *Journal of Hydrology*, 505, 312325.

Brutsaert, W. (1982). *Evaporation into the Atmosphere: Theory, History and Applications*. Dordrecht, The Netherlands, Springer.

Burian, S. J., McPherson, T., Brown, M., Streit, G. & Turin, H. (2002). Modeling the effects of air quality policy changes on water quality in urban areas. *Environmental Modeling & Assessment*, 7, 179190.

Camuffo, D. & Bernardi, A. (1982). An observational study of heat fluxes and their relationship with net radiation. *Boundary-Layer Meteorology*, 23, 359368.

Christen, A. (2005). Atmospheric turbulence and surface energy exchange in urban environments, PhD thesis, University of Basel, Stratus. ISBN 385977266.X.

Christen, A., Coops, N., Crawford, B., Kellett, R., Liss, K., Olchovski, I., Tooke, T., van der Laan, M. & Voogt, J. (2011). Validation of modeled carbon-dioxide emissions from an urban neighborhood with direct eddy-covariance measurements. *Atmospheric Environment*, 45, 60576069.

Christen, A. & Vogt, R. (2004). Energy and radiation balance of a central European city. *International Journal of Climatology*, 24, 13951421.

Chrysoulakis, N., Lopes, M., San Jos, R., Grimmond, C. S. B., Jones, M. B., Magliulo, V., Klostermann, J. E. M., Synnefa, A., Mitraka, Z., Castro, E., Gonzlez, A., Vogt, R., Vesala, T., Spano, D., Pigeon, G., Freer-Smith, P., Staszewski, T., Hodges, N., Mills, G. & Cartalis, C. (2013). Sustainable urban metabolism as a link between bio-physical sciences and urban planning: the BRIDGE project. *Landscape and Urban Planning*, 112, 100117.

Clark-Thorne, S. & Yapp, C. (2003). Stable carbon isotope constraints on mixing and mass balance of $CO_2$ in an urban atmosphere: Dallas metropolitan area, Texas, USA. *Applied Geochemistry*, 18, 7595.

Coutts, A., Beringer, J. & Tapper, N. (2007). Characteristics influencing the variability of urban $CO_2$ fluxes in Melbourne, Australia. *Atmospheric Environment*, 41, 5162.

Crawford, B., Grimmond, C. & Christen, A. (2011). Five years of carbon dioxide fluxes measurements in a highly vegetated suburban area. *Atmospheric Environment*, 45, 896905.

Denman, K., Brasseur, G., Chidthaisong, A., Ciais, P., Cox, P., Dickinson, R., Hauglustaine, D., Heinze, C., Holland, E., Jacob, D., Lohmann, U., Ramachandran, S., da Silva Dias, P., Wofsy, S. & Zhang, X. (2007). Couplings between changes in the climate system and biogeochemistry. In: *Climate Change 2007: The Physical Science Basis. Contribution of Working Group I to the Fourth Assessment Report of the Intergovernmental Panel on Climate Change*, Cambridge University Press, Cambridge, UK and New York, USA.

Ellefsen, R. (1990/91). Mapping and measuring buildings in the urban canopy boundary layer in ten US cities. *Energy and Buildings*, 1516, 10251049.

Feigenwinter, C., Vogt, R. & Christen, A. (2012). Eddy covariance measurements over urban areas. In M. Aubinet, T. Vesala & D. Papale, eds, *Eddy Covariance - A Practical Guide to Measurement and Data Analysis*. Dordrecht, The Netherlands, Springer Atmospheric Sciences, p. 430.

Foken, T., ed. (2008). *Micrometeorology*. Berlin, Germany, Springer-Verlag Berlin Heidelberg.

Goldbach, A. & Kuttler, W. (2013). Quantification of turbulent heat fluxes for adaptation strategies within urban planning. *International Journal of Climatology*, 33, 143159.

Grimmond, C. (1992). The suburban energy balance: methodological considerations and results for a mid-latitude west coast city under winter and spring conditions. *International Journal of Climatology*, 12, 481497.

Grimmond, C. (2006). Progress in measuring and observing the urban atmosphere. *Theoretical and Applied Climatology*, 84, 322.

Grimmond, C., King, T., Cropley, F., Nowak, D. & Souch, C. (2002). Local-scale fluxes of carbon dioxide in urban environments: methodological challenges and results from Chicago. *Environmental Pollution*, 116, 243254.

Grimmond, C. & Oke, T. (1986). Urban water-balance 2: Results from a suburb of Vancouver, British-Columbia. *Water Resources Research*, 22, 14041412.

Grimmond, C. & Oke, T. (1991). An evapotranspiration-interception model for urban areas, *Water Resources Research*, 27, 17391755.

Grimmond, C. & Oke, T. (1995). Comparison of heat fluxes from summertime observations in the suburbs of four North American cities. *Journal of Applied Meteorology*, 34, 873889.

Grimmond, C. & Oke, T. (1999). Aerodynamic properties of urban areas derived from analysis of surface form. *Journal of Applied Meteorology*, 38, 12621292.

Grimmond, C., Oke, T. & Steyn, D. (1986). Urban water-balance 1. A model for daily totals. *Water Resources Research*, 22, 13971403.

Hathway, E. & Sharples, S. (2012). The interaction of rivers and urban form in mitigating the urban heat island effect: a UK case study. *Building and Environment*, 58, 1422.

Helfter, C., Famulari, D., Philipps, G., Barlow, J., Wood, C., Grimmond, C. & Nemitz, E. (2011). Controls of carbon dioxide concentrations and fluxes above central London. *Atmospheric Chemistry and Physics*, 11, 19131928.

Hollis, G. E. & Ovenden, J. (1988). The quantity of stormwater runoff from 10 stretches of road, a car park and 8 roofs in Hertfordshire, England during 1983. *Hydrological Processes*, 2, 227243.

Iamarino, M., Beevers, S. & Grimmond, C. (2012). High-resolution (space, time) anthropogenic heat emissions: London 19702025. *International Journal of Climatology*, 32, 17541767.

Inkiläinen, E., McHale, M., Blank, G., James, A. & Nikinmaa, E. (2013). The role of the residential forest in regulating throughfall: a case study in Raleigh, North Carolina, USA. *Landscape and Urban Planning*, 119, 91103.

Järvi, L., Grimmond, C., Taka, M., Setälä, H., Nordbo, A. & Strachan, I. (2014, in review). Development of the Surface Urban Energy and Water balance Scheme (SUEWS) for cold climate cities. *Geoscientific Model Development*, MS No.: gmd-2013163

Järvi, L., Mammarella, I., Eugster, W., Ibrom, A., Siivola, E., Dellwik, E., Keronen, P., Burba, G. & Vesala, T. (2009). Comparison of net $CO_2$ fluxes measured with open- and closed-path infrared gas analyzers in an urban complex environment. *Boreal Environment Research*, 14, 499514.

Järvi, L., Nordbo, A., Junninen, H., Riikonen, A., Moilanen, J., Nikinmaa, E. & Vesala, T. (2012). Seasonal and annual variation of carbon dioxide surface fluxes in Helsinki, Finland, in 2006 2010. *Atmospheric Chemistry and Physics Discussions*, 12, 83558396.

Jia, Y., Ni, G., Kawahara, Y. & Suetsugi, T. (2001). Development of WEP model and its application to an urban watershed. *Hydrological Processes*, 15, 21752194.

Kordowski, K. & Kuttler, W. (2010). Carbon dioxide fluxes over an urban park area. *Atmospheric Environment*, 44, 27222730.

Kotthaus, S. & Grimmond, C. (2012). Identification of micro-scale anthropogenic $CO_2$, heat and moisture sources - processing eddy covariance fluxes for a dense urban environment. *Atmospheric Environment*, 57, 301316.

Kotthaus, S. & Grimmond, C. S. B. (2013a). Energy exchange in a dense urban environment Part I: Temporal variability of long-term observations in central London. *Urban Climate* In Press, Corrected Proof, doi:10.1016/j.uclim.2013.10.002.

Kotthaus, S. & Grimmond, C. S. B. (2013b). Energy exchange in a dense urban environment Part II: Impact of spatial heterogeneity of the surface. *Urban Climate* In Press, Corrected Proof, doi: 10.1016/j.uclim.2013.10.001.

Lemonsu, A. & Masson, V. (2002). Simulation of a summer urban breeze over Paris. *Boundary Layer Meteorology*, 104, 463490.

Lemonsu, A., Masson, V. & Berthier, E. (2007). Improvement of the hydrological component of an urban soilvegetation- atmosphere-transfer model. *Hydrological Processes*, 21, 21002111.

Lietzke, B. & Vogt, R. (2013). Variability of $CO_2$ concentrations and fluxes in and above an urban street canyon. *Atmospheric Environment*, 74, 6072.

Lietzke, B., Vogt, R., Feigenwinter, C. & Parlow, E. (2014, in review). On the variability of carbon-dioxide flux and its controlling factors in a heterogeneous urban environment. *International Journal of Climatology.*

Lindberg, F., Grimmond, C., Yogeswaran, N., Kotthaus, S. & Allen, L. (2013). Impact of city changes and weather on anthropogenic heat flux in Europe 19952015. *Urban Climate*, 4, 115.

Loridan, T. & Grimmond, C. S. B. (2012). Characterization of energy flux partitioning in urban environments: links with surface seasonal properties. *Journal of Applied Meteorology and Climatology*, 51, 219241.

Loridan, T., Grimmond, C. S. B., Offerle, B. D., Young, D. T., Smith, T. E. L., Jarvi, L. & Lindberg, F. (2011). Local-scale urban meteorological parameterization scheme (lumps): longwave radiation parameterization and seasonality related developments. Journal of *Applied Meteorology and Climatology*, 50, 185202.

Loridan, T., Lindberg, F., Jorba, O., Kotthaus, S., Grossman-Clarke, S. & Grimmond, C. S. B. (2013). High resolution simulation of the variability of surface energy balance fluxes across central London with urban zones for energy partitioning. *Boundary-Layer Meteorology*, 147, 493523.

Mitchell, V., Mein, R. & McMahon, T. (2001). Modelling the urban water cycle. *Environmental Modelling & Software*,16, 615629.

Moriwaki, R. & Kanda, M. (2004). Seasonal and diurnal fluxes of radiation, heat, water vapor, and carbon dioxide over a suburban area. *Journal of Applied Meteorology*, 43, 17001710.

Moriwaki, R., Kanda, M., Senoo, H., Hagishima, A. & Kinouchi, T. (2008). Anthropogenic water vapor emissions in Tokyo. *Water Resource Research*, 44, W11424

Morris, B., Rueedi, J., Cronin, A., Diaper, C. & DeSilva, D. (2007). Using linked process models to improve urban groundwater management: an example from Doncaster England. *Water and Environment Journal*, 21, 229240.

Nouri, H., Beecham, S., Kazemi, F. & Hassanli, A. M. (2012). A review of ET measurement techniques for estimating the water requirements of urban landscape vegetation. *Urban Water Journal*, 10, 247259.

Offerle, B., Grimmond, C. S. B. & Fortuniak, K. (2005). Heat storage and anthropogenic heat flux in relation to the energy balance of a Central European city centre. *International Journal of Climatology*, 25, 14051419.

Oke, T. (1979). Advectively-assisted evapotranspiration from irrigated urban vegetation. *Boundary-Layer Meteorology*, 17, 167173.

Oke, T. (2006). Towards better scientific communication in urban climate. *Theoretical and Applied Climatology*, 84, 179190.

Oke, T., Kalanda, B. & Steyn, D. (1981). Parameterization of heat storage in urban areas. *Urban Ecology*, 5, 4554.

Oke, T. R. (1987). *Boundary Layer Climates*. Routledge, London.

Pataki, D., Bowling, D. & Ehleringer, J. (2003). Seasonal cycle of carbon dioxide and its isotopic composition in an urban atmosphere: anthropogenic and biogenic effects. *Journal of Geophysical Research*, 108(D23), 47354742.

Pigeon, G., Legain, D., Durand, P. & Masson, V. (2007a). Anthropogenic heat release in an old European agglomeration (Toulouse, France). *International Journal of Climatology*, 27, 19691981.

Pigeon, G., Lemonsu, A., Grimmond, C., Durand, P., Thouron, O. & Masson, V. (2007b). Divergence of turbulent fluxes in the surface layer: case of a coastal city. *Boundary-Layer Meteorology*, 124, 269290.

Piringer, M., Grimmond, C., Joffre, S., Mestayer, P., Middleton, D., Rotach, M., Baklanov, A., De Ridder, K., Ferreira, J., Guilloteau, E., Karppinen, A., Martilli, A., Masson, V. & Tombrou, M. (2002). Investigating the surface energy balance in urban areas  recent advances and future needs. *Water, Air and Soil Pollution*: Focus, 2, 116.

Ragab, R., Bromley, J., Rosier, P., Cooper, J. & Gash, J. (2003a). Experimental study of water fluxes in a residential area: 1. rainfall, roof runoff and evaporation: the effect of slope and aspect. *Hydrological Processes*, 17, 24092422.

Ragab, R., Rosier, P., Dixon, A., Bromley, J. & Cooper, J. (2003b). Experimental study of water fluxes in a residential area: 2. road infiltration, runoff and evaporation. *Hydrological Processes*, 17, 24232437.

Ramamurthy, P. & Pardyjak, E. (2011). Toward understanding the behavior of carbon dioxide and surface energy fluxes in the urbanized semi-arid Salt Lake Valley, Utah, USA. *Atmospheric Environment*, 45, 7384.

Raupach, M., Antonia, R. & Rajagopalan, S. (1991). Roughwall turbulent boundary layers. *Applied Mechanics Reviews*, 44, 125.

Roberts, S., Oke, T., Grimmond, C. & Voogt, J. (2006). Comparison of four methods to estimate urban heat storage. *Journal of Applied Meteorology*, 45, 17661781.

Rotach, M. (2001). Simulation of urban-scale dispersion using a Lagrangian stochastic dispersion model. *Boundary-Layer Meteorology*, 99, 379410.

Rotach, M., Vogt, R., Bernhofer, C., Batchvarova, E., Christen, A., Clappier, A., Feddersen, B., Gryning, S.-E., Martucci, G., Mayer, H., Mitev, V., Oke, T., Parlow, E., Richner, H., Roth, M., Roulet, Y., Ruffieux, D., Salmond, J., Schatzmann, M. & Voogt, J. (2005). BUBBLE - an urban boundary layer meteorology project. *Theoretical and Applied Climatology*, 81, 149156.

Roth, M. & Oke, T. (1994). Comparison of modelled and measured heat storage in suburban terrain. *Beitraege zur Physik der Atmosphaere*, 67, 149156.

Roth, M. & Oke, T. (1995). Relative efficiencies of turbulent transfer of heat, mass and momentum over a patchy urban surface. *Journal of Atmospheric Sciences*, 52, 18641874.

Sailor, D. (2010). A review of methods for estimating anthropogenic heat and moisture emissions in the urban environment. *International Journal of Climatology*, 31, 189199.

Semadeni-Davies, A. F. & Bengtsson, L. (1999). The water balance of a sub-Arctic town. *Hydrological Processes*, 13, 18711885.

Spronken-Smith, R. A., Oke, T. & Lowry, W. (2000). Advection and the surface energy balance across an irrigated urban park. *International Journal of Climatology*, 20, 10331047.

Spronken-Smith, R., Kossmann, M. & Zawar-Reza, P. (2006). Where does all the energy go? Surface energy partitioning in suburban Christchurch under stable wintertime conditions. *Theoretical and Applied Climatology*, 84, 137149.

Steeneveld, G. J., Koopmans, S., Heusinkveld, B. G. & Theeuwes, N. E. (2014). Refreshing the role of open water surfaces on mitigating the maximum urban heat island effect. *Landscape and Urban Planning*, 121, 9296.

Stephenson, D. (1994). Comparison of the water-balance for an undeveloped and a suburban catchment. *Hydrological Sciences Journal*, 39, 295307.

Stewart, I. D. & Oke, T. R. (2012). Local climate zones for urban temperature studies. *Bulletin of the American Meteorological Society*, 93, 18791900.

Trusilova, K. & Churkina, G. (2008). The response of the terrestrial biosphere to urbanization: land cover conversion, climate, and urban pollution. *Biogeosciences*, 5, 15051515.

Vieux, B. & Bedient, P. (2004). Assessing urban hydrologic prediction accuracy through event reconstruction. *Journal of Hydrology*, 299, 217236.

Vogt, R., Christen, A., Rotach, M. W., Roth, M. & Satyanarayana, A. N. V. (2006). Temporal dynamics of $CO_2$ fluxes and profiles over a Central European city. *Theoretical and Applied Climatology*, 84, 117126.

Wang, J., Endreny, A. & Nowak, D. J. (2008). Mechanistic simulation of tree effects in an urban water balance model. *Journal of the American Water Resources Association*, 44, 7585.

Ward, H., Evans, J. & Grimmond, C. (2013). Multi-season eddy covariance observations of energy, water and carbon fluxes over a suburban area in Swindon, UK. *Atmospheric Chemistry and Physics*, 13, 46454666.

Xiao, Q., McPherson, E., Simpson, J. & Ustin, S. (2007). Hydrologic processes at the urban residential scale. *Hydrological Processes*, 21, 21742188.

# 3 Observational sites and measurements

This chapter is meant to give a brief overview. Detailed site descriptions can be found for Basel Klingelbergstrasse (BKLI) in Section P2-2.2 and for Basel Aeschenplatz (BAES) in Section P3-2.1.

Basel, Switzerland, is a central European city with 173'000 inhabitants, situated at the border to Germany in the Northeast and France in the West. The administrative unit of the City of Basel covers an area of 23.9 $km^2$ and has an average population density of 7140 inh./$km^2$. Basel represents also one of the 26 cantons of Switzerland with an area of about 1.5 times (195'000 inhabitants) the size of the city (data source: Statistisches Amt Basel-Stadt). Statistical data maintained by the city authorities is often related to the canton area (e.g. in Section P3-2.1).

The river Rhine embossed the topography around Basel, coming through a valley from the east between the Jura mountains in the south and the Black Forest in the north and bending northwards where the city is. It leaves towards the broad Upper Rhine rift valley between the Black Forest to the east and the Vosges mountains to the West. This orographic structure has a decent effect on the typical wind field over Basel as described in Section P2-3.1.

The measurement sites (Fig. 3.1) are located close to the center of the city but on opposite sides of it and about 1.6 km apart from each other. At both sites, the presence of major roads is a late consequence of the fact that in medieval times the city wall was built at these places. It was teared down in the 19th century, offering new space for increasing traffic needs and leading to the development of the outer districts of the city. This development had more space than within the borders of the former city wall and lead to the comparatively less densely built residential areas faced nowadays.

Measurements at BAES started in June 2009 and are located on top of a tower-like building at 41 m above street level. The building is situated right at the eastern border of the Aeschenplatz, a place with six arterial roads, solely intended for managing the interlacing pathways of private and public transport. At BKLI fluxes are sampled at the top of the long term flux tower (tower A, 39 m above street level, 18 m above the roof top). In the center of the street canyon adjacent to the east (BKLIC), a 19 m tower (tower B, 10/2009 – 03/2011) was sampling $CO_2$ flux at the top of the canyon and a five-level in-canyon concentration profile of $CO_2$. Four additional samples were taken at the building wall allowing for cross-section analyses in the canyon. One sample was taken at the top of tower A. The street canyon has a non-ideal cross section (Fig. 3.2). The height to width ratio is 0.7 for the building to the west and 0.34 for the building to the east.

Average building heights and surface cover data around the sites are very similar and given in Table 3.1. Section P3 shows that these features vary considerably for sectoral segments of the surroundings and that a more detailed image of the spatial surface cover distribution is of advantage when looking for the controlling factors of $F_C$. $CO_2$ concentration and flux were measured at all locations with high-frequency open-path $CO_2/H_2O$ gas

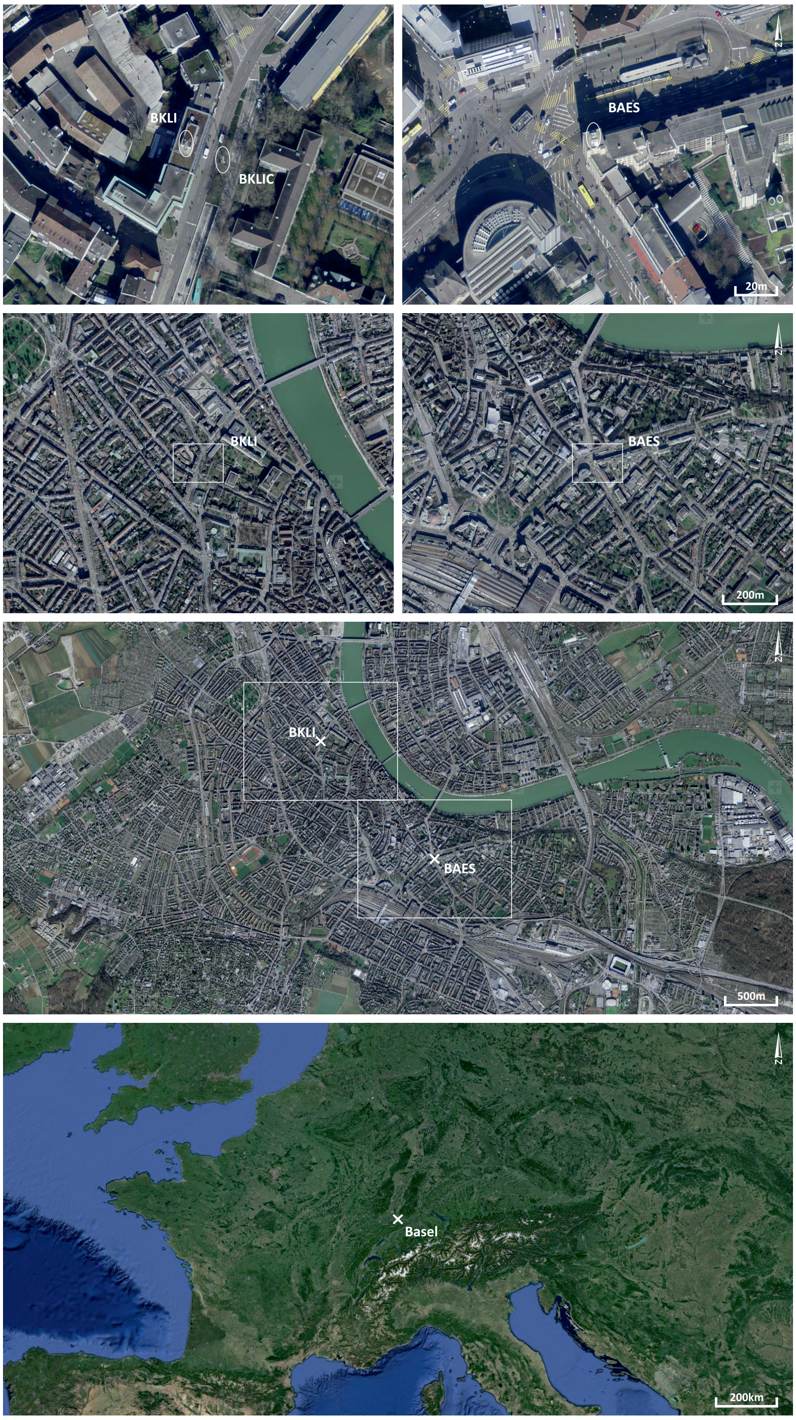


Figure 3.1: Aerial and satellite images showing (from the bottom): the location of Basel in Europe; the urban region with the location of the sites on the city scale; the neighborhood of the sites, representing the local scale; and the location of the towers on the block level, approaching the micro scale. Image sources: http://map.geo.admin.ch (top five) and http://maps.google.com (bottom).

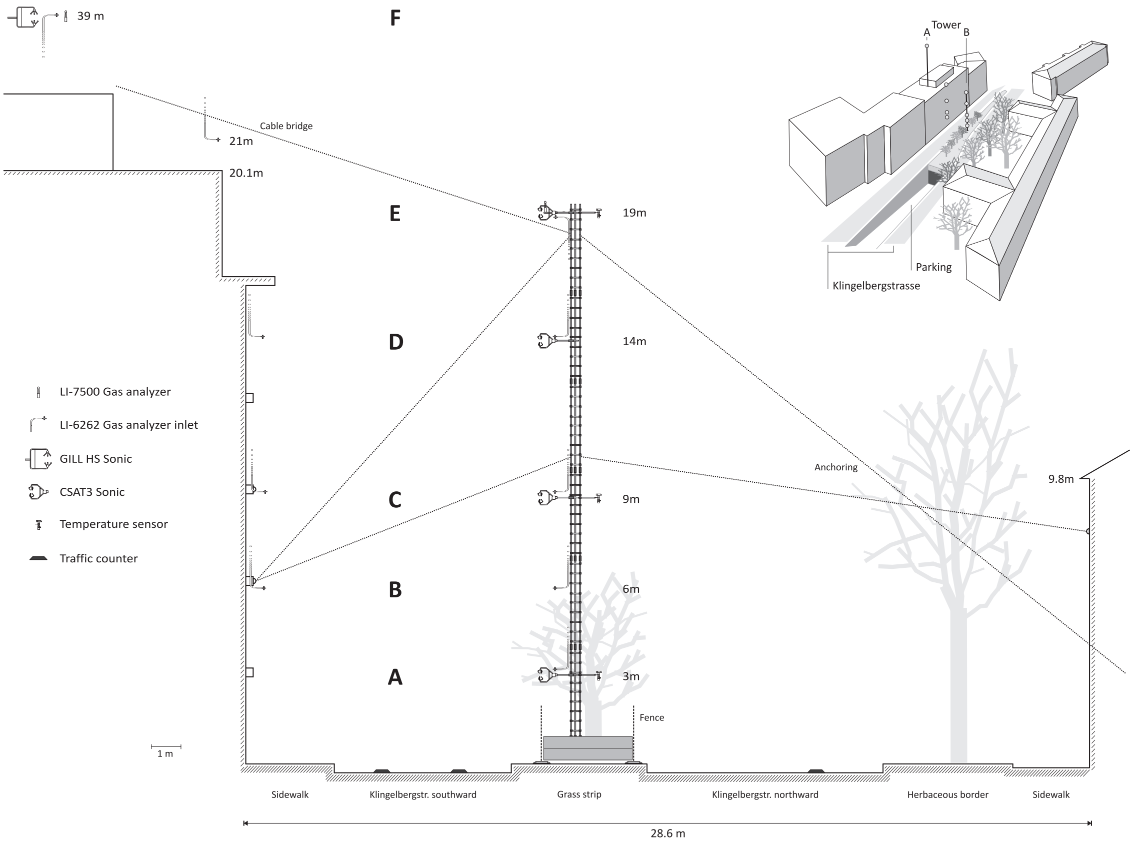


Figure 3.2: West (left) to East (right) cross section of the street canyon at Basel Klingelbergstrasse with a schematic view of the instrumented tower (including a 3D-view inlet where all measurement points are also marked). Canyon, buildings and measurement heights in the canyon (levels A–E) are to scale. In the cross section the rooftop tower is not depicted and level F not to scale.

analyzers (Table 3.1) in combination with ultrasonic-anemometers. At BKLIC a closed-path $CO_2/H_2O$ gas analyzer was sampling air probes from the 10 inlets in and above the canyon.

Data processing at all sites consisted of despiking and 30 min Reynolds block averaging. Streamline rotation and detrending was applied at BAES, but omitted at BKLI/BKLIC to keep data in the same coordinate system and to retain a common frame of reference for all levels. As stated in Section P2-2.3, this implies a non-zero average vertical wind component $\overline{w}$ if the sonic is not aligned perpendicular to the average wind vector, and thus adds uncertainties to the flux density interpretations and introduces an advective term. Sensible heat flux was corrected after Schotanus et al. (1983) and $F_C$ after Webb et al. (1980) (WPL-correction). Only at BAES a stationarity filter (Foken and Wichura, 1996) followed by a gapfilling procedure based on a set of median diurnal cycles was applied. Filtering for non-stationary cases was not applied at BKLIC because it would have had reduced data availability to one-third only. Most of the analyses there were focusing on the qualitative aspects of the flux characteristics and not on exact quantitative determination.

Table 3.1: Instrumentation, results and characteristic features of the sites and the urban structure around them (for more information, see Section P2 and Section P3). Average building height ($z_h$) and surface cover fractions for vegetation ($\lambda_v$), buildings ($\lambda_b$) and impervious ground ($\lambda_g$) are given at BKLI for a radius of $r$=400 m, at BAES for $r$=500 m. $z$ is the measurement height, $\upsilon$ is the average daily traffic density and LCZ the local climate zone classification (Stewart and Oke, 2012).

| Site | BAES | BKLI | BKLIC |
|---|---|---|---|
| Coordinates [WGS 84 long/lat] | 7.5956 / 47.5512 | 7.5805 / 47.5617 | 7.5807 / 47.5616 |
| Elevation at street level [m a.s.l.] | 270.6 | 264 | 264 |
| Sampling period | 06/2009–* | 03/2004–* | 10/2009–03/2011 |
| Data period in publications | 06/2009–05/2013 | 01/2010–12/2010 | 01/2010–12/2010 |
| *Instruments:* | | | |
| Sonic-Anemometer | CSAT3 | Gill HS | CSAT3 |
| $CO_2$ / $H_2O$ gas analyzer | LI-7500 | LI-7500 | LI-7500, LI-6262 |
| $z$ [m] | 41 | 39 | 3–19 (39) |
| $z_h$ [m] | 16 | 17 | |
| $z/z_h$ | 2.5 | 2.3 | |
| LCZ | compact midrise & open midrise to lowrise | compact to open midrise | |
| $\lambda_v$ [%] | 27 | 24 | |
| $\lambda_b$ [%] | 35 | 38 | |
| $\lambda_g$ [%] | 38 | 38 | |
| $\upsilon$ [veh d$^{-1}$] | 30500 | 15000 | |
| $F_C$ data availability [%] | 56 (100 gap-filled) | 66 | 75 |
| Average $F_C$ [$\mu$mol m$^{-2}$s$^{-1}$] | 16.35 | 11.15 | 21.58 |

Traffic density ($\upsilon$) was monitored over two weeks at BKLIC and then up-scaled as described in Section P2-2.4 using continuous data from a nearby counter of the city authorities. The same data was adapted via a factor from a traffic model to BAES (Section P3-2.1.5).

## 3.1 Instrumental issues measuring $CO_2$

Comparisons of absolute $CO_2$ concentration values from different instruments generally have to be considered with care as they are prone to device-related uncertainties. The exact determination of the mole fraction of $CO_2$ in air via the absorption of an infrared signal is not straightforward. The absorption rate shows cross sensitivities to other gases as e.g. water vapor and small deviations in the high frequency range accumulate on longer time scales. Each individual instrument has other characteristic sensitivities which may also change with time, depending e.g. on material components and the ability of the internal chemicals to clean the air in the internal reference cell from $CO_2$ and $H_2O$.

A calibration of the individual instruments with zero and span gases and the replacement of the internal chemicals helps to adjust the devices to each other but does not affect deviations between different types of instruments. Results from a parallel calibra-


Figure 3.3: Photographs of the measurement sites: (a) Basel Klingelbergstrasse, showing the street canyon tower and the rooftop tower; Basel Aeschenplatz showing (b) the EC system and the view over the city approximately to the north and (c) the view across the Aeschenplatz toward the Turmhaus building with the instrumented flagpole on top.

tion procedure of all three LI-7500 gas analyzers in August 2009 show that the correlation between the instruments was enhanced afterward (Koller, 2010), but a in-situ comparison was not conducted. The scattering and the regression in Fig. 3.4c are thus affected by the different measurement heights.

Average concentration data delivered by the LI-7500 open-path analyzers and the LI-6262 closed-path analyzer used in this study were of considerably different size which disallows a direct comparison in most cases. 30 min average mole fractions of the two instrument types, measured at 19 m and 39 m at BKLI, show large scattering but are basically related through simple linear correlations as depicted in Fig. 3.4a & b. For the LI-6262 data points are up-scaled averages of $6 \times 23$ s and the signal is damped by the long tubes (Section P1). This leads to outliers in the open-path data, not adequately captured by the LI-6262. Differences of a similar range were also found in 30 min averages of high frequency data sampled with the similar but newer closed-path model LI-7000 (Diethelm, 2011)).

The steep slope and low intercept in Fig. 3.4b suggest for the LI-6262 a different response on absolute concentration values at 39 m than at 19 m. Data points lie closer to

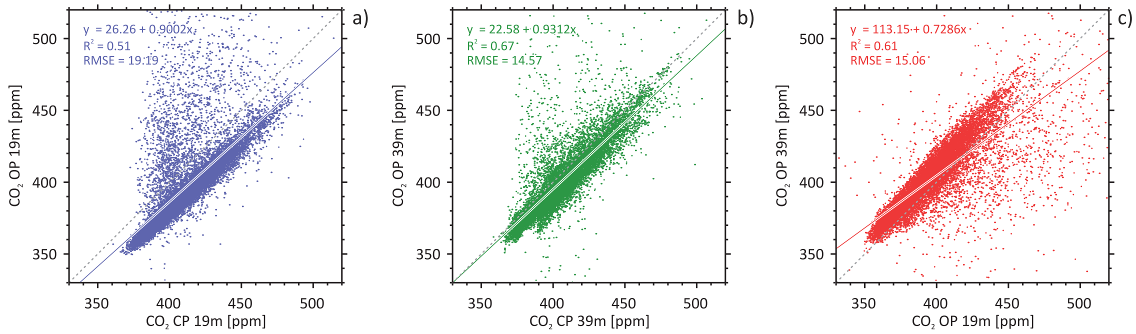


Figure 3.4: Comparison of $CO_2$ concentrations measured by the closed-path (CP) and open-path (OP) gas analyzers at BKLI/BKLIC. Points represent half-hourly averages for the year 2010.

the equal line at 19 m while deviations at 39 m become greater the lower the concentration is (typically daytime values in Summer). The open-path comparison (Fig. 3.4c) shows that vertical differences are highest in these cases, so it must be assumed that the LI-6262 experienced a lag effect when switching through the sampling tubes. A longer discarding time or sampling interval (Section P1) would probably have been necessary for such abrupt concentration changes to entirely flush the sampling cell of the instrument.

Only concentration values sampled by the LI-6262 were considered for spatial and temporal analyses in the street canyon experiment (Section P2) whereas site-comparisons between BKLI and BAES rely usually on $CO_2$ concentrations sampled by the LI-7500.

As flux calculations rely on small-size high frequency fluctuations around a temporal mean measured under stationary conditions, they are not affected by the size of the temporal mean itself and comparisons between different instruments of the same type are justifiable.

# 4 Discussion of Results

The key results from the two research papers are briefly discussed in this section and complemented by additional findings. The first paper (Section P2) on the variability of $CO_2$ fluxes and concentrations in and above the street canyon presents results from the site Basel Klingelbergstrasse and focuses on micro to local scale processes. In the second paper (Section P3) the controlling factors for the variability at the site Basel Aeschenplatz are investigated. By recapitulating, combining and complementing the key findings from the two measurements, the scope is extended beyond the local scale and the variability of $F_C$ and $CO_2$ concentrations within the city and on time scales longer than a year is addressed.

## 4.1 The controlling factors and their time scales

### 4.1.1 Summary of key results

The cyclical variations of $F_C$ can be clearly attributed to source characteristics on the respective time scales. Controlling factor for the diurnal course is at both sites traffic density, i.e. the related emissions, with distinct differences between working days and weekends/holidays (Fig. P2-8). The annual course of monthly average $F_C$ is dependent on heating emissions in Winter and their absence in Summer (Fig. 4.1). Sink effects through vegetation are expected to be low and usually of no significant relevance compared to the strong sources. In Summer months a reducing influence on $F_C$ exists that becomes visible in situations or for sectors where emissions are on a lower level, e.g. during weekends and west wind situations at BKLI (Fig. P2-8c1). Systematical patterns and occasional variability are added to $F_C$ through the distinct dependency on the prevailing wind direction and the dynamics and spatial distribution of strong sources in the respective footprint of the flux. Data from BAES suggests that local $F_C$ is to 70% determined by traffic emissions and to 30% by heating related emissions and that these fractions are varying with sectoral emission characteristics. Similar partitioning was found by Christen et al. (2011) and Koerner and Klopatek (2002), lower traffic shares of around 40% − 50% by Dahlkötter et al. (2010), Helfter et al. (2011), Nemitz et al. (2002) and Soegaard and Möller-Jensen (2003). Inventory data for the city of Basel suggests a ratio of household combustion to traffic emissions of 55/45%. This shows that observed $F_C$ is extremely influenced by local traffic emissions and is neither comparable to the city-wide emission inventory nor representative for the city scale.

### 4.1.2 Diurnal cycle of traffic emissions

Traffic density in Basel follows typical diurnal cycles as shown in Fig. P2-8. The morning rush hour is distinct and occurs at the same time and with the same intensity each morning on working days. On weekends and public holidays, traffic is reduced and rush hours are

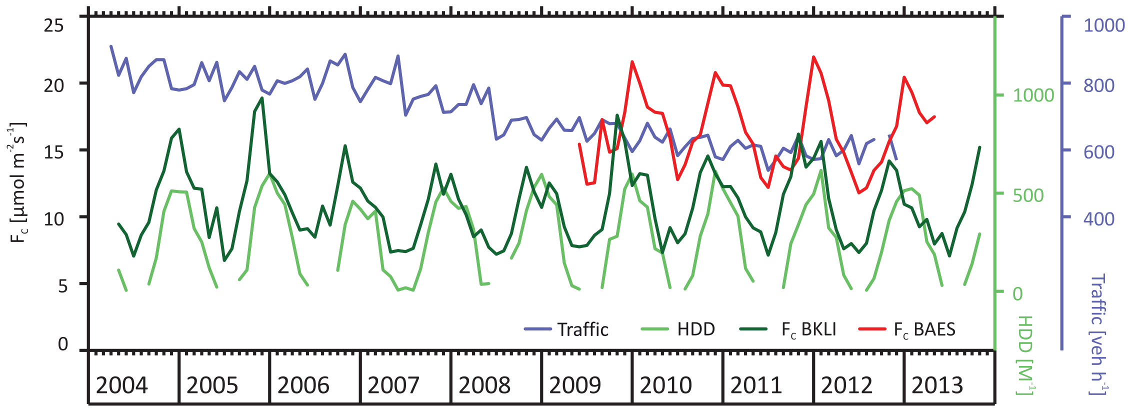


Figure 4.1: Long term courses of $F_C$, traffic density and HDD at BKLI and $F_C$ at BAES. $F_C$ and traffic density are shown as monthly averages, HDD (an indicator for heating activity) as monthly total.

absent but nighttime density is higher. A typical seasonal variability does not exist but a holiday related reduction in Summer is observed (Fig. 4.1). Long term data shows a declining trend in average traffic density from 2004 to 2011 at BKLI. The drop in 2008 can be attributed to the opening of the 'Nordtangente', a highway bypass that attracted traffic from the Klingelbergstrasse. Traffic density on the Aeschenplatz at BAES is two times higher than on the Klingelbergstrasse (Section P3-3.5.2) but is likely having similar temporal characteristics. If weekly or longer averages are regarded, traffic density does not considerably vary and is a constant contributor to $F_C$.

For situations where the almost directly underlying traffic sources (Klingelbergstrasse at BKLI, Aeschenplatz at BAES) are upwind of the measurements, their explicit influence on $F_C$ is obvious at both observational sites. The contributions of these spatially confined but very strong sources reduces the influence of the rest of the source area to an insignificant share. From the presented data it can be derived, that urban $CO_2$ fluxes at a height of approximately $2z_h$ are extremely sensitive to the location of the tower in relation to strong nearby sources.

As in many other European countries, Central European Summer Time (CEST) applies in Switzerland between the last Sunday in March and the last Sunday in October (Hereafter, Summer Time (ST) is the period when CEST is active and Winter Time (WT) is the period when it is not). Clocks are set one hour plus (CET+1) during this period and in many aspects of everyday life, human behavior experiences a one hour shift as well. So does the morning rush hour of traffic, which occurs exactly one hour later. The fact that this difference can be clearly seen in the $F_C$ signal in all three observations of $F_C$ is a distinct sign that traffic density is the dominant controlling factor for the diurnal course.

### 4.1.3 Seasonal cycle of heating emissions

To extract useful information on the influence of heating emissions on $F_C$ from inventory data, such data has to be available in a certain temporal (e.g. daily, weekly or monthly) and spatial resolution (e.g. building or block level). Unfortunately, this is not the case for Basel at the desired scales, thus an indicator for heating activity and the related emissions becomes necessary to identify the share of heating emissions on $F_C$. For this purpose, the unit 'heating degree days' (HDD) is introduced in Section P3. As a function of air temperature, HDD follow a typical seasonal cycle (Fig. 4.1). On a daily basis, the relation to $F_C$ is not that distinct, as Fig. 4.2 shows. Included in the variability are lag effects due to the non linear dependence of heating on air temperature on short time scales and the day-to-day variance of traffic and wind direction that affect $F_C$. The difference between the regressions for working days and weekends in Fig. 4.2 is related to the respective difference in traffic activity. On longer time scales, e.g. months, HDD are a better reference for $F_C$ (Fig. P3-9a) and the splitting into traffic (represented through the y-axis intercept) and heating induced parts becomes more reliable. On the other hand, the y-axis intercept of the regression through all daily values is very similar to the intercept of the monthly averages, suggesting that the average image of a set of daily values may also be taken as an indicator, e.g. for separating weekend and working day contributions as in Table P3-4.

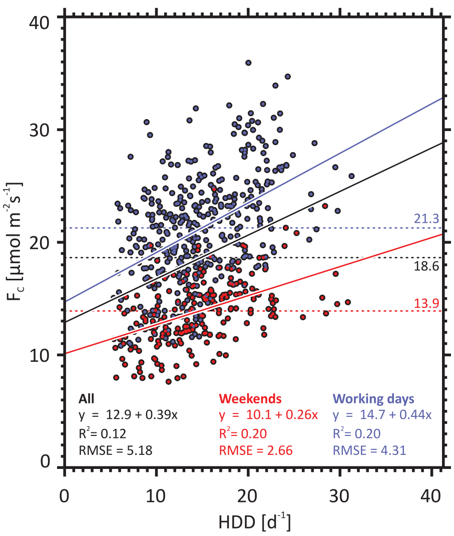


Figure 4.2: Daily averages of $F_C$ as a function of HDD per day, separated by working days and weekends. Straight lines are the regression lines and dotted horizontal lines the respective average $F_C$.

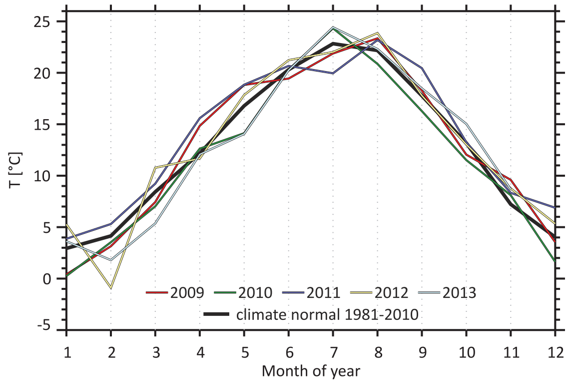


Figure 4.3: Yearly course of average monthly air temperatures at BAES. The climate normal temperature is plotted as a reference.

Heating emissions increase with colder temperatures. Their seasonal course is thus affected by periods when air temperature deviates from its typical average values, in either direction. Fig. 4.3 shows the course of the average monthly air temperature at Basel for the years 2009-2013. The climate normal temperature represents the average course for

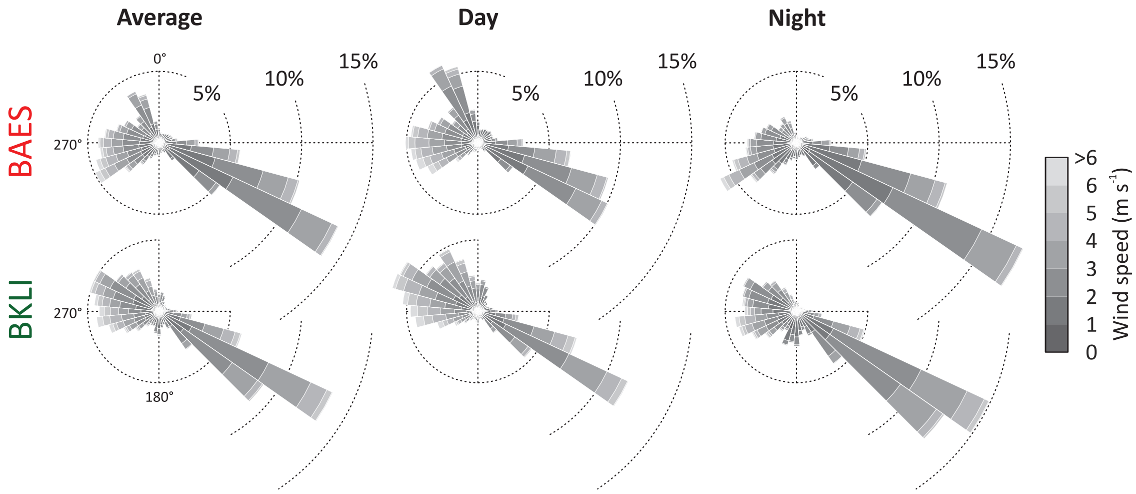


Figure 4.4: Wind direction frequencies and velocities at BAES and BKLI for the period 06/2009–06/2013. (a) all cases, (b) day- and (c) nighttime. Data is binned into 36 10°-classes.

the years 1981-2010, measured at the MeteoSchweiz station Basel-Binningen at the city border. It was scaled to BAES via linear regression coefficients to account for the slightly higher average temperatures in the urban center. The deviations from the climate normal temperature are greatest in Winter. February 2012 and January 2010 were comparatively cold months in the measurement period which lead to higher heating emissions, reflected by increased average monthly $F_C$. This and further temperature related peculiarities of $F_C$ are discussed in Section P3-3.5.3.

### 4.1.4 Wind direction cycles and their variability

As described in Section P2-3.1, two typical wind direction sectors are observed for Basel, a narrow south-east sector and a broader western sector. Distribution, frequency and velocity of half-hourly wind data at BAES and BKLI is shown in Fig. 4.4. The general pattern is valid at both sites, an exception is the separate and comparatively frequent daytime north-west sector that is only seen at BAES and probably a result of locally induced flow deviations by the urban structure. Winds from the broader western sector are on average stronger, with their highest frequencies slightly shifted toward 240°at BAES and toward 290°at BKLI.

A typical diurnal cycle can be observed, with east winds dominating at night and west winds at daytime (Fig. 4.5). In Spring and Summer afternoon, west wind covers up to 75% of all cases. Winter shows a lower amplitude and less frequent east winds at night, but a higher monthly variability (Fig. P3-8). On summer days with a clear diurnal pattern, the change from east to west in the morning can happen within an hour or less. Opposed, Winter days may be dominated by constant east wind situations. A better impression of the variability of the wind directions on the diurnal and seasonal scale is given by Fig. P3-8 where the average diurnal courses for each month are depicted and inter-annual

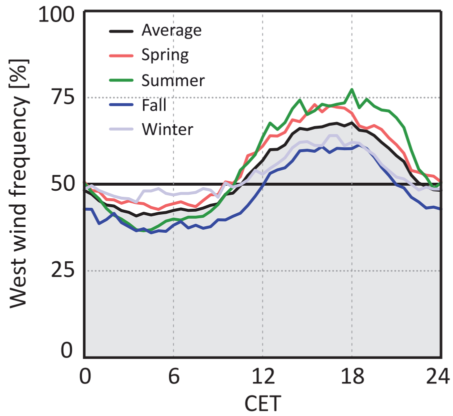


Figure 4.5: Relative frequency of west wind (180–360°) depicted as diurnal course for the different seasons at BKLI. The area below a line represents west wind cases, the area above east wind cases. The average course is shaded in gray. Data period is 06/2009-06/2013.

variations for single months can be seen.

Wind direction patterns are important for the understanding of measured $F_C$ at urban sites in heterogeneous surroundings, where emissions are not equally distributed in space and time. They interact on the diurnal scale with the course and spatial distribution of traffic and on the seasonal scale with heating emissions. Typical and constant wind patterns on either scale result in typical courses of $F_C$, while deviations can lead to peculiarities.

## 4.2 Spatial dependencies – local and city scale variability

A good impression of the variability of $F_C$ on the city scale is given by Fig. 4.6, where for all three $F_C$ measurements the average monthly diurnal courses are compared. The traffic influence can be seen in each month and for all observations. At BKLIC, the diurnal course is often unsteady but gives the clearest representation of traffic density throughout the year, due to the sampling location in the street canyon. The traffic pattern is also distinct at BAES and during the morning increase at BKLI. At the latter, the afternoon reduction through the shift to source areas to the west leads to substantially lower $F_C$ in the Summer months (Section P2-3.4). At BAES, west winds result correspondingly in higher fluxes whereas the slower morning increase is related to source areas to the east. Nighttime values are in Summer similar at all three sites. In Winter, nighttime differences reflect the contribution of heating emissions: $F_C$ is highest at BAES and often lowest at the top of the street canyon where heating contributions to $F_C$ are expected to be negligible.

The cases where $F_C$ is of similar size at BAES and BKLI (e.g. the morning increase in Summer, the courses in October and November) indicate, that, without the typical diurnal wind direction change, both sites might deliver comparable fluxes. In these months, daytime east winds get more dominant and average monthly $F_C$ at BKLI occasionally

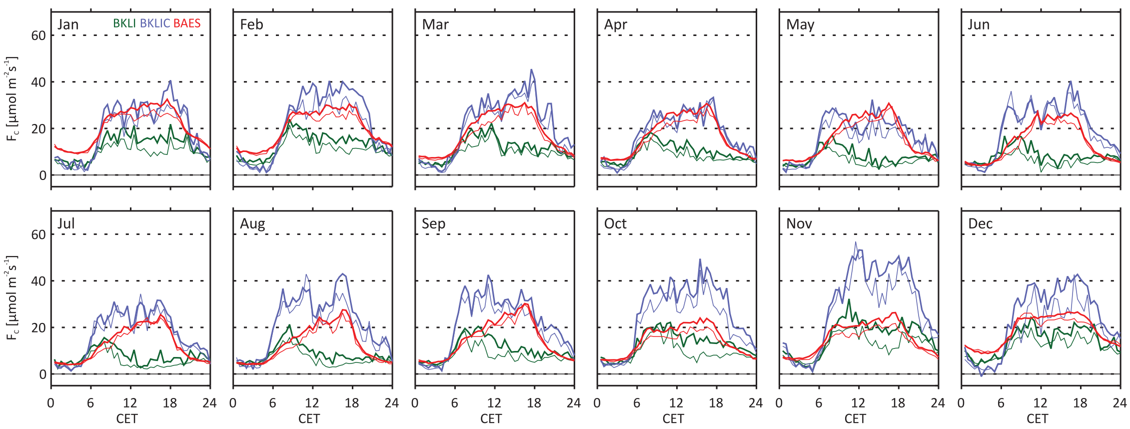


Figure 4.6: Monthly average diurnal courses of $F_C$ at the three measurements. Data period is for BAES and BKLI four years (06/2009-05/2013) and for BKLC one year (2010). Thick lines represent the mean, thin lines the median.

outreaches its usually higher opponent (Fig. 4.1). The major differences between the diurnal courses at BKLI and BAES are explainable with the fact that close-by traffic is for both the strongest contributor but located in opposite directions at the sites: to the east at BKLI and to the west at BAES. During a typical Summer day, west wind and high traffic co-occur, leading to high $F_C$ at BAES. At the same time at BKLI, traffic emissions are vented away from the site. Later on after sunset, when wind blows from the east, BKLI captures the emissions that originate from the Klingelbergstrasse, but they are on a low level. Figure 4.7 illustrates the dependencies. Together with the two times higher traffic density at the Aeschenplatz, this interdependency accounts for a great part of the about 1.5 times higher average $F_C$ at BAES.

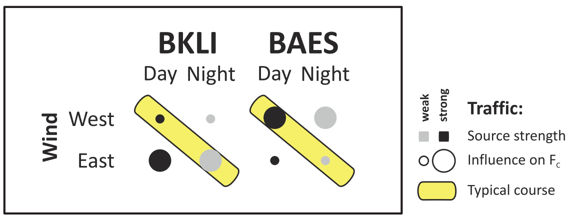


Figure 4.7: Illustrated dependence of $F_C$ on the diurnal differences of wind directions and traffic at BAES and BKLI. The size of the circles represents the strength of the dependence of $F_C$ on traffic, the color the source strength in its diurnal course. Typical cases are marked by the yellow bar and lead to higher measured fluxes at BAES.

The strong dependence of summed up $F_C$ on the prevailing wind directions is visualized in Fig. 4.8. Net ecosystem exchange (NEE) values were calculated separately for each wind sector and are depicted as average totals for each month in $\mathrm{g\,C\,m^{-2}}$. The narrow south-east wind sector accounts almost singularly for the total of measured $F_C$ at BKLI and

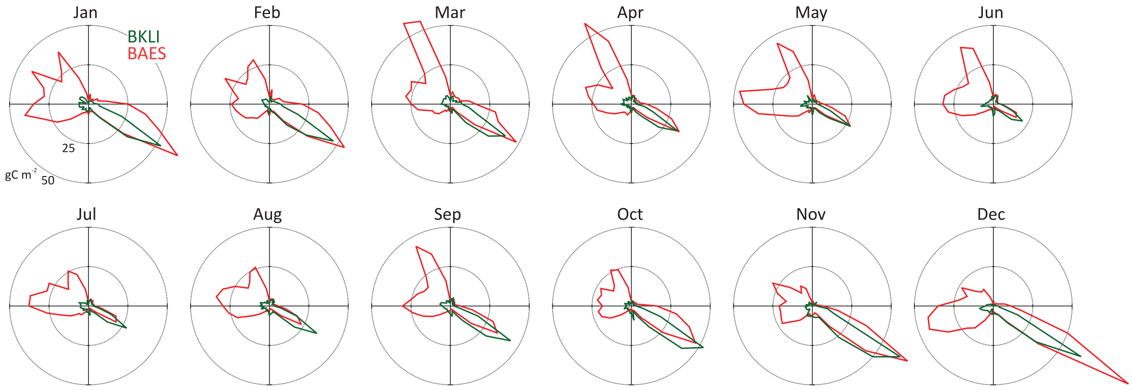


Figure 4.8: The dependence of the monthly averages of NEE on the wind direction. Depicted as average monthly totals for individual 10° sectors at BKLI and BAES for the period 06/2009–06/2013.

is often similar in size at BAES. Here, the shape of the lines reflects the average wind direction frequencies in Fig. 4.4. The equality of the size of the south-east sector for most months shows that the traffic on the Aeschenplatz is the 'additional source' for BAES that leads to the higher $F_C$. Higher south-east contributions to BAES in Winter are related to higher heating activities.

Even if the shape of the lines suggests the impression of a source area, they should not be mistaken for representing actual footprints. Neither distance and wind velocity nor cross-wind and stability effects are accounted for (Section 2.3).

## 4.3 Seasonality of $CO_2$ concentrations

As stated in Section P2, the diurnal course of the $CO_2$ concentration level inside the UBL is basically coupled to the height of the UBL itself. Traffic has only a minor, superimposed effect which gets smaller with height.

The seasonality of the four year course of $CO_2$ concentrations at BAES (Fig. P3-10) shows a good correlation with $F_C$, HDD and air temperature. Even if data from the measurement gaps in Winter 2011/12 and 2012/13 are missing, the global trend towards higher atmospheric $CO_2$ concentrations is well reflected by the data, e.g. by the increase of the yearly minima. On a longer time scale of ten years (Fig. 4.9), the trend for Basel is obvious and follows in its rate the trend at the regional Global Atmosphere Watch (GAW) background station Schauinsland (Section P3-3.5.3). The lower amplitude and the slight phase shift at the latter is a result of the altitude (1205 m.a.s.l) of the station. It is less affected by surface processes in the PBL in general and not directly influenced by sources and sinks in the lower layers. A fact that is also represented by the stability of the trend, compared to the more undulating trend at BKLI.

The courses at BAES, BKLI and BKLIC are similar in their amplitude. Higher street level concentrations as seen in Fig. P2-5 (measured with one single instrument) are not reflected by the differences between the courses of BKLI and BKLIC in Fig. 4.9 (measured with two different instruments). This is due to the difficulties of exact concentration

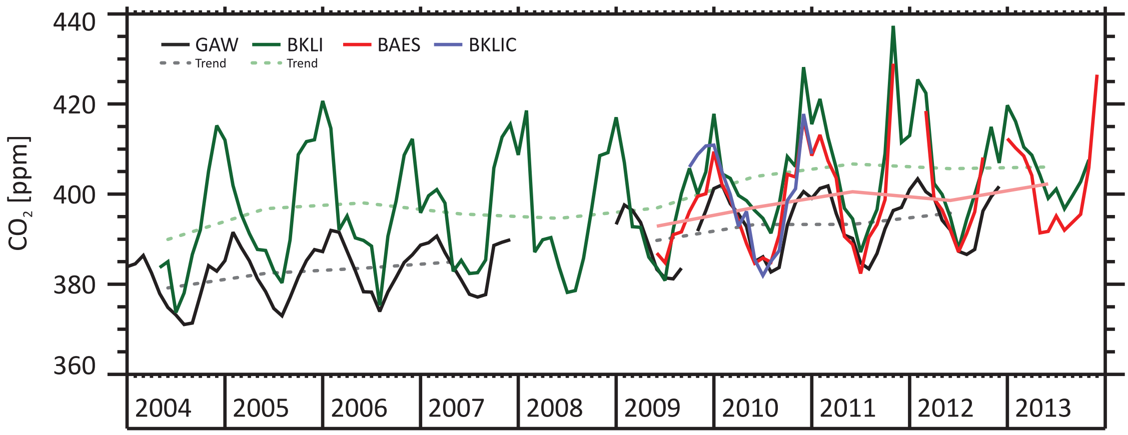


Figure 4.9: Long term $CO_2$ concentration (monthly averages) measured at the three sites and the GAW station Schauinsland. Dashed lines are trend values for BKLI and GAW based on yearly averages. This comparison is prone to uncertainties as it relies on different instruments (Section 3.1).

measurements mentioned in Section 3.1 which have to be kept in mind when analyzing Fig. 4.9. The significance and comparability of the depicted values is restricted. Trends and phase shifts are nonetheless of good explanatory power.

BAES shows lower minima and maxima than BKLI which might be – besides the instrumental issues – due to source area differences (source areas for concentrations are usually larger than for fluxes but have not been calculated). Opposed to fluxes, which depend on the diurnal course of traffic, concentrations in the ISL are primarily a function of the UBL height. Thus they rely differently on wind direction patterns. An indicator for a distinct wind direction or source area dependence are the months in Winter 2011/12. High values in November are followed by unusually low values in December and January. Referring to Fig. P3-8, it can be seen that November experienced an atypically high share of east wind while this pattern is flipped for the following months where west winds were more common. For BKLI, this results in a stronger contribution of heating emissions from the residential area to the west in November and a lower contribution from the east in January/February, showing that traffic emissions are less important for measured concentrations than for fluxes (Section P2-3.3.1). Wind direction anomalies in Summer are less frequent and have a minor effect on average $CO_2$ concentrations due to less stable atmospheric conditions and a generally enhanced vertical dilution of $CO_2$.

## 4.4 Reoccurring vortex patterns in the street canyon

Flow patterns inside the street canyon at BKLI are found to be highly three-dimensional, showing a lateral helical flow structure strongly dependent on the prevailing wind direction. The in-canyon vortex itself develops independently on the wind direction, except for nearly canyon-parallel winds, with its size determined by the height of the respective upwind building. While visible in the average wind field, the vortex is assumed to be not persistent and continuously re-evolving on the high-frequency time scale (Christen, 2005).

In Section P2-3.3.2, estimations on the size and location of the different vortex structures are presented, based on average wind vectors inside the canyon. This section presents additional calculations of the location of the center of the rotational flow for different ambient wind directions.

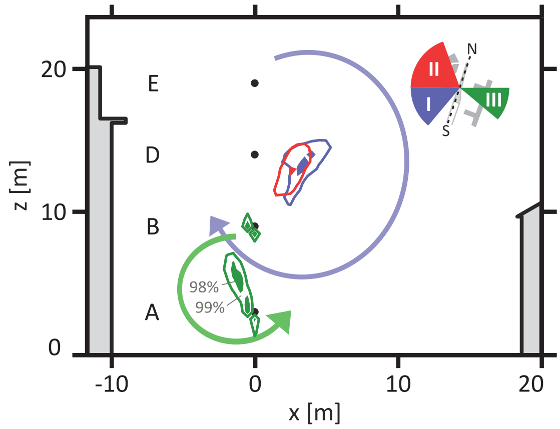


Figure 4.10: The expected street canyon vortex in the canyon cross section and the location of its center (contour lines) for all half-hourly cases in 2010. Three ambient wind sectors are distinguished: (I) 220-270°in blue, (II) 270-340°in red and (III) 90-130°in green. Arrows sketch the expected vortex location (I and II in blue, III in green). Sampling points (A, B, D, E) are given as a reference. This figure relates to Fig. P2-4. For the meaning of the contour lines, see Section 4.4.

In Fig. 4.10 the expected vortices for three wind sectors are sketched in the cross canyon plane. This figure aggregates and extends the information given in Fig. P2-4. If an idealized symmetric vortex is assumed, the intersection of vectors that are normal to its average rotational flow gives the rotational axis or, in the depicted plane, the center point of the vortex. In the non-ideal case the vortex is stretched or otherwise deformed and has no unique center point but rather a center area around which it rotates. The average location and extent of this center area can be statistically approached. We can assume that the measured wind vectors in the canyon are part of the rotational flow. The wind vectors are projected to the cross canyon plane in which their normal vectors are calculated. Intersections are then calculated for each possible combination of two normal vectors, giving several possible center points for one vortex case. This procedure was applied for each half hour in the year 2010 and the resulting set of center points was separated by the three wind sectors shown in Fig. 4.10. For west wind, all four heights (A, B, D, E) were assumed to be in the vortex structure. For east wind, only center points calculated for A&B and A&D were considered.

Figure 4.10 gives an impression of the location and size of the center area for the three ambient wind direction sectors and supports the assumed vortex structures depicted in Fig. P2-4. Contour lines enclose 99% (the filled inner part 98%) of all center points calculated (their color refers to the wind sector). The size of the contour areas indicates that for ambient winds within one of the sectors the axis of the rotational flow is always located at more or less the same place in space. It can thus be assumed that the structure of the vortex is also similar.

Daytime in-canyon distribution of $CO_2$ (Fig. P2-7) and other pollutants emitted by passing vehicles depends heavily on these vortex structures, as described in Section P2-3.3.2. A highly turbulent shear layer usually forms during west wind situations at the top of the canyon (Gartmann et al., 2011), leading to a reduced vertical exchange with the RSL above and a persistent vortex structure (the blue vortex sketched in Fig. 4.10). Fig. P2-7 shows, that this results in a good mixing with a vertically homogeneous $CO_2$ distribution in the canyon center and a strong accumulation at the leeward wall (the left side of the figure). The maximum concentration is found in the upper half of the wall where the vortex has less removing effect and small counter-rotating vortices can be assumed which support dispersive accumulation processes.

### 4.4.1 Methodical issues

Despite methodical limitations of the EC method inside the RSL (Section 2), measurements near the top of the UCL deliver average $CO_2$ fluxes that show an excellent qualitative agreement with diurnal traffic patterns on the street below (Fig. P2-8 and Fig. P2-9). Mixing inside the canyon seems to be sufficient to blend the traffic emissions to a representative flux. Except for along-canyon winds from the north, the three-dimensionality of the vortex flow leads to vertically upward inclined average streamlines at canyon top of up to 20°or more (Fig. P2-3). Omitting a streamline correction of the flux data means that in most cases a vertical advective transport of $CO_2$ must be assumed, not captured as flux by the EC system. Nevertheless, for qualitative analyses that aim at increasing the knowledge on processes on the micro scale, the measurements are legitimated by their results.

# P2 Variability of $CO_2$ concentrations and fluxes in and above an urban street canyon

**Lietzke, B.** and Vogt, R. (2013):
Variability of $CO_2$ concentrations and fluxes in and above an urban street canyon.
*Atmospheric Environment*, 74, p. 60–72.

Available at http://dx.doi.org/10.1016/j.atmosenv.2013.03.030

Atmospheric Environment 74 (2013) 60–72

Contents lists available at SciVerse ScienceDirect

Atmospheric Environment

journal homepage: www.elsevier.com/locate/atmosenv

# Variability of $CO_2$ concentrations and fluxes in and above an urban street canyon

Björn Lietzke*, Roland Vogt

*MCR Lab, Department of Environmental Sciences, University of Basel, Klingelbergstr. 27, 4052 Basel, Switzerland*

HIGHLIGHTS

- $CO_2$ fluxes and concentrations were measured at an urban street canyon over one year.
- Fluxes at the top of the canyon show a distinct qualitative correlation with traffic density.
- Fluxes above also strongly depend on traffic but only for eastern wind directions.
- Wind may act as a lid on top of the canyon and reduce turbulent vertical exchange.
- In-canyon vortex has corkscrew like lateral motion and strong influence on $CO_2$ distribution.

ARTICLE INFO

*Article history:*
Received 28 March 2012
Received in revised form
14 March 2013
Accepted 16 March 2013

*Keywords:*
Carbon-dioxide
Urban
Street canyon
Flux measurements
Concentration profiles
Eddy-covariance
Basel

ABSTRACT

The variability of $CO_2$ concentrations and fluxes in dense urban environments is high due to the inherent heterogeneity of these complex areas and their spatio-temporally variable anthropogenic sources. With a focus on micro- to local-scale $CO_2$-exchange processes, measurements were conducted in a street canyon in the city of Basel, Switzerland in 2010. $CO_2$ fluxes were sampled at the top of the canyon (19 m) and at 39 m while vertical $CO_2$ concentration profiles were measured in the center and at a wall of the canyon. $CO_2$ concentration distributions in the street canyon and exchange processes with the layers above show, apart from expected general diurnal patterns due mixing layer heights, a strong dependence on wind direction relative to the canyon. As a consequence of the resulting corkscrew-like canyon vortex, accumulation of $CO_2$ inside the canyon is modulated with distinct distribution patterns. The evaluation of diurnal traffic data provides good explanations for the vertical and horizontal differences in $CO_2$-distribution inside the canyon. Diurnal flux characteristics at the top of the canyon can almost solely be explained with traffic density expressed by the strong linear dependence. Even the diurnal course of the flux at 39 m shows a remarkable relationship to traffic density for east wind conditions while, for west wind situations, a change toward source areas with lower emissions leads to a reduced flux.



## 1. Introduction

Dense population, a high amount of traffic and a small fraction of green areas are the main factors that lead to higher emissions of $CO_2$ in cities when compared to rural areas. Measuring and quantifying these emissions reliably is difficult because the urban surface is often very heterogeneous and the spatial and temporal distribution of sources is highly variable. Hence, the contribution of cities to the global carbon cycle is a crucial, yet not adequately investigated phenomenon. Quantification attempts, e.g. in modeling studies, are often based on estimations of fossil fuel consumption averaged over long time periods and large areas, even on a city scale (Grimmond et al., 2002), and sometimes adapted to smaller scales using different patterns of urban development as proxy data (Parshall et al., 2010).

It is only recently that investigations in the area of urban metabolism approaches started to become more spatially detailed and more integrated in terms of which processes and factors are included. Christen et al. (2011) for example found a good agreement between measured and holistically modeled carbon fluxes that supported the idea of deriving carbon budgets from bottom-up modeling of emission processes. The question remains as to how well this works for different urban structures, e.g. dense city centers or other more diversified areas.

In this paper we present results from a measurement study on micro- to local-scale $CO_2$ transport processes in and above a street canyon at a central and diverse urban site. It was not possible to compare our results to modeled carbon fluxes but instead the

* Corresponding author.
*E-mail address:* bjoern.lietzke@unibas.ch (B. Lietzke).

1352-2310/$ – see front matter © 2013 Elsevier Ltd. All rights reserved.
http://dx.doi.org/10.1016/j.atmosenv.2013.03.030

research tries to provide insights into the linking of flux tower data to processes associated with the underlying urban structure.

One year of data is presented and analyzed to understand what factors are eminent for local atmospheric transport processes of $CO_2$ and the resulting spatial and temporal patterns of the fluxes and concentrations close to the urban surface. The effect of the urban structure i.e. the street canyon on micro-scale in-canyon wind patterns is illustrated. At two different heights the dependence of $CO_2$ fluxes on wind patterns and traffic, which is the major source of $CO_2$ in the canyon, is analyzed.

### 1.1. $CO_2$ concentrations

Dense urban areas are characterized by a high amount of impervious surfaces and sparse vegetation. Urban boundary layer (UBL) $CO_2$ concentrations over such areas show generally similar behaviors as over other surface types, e.g. forests. Characteristics are the relative independence of local sources, especially during daytime, and a large diurnal amplitude with an early morning maximum and a midday/afternoon minimum. This diurnal pattern is mainly thought to be a direct effect of UBL height coupled with a dilution of $CO_2$ during its growth and an accumulation during its decrease in the evening and throughout the night (Vogt et al., 2006). Despite some slight deviations in the size of the amplitude, this characteristic is independent of the height of the measurement inside the roughness sublayer (RSL). Nevertheless, the horizontal concentration distribution close to the ground may show a greater dependence on the spatial source and sink distribution as well as on their strengths. From transect measurements Henninger (2008) statistically derives that on a city scale the differences in near surface ($z = 1.5$ m) $CO_2$ concentration depend 71% on local traffic density and urban canopy layer (UCL) stability. Similarly, photosynthesis can be expected to have only a very local effect on the diurnal course of $CO_2$ concentrations in dense urban areas. According to Strong et al. (2011) it becomes relevant during summer mornings within shallow mixing heights.

Several studies (e.g. Helfter et al., 2011; Reid and Steyn, 1997; Strong et al., 2011; Vogt et al., 2006) postulate that entrainment of tropospheric air as well as large-scale horizontal advection of air masses, both with low $CO_2$ concentrations, must take place during the day. Otherwise, the afternoon drop of $CO_2$ levels close to background concentration could not be explained as there is normally a high input through emissions at that time of the day. In contrast, nocturnal courses, often under relatively stable atmospheric conditions, are explainable with local source characteristics (Vogt et al., 2006). Strong et al. (2011) provide evidence for these postulations with model results where, on average, advection was the most important $CO_2$ reduction process at Salt Lake Valley, USA, except for hours with a strong UBL growth where there was stronger fresh air entrainment from above.

### 1.2. $CO_2$ fluxes

Cities are generally a net source of $CO_2$. Reported average $F_C$ from direct measurement studies in urban or suburban areas range from 0.92 (Ramamurthy and Pardyjak, 2011) to 26.0 $\mu$mol m$^{-2}$ s$^{-1}$(Nemitz et al., 2002). While these two studies – as well as many others – only cover a part of the year, long-term studies confirm the range (0.95 (Crawford et al., 2011) to 25.58 $\mu$mol m$^{-2}$ s$^{-1}$ (Helfter et al., 2011)). Traffic and domestic heating (or cooling) are the main emitters in urban or suburban surroundings while human and vegetation/soil respiration play a minor part. Daytime vegetation uptake has a limiting effect on fluxes (Coutts et al., 2007; Kordowski and Kuttler, 2010) but it usually can not compensate anthropogenic sources. The vegetation fraction ($\lambda_v$) of a study area can be taken as a rough indicator for the influence of plant uptake, even if the effective uptake rate depends on other factors like e.g. plant species or local climate conditions. Measurements over suburban neighborhoods with a high $\lambda_v$ (e.g. Crawford et al., 2011; Ramamurthy and Pardyjak, 2011) often report – not surprisingly – greater influences than such over more sealed urban surfaces (e.g. Grimmond et al., 2004; Matese et al., 2009). Nevertheless, establishing a dependency between reported $\lambda_v$ and $F_C$ is not as straightforward as many other factors like the amount and spatial distribution of traffic, the measurement period or the types of the combusted fuels for domestic heating influence $F_C$.

Thus, contrary to $CO_2$ concentrations, comparing the diurnal courses of vertical $CO_2$ fluxes ($F_C$) between cities reveals patterns that are very different from each other. There is a clear correlation to source dynamics, a fact that can, for example, be seen if fluxes are compared with estimated emissions. A major road's street canyon, like the one investigated in this study, is therefore an ideal experimental site as the dominant source inside the canyon – considering human and plant respiration as negligible in this case – is the directly underlying traffic.

A well established way to assess vertical $CO_2$ fluxes to and from the atmosphere is the eddy-covariance (EC) technique. It has proven to deliver reliable results over various, relatively homogeneous surfaces, e.g. in the FLUXNET community (Baldocchi, 2008). Its use at urban sites has only recently been intensified with several papers that were published primarily during the last decade. Nevertheless, long-term studies and comparisons between parallel measurements in the same city are still rare.

Major uncertainties with EC measurements in the urban inertial sublayer (ISL) arise through the aforementioned problems of the highly diversified surface structure and non-uniform sources. Thus, proper placement of the sensors in relation to dominant $CO_2$ sources such as major roads is an important task. Christen et al. (2011) found that due to the location of their tower close to an intersection, the fraction from transportation in the total $CO_2$ signal measured increased from 47% for the entire homogeneous study area to 70% at that specific location. This is a remarkable increase and it indicates how challenging it is to properly relate source areas to measured fluxes (see e.g. Bergeron and Strachan, 2011; Järvi et al., 2012; Kordowski and Kuttler, 2010).

EC measurements inside the urban RSL are affected by the 3D nature of the flow resulting from the high spatial variability of local roughness elements (Feigenwinter et al., 2012) and fluxes are height dependent inside the RSL (Rotach, 2001). Vertical turbulent transport can be calculated for a point in space but the flux can not be directly attributed to a source area like when EC measurements are done in the ISL, i.e. we do not know a priori what the flux represents. Despite these limitations, we placed an EC system on top of the street canyon in order to capture the influence of the traffic on $CO_2$ fluxes.

### 1.3. Street canyon effects

The closer to the ground that measurements are taken, the better they may be verified and related to single local sources but the more they are affected by the surface and its heterogeneities. Which processes influence the vertical transport of $CO_2$ from source level to measurement level is an important question in urban surroundings. A major focus of this study thus lies on the relationship between traffic as a primary source of $CO_2$, micro-scale distribution patterns in a street canyon and local-scale (following the definition of scales according to Oke (1987)) flux characteristics in a dense urban environment.

Flow patterns and concentration dispersion in and around urban street canyons can be studied using different means. Besides field experiments on wind, turbulence or concentrations (e.g. DePaul and Sheih, 1985; Rotach, 1995), modeling and wind tunnel studies are other common approaches (e.g. Hoydysh and Dabberdt, 1988; Kastner-Klein and Plate, 1999; Barlow et al., 2004; Harman et al., 2004; Balczó et al., 2009; Gromke and Ruck, 2009; Gartmann et al., 2011 or a review by Vardoulakis et al., 2003).

Despite the different types of approaches, one of the main results from this kind of studies is that transport processes are often determined by in-canyon vortices, the orientation of which are strongly dependent on wind direction as well as on canyon and roof geometries. Also, building dimensions and upwind building configuration have an influence on the vertical exchange: in a wind tunnel study, Kastner-Klein and Plate (1999) found concentrations of pollutants to be up to 10 times higher at the leeward compared to the windward wall of a street canyon. For wind directions not perpendicular to the canyon, different positions of the sampling profiles along the canyon axis resulted in different concentration values.

Modeling and wind tunnel studies have limitations compared to real world studies. Analyses are typically done only for perpendicular wind directions and street canyons are often of ideal geometry, e.g. with a height to width ratio of 1, buildings with flat roofs and without additional obstacles inside the canyon. They can therefore only give a reduced image of real street canyons. For example, the presence of vegetation inside a canyon has an influence on pollutant transport according to Balczó et al. (2009). As one of the few studies, they compare modeling and wind tunnel data for a street canyon with vegetation of different Leaf Area Density (LAD) (see also Gromke and Ruck, 2009 for the wind tunnel part of that study). They found pollutant concentrations to be increased by 20–40% on average with increasing LAD and, in agreement with Kastner-Klein and Plate (1999), higher values at the leeward wall and decreased concentrations at the windward wall. Their vegetation volume filled about half the canyon volume, thus their results are not directly comparable to the situation described in this paper where the trees in the canyon center are a lot smaller. Nevertheless, it shows that the presence of trees has a significant influence on the flow structures and therefore also on the dispersion of pollutants in a street canyon.

## 2. Methods

### 2.1. Winter- and summertime

Time declarations in this paper are all given in Central European Time (CET = UTC+1). Summertime (ST) is the period from 28.03. to 31.10.2010 when Central European Summer Time (CEST = CET+1) is active and wintertime (WT) is the period when it is not (01.01.–27.03. and 01.11.–31.12.2010).

### 2.2. Site characteristics

Since 2003, the University of Basel's MCR Lab (Meteorology, Climatology and Remote Sensing) has been operating a long-term urban meteorological site in the city of Basel, Switzerland (Fig. 1; WGS 84: 7.5805 E/47.5617 N; Elevation 264 m a.s.l.). The permanent part of the site is an 18 m tall tower (tower A, see Fig. 2c) mounted on the flat roof of a 20 m high University building. An additional 18 m high triangular lattice-tower (tower B) was erected on a 1 m high concrete block at the center of the adjacent street canyon (Klingelbergstrasse) at a distance of 11 m from the building. The tops of the towers are 39 m and 19 m above street level. Tower B was operated from mid October 2009 until the end of March 2011 whereas data presented in this study cover only the year 2010.

The Klingelbergstrasse is part of an inner ring road around the city center of Basel and has an approximate north-south orientation of a 20° angle to the east. At the location where the street canyon measurements were taken, the road consists of three lanes, one northbound and two southbound, all highly frequented by individual traffic and public transport buses throughout the day. Tower B itself is placed on a 3 m wide grass strip between the lanes. A row of six approximately 6 m tall trees is sparsely planted on that strip. 21 m south and 67 m north of tower B are entrances to a large multi-story public underground parking garage. Adjacent east of the road is an herbaceous border with 15–20 m tall mature sycamore trees and an 11 m tall building with an open courtyard facing the road.

The average building height $z_h$ in the area around the site is 17 m for a radius of 400 m, thus the measurements at the top of tower A ($z/z_h = 2.3$) can be considered to take place above the RSL and inside the ISL, assuming that the upper level of the RSL is around $2z_h$ (Feigenwinter et al., 2012). Most of the buildings west of the site are residential, forming blocks with green backyards. This area consists of a regular structure of buildings whereas in the east and north there are a few larger university buildings including the 40 m high University Hospital about 250 m north-east of the site. The plan area within a 400 m radius around the site has a vegetation fraction of $\lambda_v = 23.8\%$, a building fraction of $\lambda_b = 38.3\%$ and $\lambda_g = 37.9\%$ impervious ground surface.

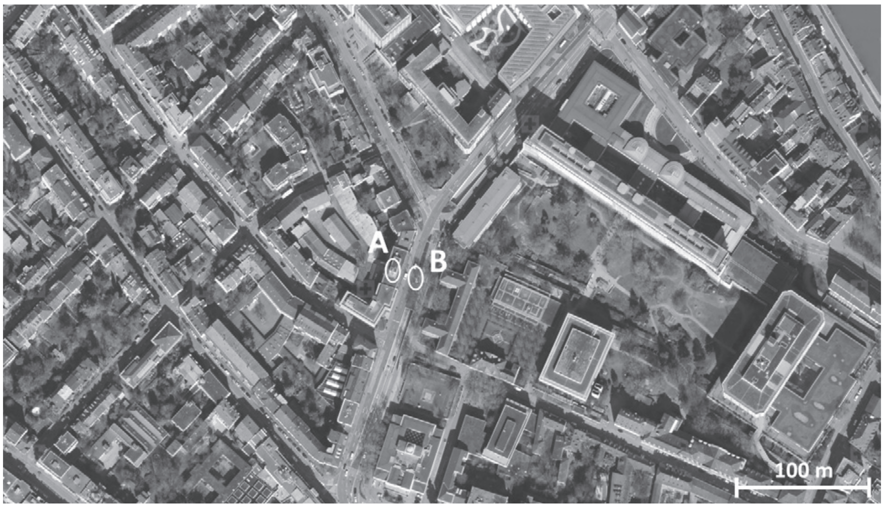


**Fig. 1.** Aerial image of the surroundings of the site with the locations of towers A and B marked. Image source: http://map.geo.admin.ch

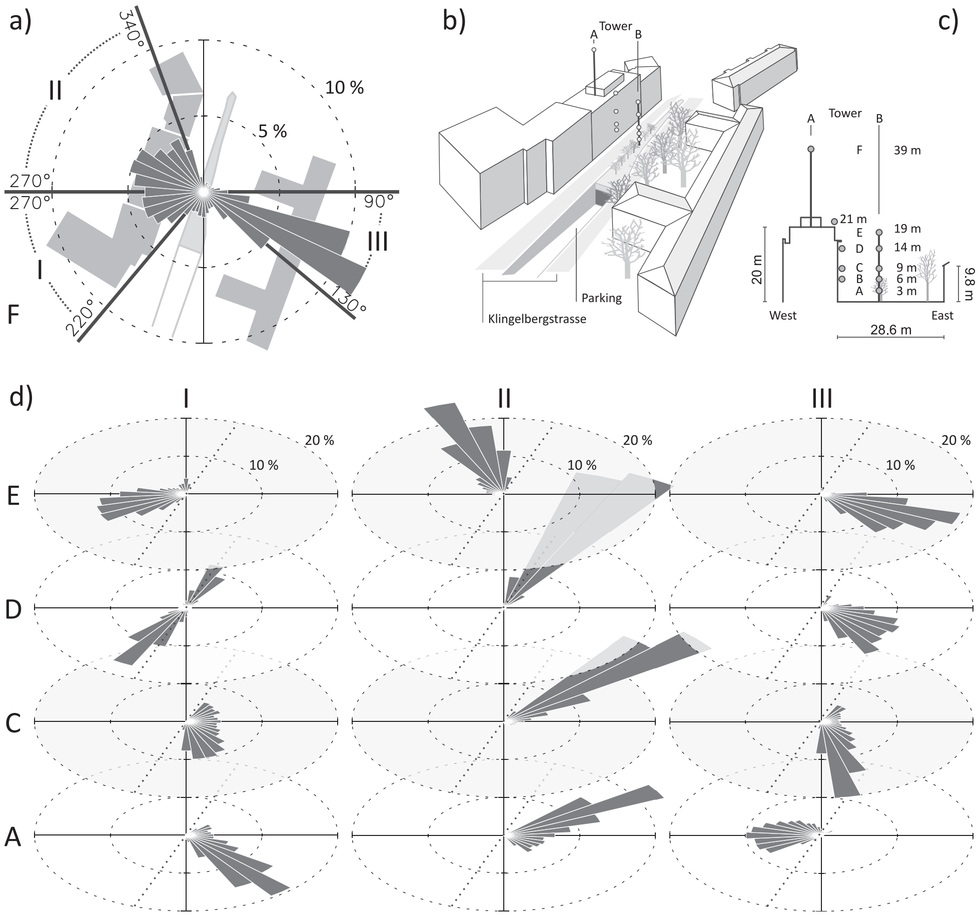


**Fig. 2.** (a) Wind rose at 39 m (F) and plan area of the surroundings. (b) 3D-view from the south. (c) cross section at the tower location. (d) wind roses down into the street canyon at the heights E, D, C and A for the wind sectors I, II and III. Canyon axis orientation is 20° and is denoted by the dotted line in the in-canyon wind roses.

The flow regime of wind coming from the area west of the site is expected to be 'skimming flow' (Oke, 1987) as the underlying building structure is relatively dense. The street canyon itself has a non-ideal cross section. The height to width ratio is 0.7 for the building to the west and 0.34 for the building to the east. Thus, the local flow regime for the canyon for east wind situations might be characterized as 'wake interference flow' (Oke, 1987).

### 2.3. Instrumentation and data handling

Two $CO_2$ concentration profiles, each consisting of five levels (also depicted in Fig. 2c), were sampled with a closed-path gas analyzer (LI-6262) and a gas multiplexer system that switched through the different inlet tubes in a series, similar to the system described in Vogt et al. (2006). The LI-6262 was housed in a room on top of the building to minimize errors due to temperature changes. The inlets of the tubes (50 m, Polyethylene, $\phi$ 4 mm, FESTO AG, Dietikon, CH) were connected to particle filters (Acro 50 Vent Device with 1 μm PTFE membrane, PALL Gelman Laboratory, Ann Arbor, MI, USA) and mounted at five different heights on the street canyon tower B, four heights at the wall of the adjacent building and at 39 m on top of tower A (Table 1). The horizontal distance between canyon and wall inlets was approximately 10 m. Air was continuously sucked through all tubes with a flow rate of approximately 10 l $s^{-1}$ whereas each tube was successively probed at a lower flow rate (around 5 l $s^{-1}$) for 30 s. The first 7 s were discarded and the average value of the following 23 s was stored by a Campbell 21X data logger and considered to be the 5 min average for that inlet. The LI-6262 was calibrated for zero and span offsets at least every second week. Time lag corrections were not applied since only averaged values over 5 min were considered. Inlet filters were replaced every second week due to possible obstruction by dust to ensure constant flow rates.

Two EC systems to measure $CO_2$ flux were operated during this field work. One was mounted at 39 m ($F_{C(39)}$) and one at 19 m ($F_{C(19)}$). The installed ultrasonic-anemometers were a Gill HS at tower A and a Campbell Scientific CSAT3 at tower B (details are listed in Table 1). Both systems used LICOR LI-7500 open-path gas analyzers that were calibrated prior to the experiment. The internal data quality control value (Automatic Gain Control) of the LI-7500

**Table 1**
Instrumentation of the site and measured variables. Measurement heights are denoted for A as the rooftop tower and the building wall and B as the street canyon tower (see cross section in Fig. 2 for an illustration).

| Variable | Measurement height $z$ [m] | Storage interval [Hz] | Instrument | Manufacturer |
|---|---|---|---|---|
| $u,v,w,\theta$ | A: 39 | 20 | Gill HS | Gill Instruments Ltd, UK |
| $u,v,w,\theta$ | B: 3, 9, 14, 19 | 20 | CSAT3 | Campbell Scientific Inc., U.S.A. |
| $CO_2$ conc | A: 6, 9, 14, 21, 39<br>B: 3, 6, 9, 14, 19 | 1 | LI-6262 | LI-COR, U.S.A. |
| $CO_2$ flux ($F_C$) | A: 39; B: 19 | 20 | LI-7500 | LI-COR, U.S.A. |

from tower B was used in post-processing to remove potential erroneous data due to obstructions of the optical path (precipitation, droplets, dust) for both instruments, as the one on tower A was operated in analog mode. Despiking was applied for all variables and Reynolds decomposition based on 30 min block averaging was used to calculate fluxes. The vertical inclination angles of the three dimensional wind vectors (Fig. 3) are comparatively large for some wind directions. Nevertheless, no streamline rotation was applied for the data used in this paper in order to keep it all in the same coordinate system and to retain a common frame of reference for all levels. For similar reasons, no detrending or other filtering of the time series was done as that would have removed different amounts of energy on different levels. Double rotation (Tanner and Thurtell, 1969) would have increased the $F_{C(39)}$ fluxes by an average of 8% but did not change the diurnal characteristics. By omitting a double rotation or a planar fit method (Wilczak et al., 2001) it has to be recognized that this implies a non-zero average vertical wind component $\overline{w}$ if the sonic is not aligned perpendicular to the average wind vector, and thus adds uncertainties to the flux density interpretations and introduces an advective term.

Corrections were applied to the sensible heat flux $H$ after Schotanus et al. (1983) and to $F_C$ after Webb et al. (1980) (WPL-correction). No open-path sensor heating correction (Burba et al., 2008) was done. For the year 2010, 75% of the flux data collected at 19 m and 66% of the flux data collected at 39 m was available for further analyses.

Testing for instationarity (Foken and Wichura, 1996) revealed that 37% of the remaining $F_{C(39)}$ was measured under nonstationary conditions, which is not surprising as thermal convection is comparatively high in the RSL (Feigenwinter et al., 2012). Removing this large amount of data would have led to an availability of only 29% of $F_{C(39)}$. A stationarity-filter was also not applied because this study focuses on qualitative aspects of the flux characteristics.

Additional instruments inside the canyon were three CSAT3 sonic anemometers to monitor turbulence and flow directions at different levels and ventilated psychrometers that sampled wet and dry air temperature at three heights.

### 2.4. Traffic data

Traffic density $\upsilon_K$ was monitored over two weeks, one set in April and one set in September 2010. Inductive counters on each lane were sampling with a one hour resolution. Those two weeks of traffic data were then used to scale the data of a continuous traffic counter $\upsilon_J$ (managed by the city authorities) that is installed on a nearby part of the same ring road on a bridge (Johanniterbrücke, 0.7 km to the north). Despite the fact that there are two crossings between the two sampling points, the traffic densities showed an approximately linear relationship (Southward lanes: $\upsilon_K = -17.3 + 1.24\upsilon_J$ veh h$^{-1}$, $R^2 = 0.95$, RMSE $= 55.8$ veh h$^{-1}$; Northward lane: $\upsilon_K = 14.6 + 0.75\upsilon_J$ veh h$^{-1}$, $R^2 = 0.91$, RMSE $= 53.0$ veh h$^{-1}$). The fit was improved with a separate regression for each hour of the mean diurnal course for weekdays and weekend days since, for example, the morning rush hour is more pronounced at the Klingelbergstrasse than at the Johanniterbrücke. For the ST period, the hourly fits were shifted by one hour. The diurnal working day rhythm of the traffic density, especially the morning increase, was very clearly distinguishable between WT and ST. Finally, a continuous and reliable traffic density dataset of hourly resolution was deduced for the Klingelbergstrasse site.

## 3. Results and discussion

### 3.1. Wind

The wind field over the city of Basel is characterized by two main wind sectors (Fig. 2a): A broad western sector and a relatively narrow ESE sector. The first can be partitioned into two components: the daytime part of a regional mountain-valley wind system following the orographic structure of the Rhine valley (NW) and a synoptically driven fraction (W). The second part consists primarily of autochthonous drainage flows from the Rhine valley, a result of the nighttime part of the regional wind system. While the diurnal pattern is distinct during the Summer months (April to September), ESE directions often become more dominant during daytime in the Winter months (October to February).

In Fig. 8, the diurnal course of the dominating wind directions is depicted with gray bars for ST and WT situations. The average daily turn in direction from easterly (in relation to the axis of the street canyon, easterly here is considered as from 20 to 200°) to westerly winds (200–20°) occurs at around 10:00 CET.

The general wind pattern in combination with the approximately north–south orientated axis of the canyon leads to nearly perpendicular wind directions for most of the time of the sampling period (Fig. 2a). Such cases induce interesting in-canyon flow patterns as illustrated in Fig. 4 and are important for concentration distribution in the canyon layer and local exchange processes between the canyon layer and the above RSL.

### 3.2. $CO_2$ sources

Within the canyon, motor traffic on the Klingelbergstrasse is the major source of $CO_2$. Minor and comparatively negligible contributions may originate from human (0.39 mol s$^{-1}$ per human being according to Moriwaki and Kanda (2004)), plant or soil respiration or from entrained air masses from the flow above the canyon (e.g. household, industrial or traffic emissions from remote sources).

Source characteristics of the traffic emissions were analyzed on a diurnal basis (Fig. 8), separated for working days (Monday to Friday), Saturdays and Sundays due to the differences in their diurnal pattern. The period of ST had to be distinguished from WT as the diurnal courses showed a clear one hour shift, especially for the morning rush hour. This can also be seen in the diurnally averaged $CO_2$ fluxes. Consequently, $CO_2$ concentrations (Section 3.3.1) and fluxes (Section 3.4) were also analyzed separately for ST and WT and working days, Saturdays and Sundays respectively.

On working days (Fig. 8a), the average minimum $\tilde{x}_{hmin}$ of hourly traffic volume occurs in the early morning (Table 2). During the morning rush hour, the traffic volume first rapidly increases until 8 (ST)/9 (WT) CET, followed by a slower increase, which, apart from a

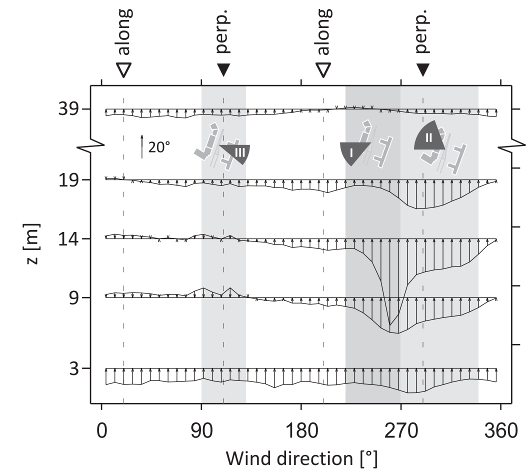


**Fig. 3.** Vertical inclination angle of the three dimensional wind vector to the horizontal plane at all measurement levels as a function of ambient wind direction at 39 m. Shaded wind direction ranges represent sectors I to III shown in Fig. 2.

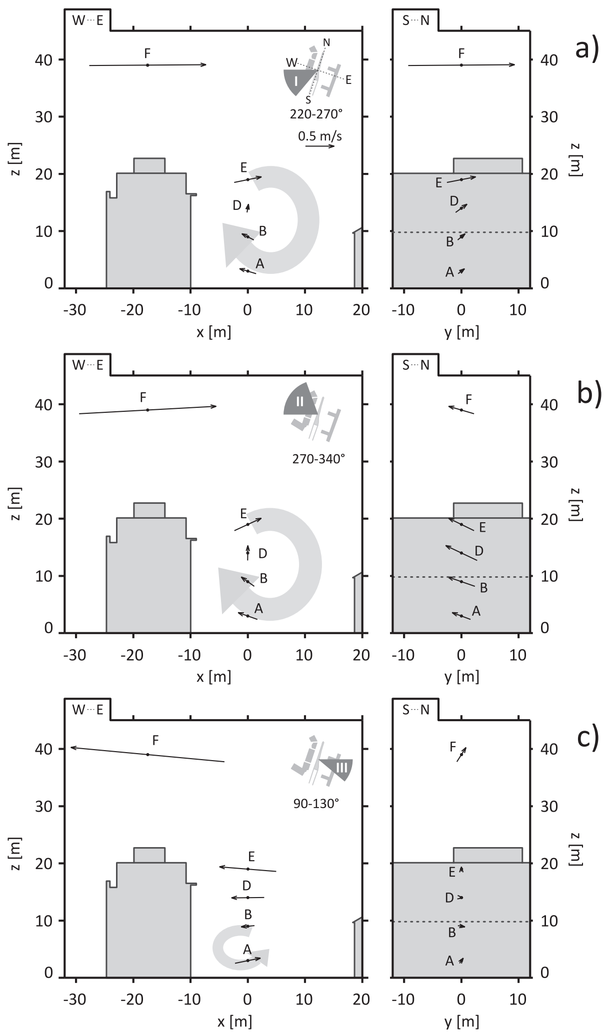


**Fig. 4.** Cross (left column, West–East) and lateral (right column, South–North) sections of the street canyon for three different ambient wind sectors (a, b & c). Arrows depict average wind vector components in the respective planes at the measurement locations A, B, D, E and F (Fig. 2c). Typical expected vortex structures are shown for each wind sector.

slight midday depression, lasts until the daily maximum $\tilde{x}_{h\max}$ is reached in the late afternoon. Afterward, traffic volume falls back to its minimum. As expected, the diurnal pattern is different on weekends (Fig. 8b and c). The amplitude is generally lower, the minimum is higher and occurs later in the early morning and the course is smoother with no morning rush hour and a less distinct evening peak.

The traffic variability from week to week (Table 2) is low with mean hourly normalized standard deviations $\overline{\sigma_{\rm rel}(x_h)}$ of 0.12 and 0.11 for ST and WT working days respectively. On weekends it is of the same size or slightly higher as people are not required to follow their working day rhythm. The variability on working days during the morning increase is remarkably low while the evening decrease shows stronger variations. Exceptions are public holidays where the diurnal pattern is similar to that of weekends. As a consequence, public holidays were previously categorized with Saturdays or Sundays according to their traffic pattern and are thus already included in the data for weekends in Fig. 8 and Table 2.

### 3.3. $CO_2$ concentrations

#### 3.3.1. Diurnal course

Analyzing the mean diurnal course of $CO_2$ concentration (Fig. 5) reveals patterns that can be considered typical for urbanized areas (e.g. Burri et al., 2009; George et al., 2007; Grimmond et al., 2002; Nemitz et al., 2002; Reid and Steyn, 1997; Strong et al., 2011; Vogt et al., 2006; Velasco, 2005). Considering the ST courses for working days (Fig. 5a) at 39 m, lowest concentrations are encountered in the late afternoon with 385 ppm. This is close to 386 ppm which is the ST average diurnal minimum recorded by the GAW (Global Atmosphere Watch, (UBA, 2012)) station Schauinsland, Germany (7.92 E, 47.90 N, 1205 m.a.s.l) and is considered to be the regional background concentration. At night $CO_2$ is accumulated in the stable nocturnal boundary layer. Concentrations rise continuously and reach their maximum in the early morning with 422 ppm. After sunrise a sudden drop occurs that can be attributed to the beginning breakup of the nocturnal boundary layer and the growth of the UBL. The morning rush hour has only a minor influence on the course of the $CO_2$ concentration at 39 m as the traffic peaks slightly after the time of the maximum concentration (see Fig. 8).

At 19 m and 3 m inside the street canyon, the diurnal courses are similar in their basic patterns but are shifted to higher values. Here, an increase in slope parallel with the rapidly increasing traffic density at around 5 CET is observed. Concentration values afterward fall abruptly until midday and reach their minimum in the late afternoon for 39 m and little earlier for the lower measurement points. The concentration differences (Fig. 5c) between the canyon and 39 m suggest a distinct relationship with the diurnal course of traffic density: A sharp increase in the morning, a short depression at noon and a sharp decrease in the evening. In general, traffic has a direct effect on the vertical differences of $CO_2$ – and hence on the vertical $CO_2$ fluxes as will be explained later – but the UBL growth superimposes its effect on the absolute $CO_2$ concentrations which can be seen, for example, in the fact that the concentration course drops in the morning while the traffic remains high throughout the day.

Also, the diurnal courses of the $CO_2$ concentrations on weekends (Fig. 5b) depend on the UBL height in their basic pattern and are thus not much different from working days (Fig. 5a). In contrast to working days, less morning traffic leads to a lower concentration level inside the canyon and the vertical gradients (Fig. 5d) are thus smaller, but increase as traffic increases throughout the day. During the first hours of the day, concentrations are higher on all levels than on working days due to higher nighttime traffic activity on weekends.

Similarly, lower UBL heights and more stable atmospheric conditions during the WT period are one reason for lower amplitudes in the diurnal courses during that time of the year. Additionally, higher emissions from combustion (district heating and combustion by industry, households, commerce and services account for 58% of all $CO_2$ emissions in 2010 in Basel (Kanton Basel-Stadt, 2010)) and less plant activity contribute to the generally higher $CO_2$ level. The working days diurnal minimum of 412 ppm at 39 m is thus higher than the 399 ppm WT background minimum at the Schauinsland GAW station. Vertical concentration differences are stronger compared to ST, especially on weekends, suggesting that vertical mixing is inhibited. The distinct one hour shift in the morning between WT and ST differences in Fig. 5c is another clear piece of evidence indicating the influence of traffic on the vertical concentration differences.

The stability of the UBL can be taken as an indicator for its height, even if the UBL is rarely stable. The stability index is calculated as $\zeta = (z - z_d)/L$ with $z = 39$ m as the measurement height, $z_d$ the zero-plane displacement height (taken to be 2/3 $z_h$,

**Table 2**
Basic statistical characteristics for diurnally averaged hourly traffic [veh $h^{-1}$] and $F_C$ [μmol $m^{-2}$ $s^{-1}$] as plotted in Fig. 8, separated for Summertime (ST), Wintertime (WT), working days (Wd), Saturdays (Sa) and Sundays (Su). With $h = \{1, 2, 3, \ldots, 24\}$ for the hours of the day and $x_h$ as the set of values of all considered days for each $h$. $\overline{n(x_h)}$ is the average number of available values per hour, $\overline{\tilde{x}_h}$ is the average of all median values, $\overline{\bar{x}_h}$ the average of all mean values and $\overline{\sigma_{\mathrm{rel}}(x_h)} = \overline{\sigma(x_h)/\bar{x}_h}$ is the average of all normalized standard deviation values. $\tilde{x}_{h\min}$ gives the minimum and $\tilde{x}_{h\max}$ the maximum of the diurnal courses of the hourly median $\tilde{x}_h$.

| Variable | Period | Days | $\overline{n(x_h)}$ | $\overline{\tilde{x}_h}$ | $\overline{\bar{x}_h}$ | $\overline{\sigma_{\mathrm{rel}}(x_h)}$ | $\tilde{x}_{h\min}$ (CET) | $\tilde{x}_{h\max}$ (CET) |
|---|---|---|---|---|---|---|---|---|
| Traffic | ST | Wd | 150.0 | 681.8 | 682.4 | 0.12 | 38.0 (04) | 1203.5 (18) |
| | | Sa | 32.0 | 580.0 | 580.2 | 0.12 | 115.0 (05) | 1006.5 (15) |
| | | Su | 35.0 | 430.8 | 433.1 | 0.13 | 113.0 (05) | 765.0 (17) |
| | WT | Wd | 95.0 | 681.6 | 683.7 | 0.11 | 39.0 (05) | 1215.0 (19) |
| | | Sa | 30.0 | 575.8 | 579.1 | 0.22 | 120.0 (06) | 1036.5 (16) |
| | | Su | 22.9 | 433.5 | 433.0 | 0.17 | 120.0 (06) | 793.0 (18) |
| | Year | All | 364.9 | 639.4 | 625.6 | 0.34 | 49.00 (03) | 1164.0 (17) |
| $F_{C(19)}$ | ST | Wd | 112.0 | 20.0 | 22.8 | 0.85 | 2.3 (04) | 33.5 (10) |
| | | Sa | 24.1 | 15.8 | 17.4 | 0.75 | 3.2 (04) | 29.7 (12) |
| | | Su | 24.5 | 9.9 | 11.9 | 0.91 | 3.3 (04) | 17.0 (16) |
| | WT | Wd | 72.2 | 22.0 | 26.4 | 1.00 | 1.9 (04) | 37.7 (19) |
| | | Sa | 24.0 | 16.5 | 19.5 | 0.83 | 3.3 (05) | 29.7 (11) |
| | | Su | 18.5 | 11.8 | 14.6 | 0.91 | 2.7 (05) | 22.0 (18) |
| | Year | All | 275.2 | 17.8 | 21.6 | 0.94 | 2.7 (04) | 29.4 (17) |
| $F_{C(39)}$ | ST | Wd | 108.5 | 8.1 | 10.9 | 2.33 | 3.8 (04) | 16.0 (11) |
| | | Sa | 22.6 | 6.9 | 8.3 | 3.90 | 4.1 (17) | 12.8 (09) |
| | | Su | 24.7 | 5.0 | 6.8 | 2.94 | 1.4 (16) | 7.2 (03) |
| | WT | Wd | 53.5 | 12.3 | 15.0 | 1.68 | 4.5 (03) | 20.1 (13) |
| | | Sa | 17.9 | 10.4 | 11.9 | 1.59 | 4.3 (03) | 17.2 (19) |
| | | Su | 14.5 | 8.5 | 9.7 | 2.07 | 5.6 (05) | 13.1 (21) |
| | Year | All | 241.7 | 8.2 | 11.2 | 2.25 | 4.6 (04) | 13.3 (10) |

which is according to Grimmond and Oke (1999) a reasonable value) and $L$ the Obukhov-Length. The mean diurnal courses of classified atmospheric stability in Fig. 6 reveal that the UBL can be considered as unstable ($\zeta < -0.05$) during the night for around 60% in both the ST and WT period. During the day unstable cases are more frequent. Slightly less unstable cases occur, on average, in the first part of the night, a fact that is more pronounced during ST (Fig. 6a). As expected, the diurnal pattern is smoothed during WT (Fig. 6b). Stable situations ($\zeta > 0.05$) are generally rare in all seasons (<20%).

*3.3.2. Vertical profiles*

The diurnal variation of vertical $CO_2$ concentration profiles is shown in detail in Fig. 7. Only cases for wind directions that were approximately perpendicular to the canyon axis were considered in this figure (from 270 to 310° (west, Fig. 7a) and 90–130° (east, Fig. 7b)). These sectors coincide well with the two main sectors of the prevailing wind directions at this site.

Regarding the profile measured at the center of the canyon, east wind situations (Fig. 7b) show a decrease with height throughout the whole day, with a higher in-canyon gradient during the day and

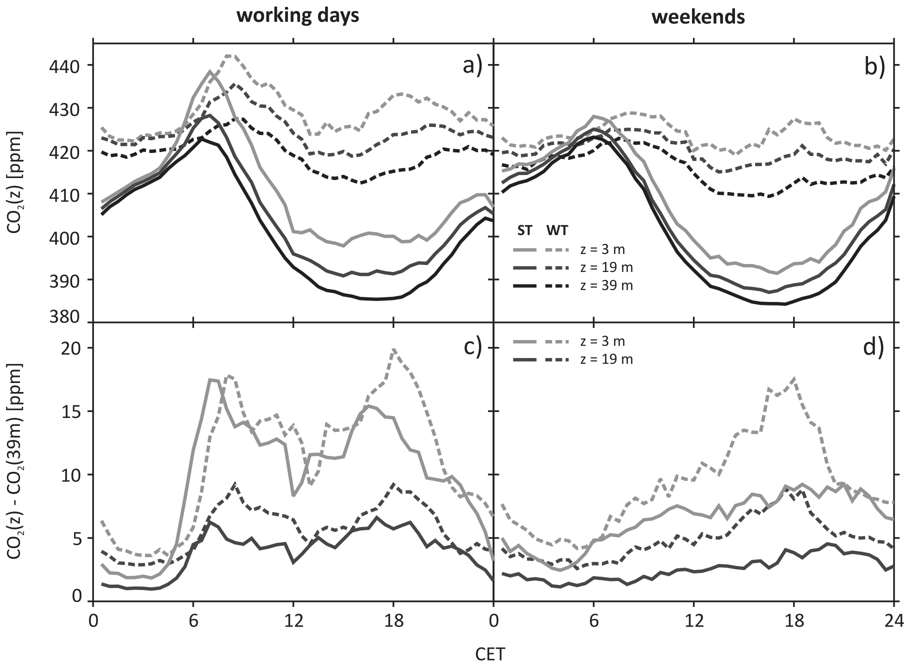


**Fig. 5.** Mean diurnal courses of $CO_2$ concentrations at two heights in the canyon center and above the roof for working days (a) and weekends (b). Data is separated for summer- (ST) and wintertime (WT). (c) & (d): Corresponding differences relative to top level.

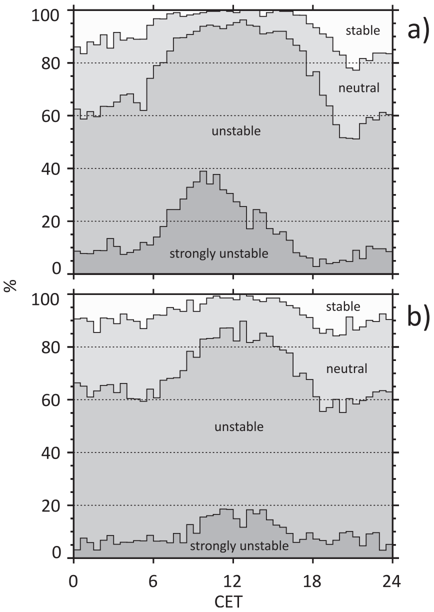


**Fig. 6.** Mean diurnal course of frequencies of UBL stability classes measured at 39 m for (a) ST and (b) WT. Stable: $\zeta > 0.05$; neutral: $|\zeta| < 0.05$; unstable: $\zeta < -0.05$; strongly unstable: $\zeta < -1$.

a lower gradient at night. In the diurnal course, the size of the vertical gradient depends on the amount of traffic, as was expected. The vertical transport of $CO_2$ from the canyon layer to the RSL is unhindered.

For west wind situations (Fig. 7a), the central profile shows a different behavior. In the middle part between 6 m and 19 m, only a small negative vertical gradient can be observed during daytime. The gradient is higher at the bottom of the canyon next to the emission sources and may also turn slightly positive for some cases in the upper half of the canyon volume between 9 m and 19 m. The $CO_2$ in the canyon center seems to be uniformly distributed, at least in the middle and upper part (Fig. 7a). Such a uniform concentration core was also observed by Caton et al. (2003) and can be attributed to a large in-canyon vortex (depicted in Fig. 4) which builds up in the lee of the western wall. The structure of this vortex can be derived from the average wind components in the cross-canyon sections (Fig. 4, left column). For west wind situations (a & b), the vortex leads to an enhanced vertical and horizontal transport of air masses inside the whole canyon. Fresh air with less $CO_2$ is entrained from the above flow close to the windward wall of the canyon. $CO_2$ rich air is transported from the bottom to the leeward wall and from there to the top of the canyon. Consequently, a fairly homogeneous vertical concentration distribution in the canyon core can be observed.

In reality the wind is rarely exactly normal to the canyon axis, thus the vortex does not only have a 2-dimensional structure (left column in Fig. 4) but elongates along the canyon axis (right column in Fig. 4) and takes on a 3-dimensional 'corkscrew' pattern. Figs. 2 and 4 show how even slightly different ISL wind directions (sector I and II marked in the topmost wind rose F) lead to diametrically opposed directions at 9 m inside the canyon which indicates opposed directions of the 'corkscrew' flow. ISL wind from sector I (220–270°) turns counter-clockwise with decreasing height and results in a south-to-north transport inside the canyon and a sector II wind (270–340°) takes on the clockwise turn and generates a north-to-south 'corkscrew' flow. The direction of the 'corkscrew' flow changes at an ISL wind direction of around 270°. This gives an angle of 70° to the axis of the canyon instead of the expected 90°. This shift is probably due to upstream modifications of the approaching flow e.g. through obstacles like the small cubic

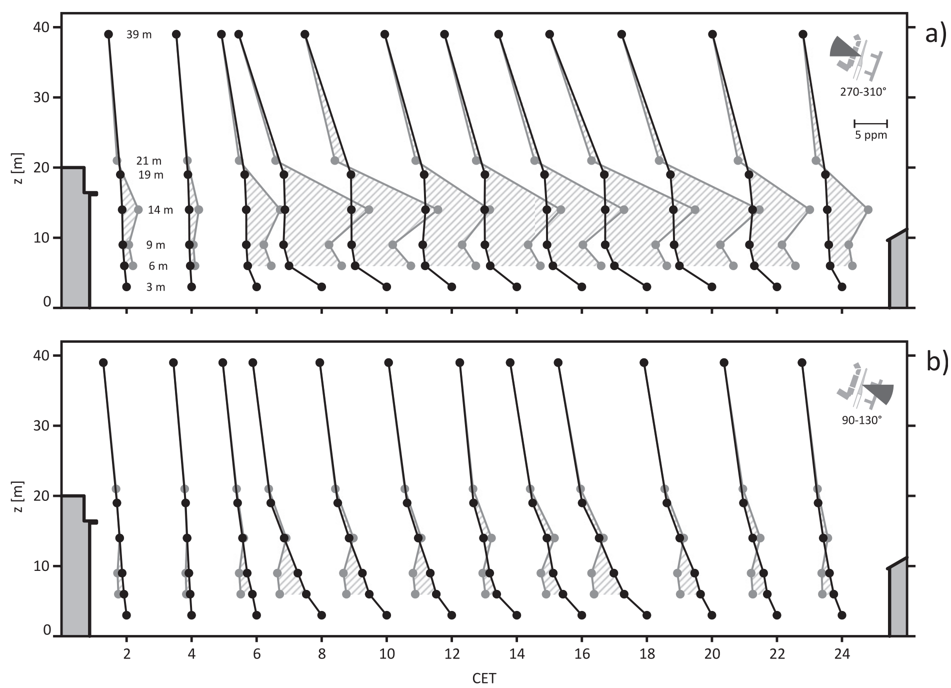


**Fig. 7.** Mean diurnal course of vertical $CO_2$ concentration profiles for nearly canyon-perpendicular winds from west (a: 270–310°) and east (b: 90–130°). Black profiles are from the canyon center and gray profiles are from the canyon wall (see cross section in Fig. 2 for sampling point locations). Each profile represents average values over two hours while the lowest dot denotes the end time of the averaging period. Contours of the adjacent buildings are shown by the gray shaded areas to the left and right (height to scale, distance not).

structure (see 3D-view in Fig. 2b) on top of the roof of the windward building.

For west wind situations shown in Fig. 7a, the turbulent vertical exchange with the layers above the canyon is reduced. The overflowing air generates shear stress and acts as a lid directly behind the building which hinders the $CO_2$ rich air from rising further and leads to an accumulation in the upper region of the wall (shown by the high concentrations at 14 m). Reduced vertical transport was also observed by Caton et al. (2003) and Salizzoni et al. (2009). The comparatively large vertical inclination angle of the wind vector at 19 m (Sector II in Figs. 3 and 4b) indicates an additional $CO_2$ transport by vertical advection and thus an enhanced venting of $CO_2$ from the canyon toward the downwind side. A quantification of the advective part of the transport is not possible with the given setup. Results from CFD calculations for the same canyon presented in Gartmann et al. (2011) show the plume-like venting of $CO_2$ and give an impression of the spatial $CO_2$ distribution as well as of the vortex structure.

While daytime vertical transfer processes are supposed to be governed by the incoming turbulence and the shear layer (Caton et al., 2003; Salizzoni et al., 2009), intermittent convective plumes can contribute to the venting of $CO_2$ during the night when weak flow conditions are unlikely to cause significant vortex circulation (Salmond et al., 2005).

The relatively strong vertical gradient between 3 and 6 m (Fig. 7a) is probably due to the presence of trees (height of approximately 6 m) in the middle of the canyon that attenuate the vortex velocity in the range below 6 m (see Balczó et al., 2009 or Gromke and Ruck, 2009 for the effect of trees on dispersion processes in street canyons).

Another effect of that in-canyon vortex is the transport of air toward the leeward building wall and the local accumulation of $CO_2$ there. During the whole diurnal course (Fig. 7a), in-canyon maximum concentrations are measured at 14 m close to the upper edge of the building whereas Kastner-Klein and Plate (1999) found concentrations to decrease with height for comparable cases. The highest horizontal gradients at this height between wall and canyon center are observed during rush hours in the morning and evening with maximum 30 min average values of >15 ppm (1.5 ppm $m^{-1}$). It is remarkable that during west wind situations, the highest concentrations inside the canyon are found next to the leeward wall and not at the bottom of the canyon next to the emission sources. The vortex has the effect that emissions from the western lanes are transported away from the sampling point in the canyon center directly toward and up the wall. On average, every sampling inlet at the wall measured a higher concentration than the bottom inlet at the center, which is the one closest to the traffic. The mean diurnal horizontal $CO_2$ concentration gradient at 14 m is always even higher than the overall vertical gradient inside the canyon. The accumulation of $CO_2$ rich air in the upper part of the leeward wall might be supported by a smaller counter-rotating vortex (Salizzoni et al., 2009) in the corner between the main vortex and the wall. The wind velocity in this part of the canyon has to be much lower than in the main vortex to allow $CO_2$ to be accumulated here.

### 3.4. $CO_2$ fluxes

To study the relationship between traffic and $F_C$, both were analyzed on an average diurnal basis. Their statistics are shown in Table 2. Fluxes in this table as well as in Figs. 8 and 9 were averaged from half-hourly to hourly values to match the temporal resolution of traffic data. The flux loss due to this low frequency filter was negligible. Note that in Fig. 8, the separate $y$-axes for traffic, $F_{C(19)}$ and $F_{C(39)}$ and the slightly different scalings for ST and WT have to be taken into account. The axes for the fluxes are scaled according

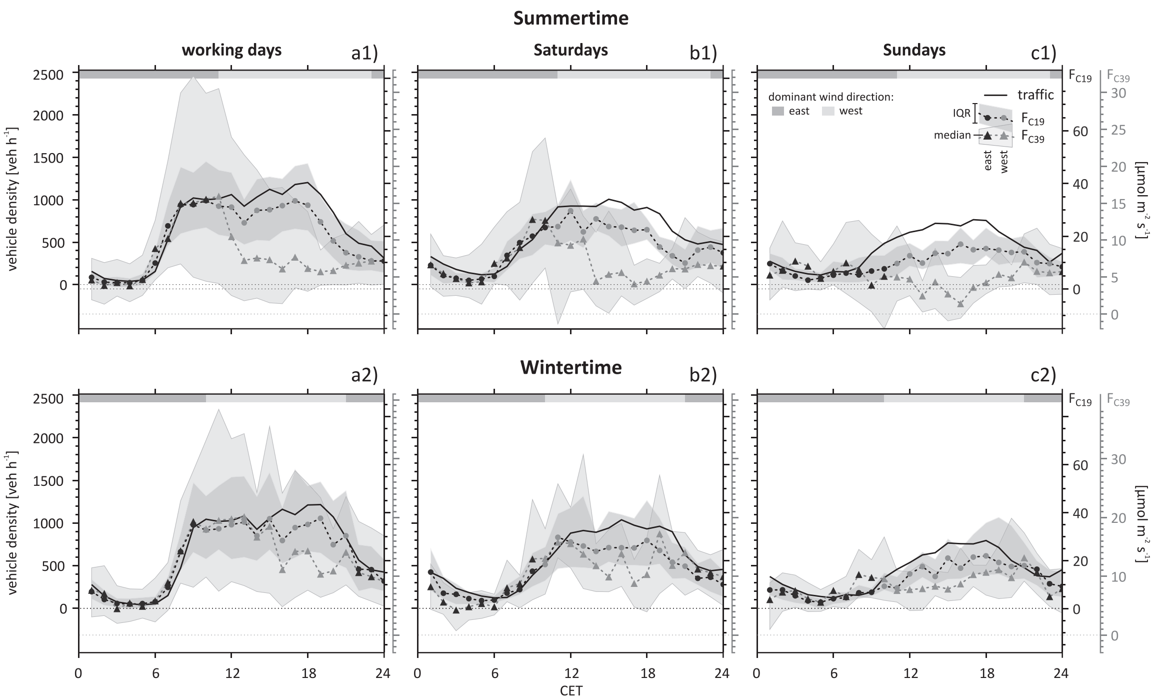


**Fig. 8.** Average diurnal courses of vehicle density (black line), $F_{C(19)}$ (circles) and $F_{C(39)}$ (triangles) for ST (upper row) and WT period (lower row). Hourly averaged median data for (a) working days, (b) Saturdays and (c) Sundays. Shaded areas represent the interquartile ranges (IQR). The $y$-axes for $F_C$ are scaled by the linear regression equations for working days in Fig. 9a1 and a2. The light gray bar at the top of each plot denotes > 50% winds from western directions (20–200°), the dark gray > 50% from eastern directions (200–20°). Correspondingly, $F_C$ values measured under west wind (east wind) influence are marked with lighter gray (darker gray) symbols.

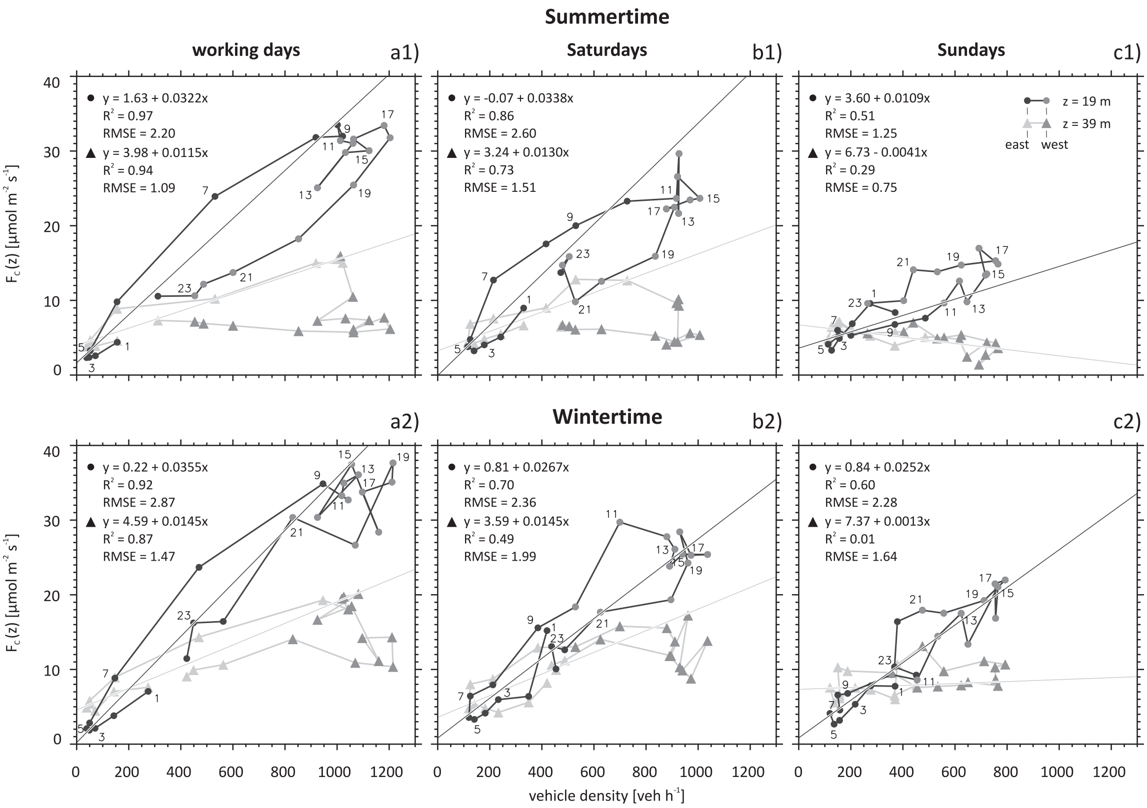


**Fig. 9.** Relation between average diurnal vehicles per hour and $F_{C(19)}$ (circles) and $F_{C(39)}$ (triangles) for summertime (upper row) and wintertime (lower row). Hourly averaged median data for working days (a), Saturdays (b) and Sundays (c). For the sake of clarity, only the odd hours of $F_{C(19)}$ are labeled next to the 19 m level points. The straight dark gray line is the linear regression for $F_{C(19)}$, the light gray line the linear regression for $F_{C(39)}$, but in both cases only for those times of the day where > 50% winds originate from eastern direction (dark gray dots and light gray triangles, see also Fig. 8).

to the equations of the linear regressions between average working day traffic and fluxes from Fig. 9a1 and a2 respectively.

By comparing the courses of the diurnal vehicle density and $F_{C(19)}$ (Fig. 8) for ST and WT, it is found that on average, the latter follow the first surprisingly well, especially on working days (Fig. 8a). Here, even the midday traffic reduction is clearly reflected by the fluxes. The regression coefficients in Fig. 9 support the finding that $F_{C(19)}$ at the top of the canyon layer is directly connected to traffic density and respective emissions at the bottom of the canyon.

Table 2 shows that, when averaged over the entire year 2010, $F_{C(19)}$ is $\overline{\overline{x}_h} = 21.6\ \mu\text{mol m}^{-2}\ \text{s}^{-1}$. WT fluxes are higher than ST fluxes and the statistical distribution is not normally but skewed toward higher values (average mean $\overline{\overline{x}_h}$ is higher than average median $\overline{\tilde{x}_h}$). This indicates that WT $F_{C(19)}$ has higher fluctuations than ST $F_{C(19)}$. Both highest $\tilde{x}_{h\max}$ and lowest $\tilde{x}_{h\min}$ of all $F_{C(19)}$ values are reached during WT working days. Minimum values always occur in the early morning when traffic is lowest, whereas maximum values occur on working days during the rush hours, on Saturdays around noon and on Sundays in the late afternoon.

In every sub-figure of Fig. 8, slightly lower $F_{C(19)}$ can be observed in the afternoon if the course of traffic is taken as a relative reference. This has to be attributed to the average diurnal change in the dominant wind direction from east (in the night and in the morning hours) to west (in the afternoon) as denoted by the gray bars. As already mentioned for Fig. 7, west wind situations come along with a reduced vertical $CO_2$ transport due to the lid-effect of the overflowing air above the street canyon. With the nightly change back to east wind, the course of $F_{C(19)}$ re-adapts to that of traffic.

As a consequence of this wind direction dependency, for both $F_{C(19)}$ and $F_{C(39)}$, only those times of the day were considered for the linear regressions in Fig. 9 where east is the dominant wind direction (>50% of all cases from 20 to 200°) and where a higher correlation with traffic density on the Klingelbergstrasse can be expected. The resulting high $R^2$ values of 0.87–0.97 for working days statistically support the visual impression of a strong dependence of $F_C$ on traffic found in Fig. 8.

On weekends, scaled $F_{C(19)}$ (Fig. 8b and c) is not as congruent with vehicular density as on working days but is still similar. The larger scatter on Saturdays and Sundays can be explained with the fact that fewer days are incorporated in the plot if compared to working days ($\overline{n(x_h)}$ in Table 2). On Saturdays (Fig. 8b) $F_{C(19)}$ again shows a good correlation with traffic in the morning and is less coupled in the afternoon when west winds are more frequent. Thus, maximum $F_{C(19)}$ occurs before the traffic peak is reached in the afternoon. Nighttime and minimum ($\tilde{x}_{h\min}$) values for traffic as well as for $F_{C(19)}$ are on weekends higher than on working days, whereas maximum values ($\tilde{x}_{h\max}$) are comparatively lower. This is especially the case on Sundays when traffic and $F_{C(19)}$ increase slowly throughout the morning and early afternoon and peak in the late afternoon with values for $F_{C(19)}$ of only about half the size of the working day $\tilde{x}_{h\max}$.

For $F_{C(39)}$ Table 2 gives a yearly average of $\overline{\overline{x}_h} = 11.2\ \mu\text{mol m}^{-2}\ \text{s}^{-1}$ which is about half the size of $F_{C(19)}$. Nighttime – and thus minimum values too – are slightly higher at 39 m, especially during WT due to additional $CO_2$ sources like heating, which contribute to the flux at this height and are not captured by the 19 m high measurements. Maximum values are again a lot smaller than at 19 m and the higher standard deviations $\overline{\sigma_{\rm rel}(x_h)}$ show that the variability of $F_{C(39)}$ is comparatively higher.

How much of the $CO_2$ that is emitted in the canyon effectively arrives at the measurement level is for the 39 m reading to a greater extent dependent on wind direction than for the 19 m reading. Working days' (Fig. 8a) nocturnal flux and the morning increase (east wind) are almost congruent with traffic for WT and ST situations – but only until the wind direction changes. Afterward, it falls back to about half (ST) or roughly two thirds (WT) of its morning maximum. The corresponding delay in WT can be attributed to the fact that during this time of the year, the atmosphere is generally less unstable (Fig. 6), the wind is more often blowing from the east and the diurnal pattern is not established as well as during ST. With the wind direction changing to east again in the late evening, the scaled courses re-adapt to those of the traffic density and $F_{C(19)}$.

Similar behavior is shown for Saturdays (Fig. 8b), except that the wind already turns while the traffic is still increasing, leading to a stronger divergence of the courses. On Sundays (Fig. 8c) $F_{C(39)}$ shows almost no diurnal pattern and no significant statistical relationship with traffic (Fig. 9c) which is a result of the late increase in traffic just after the wind turn occurs and the decrease to low values right before the wind turns back before midnight. It is noteworthy that in ST, the highest fluxes occur between midnight and the early morning. This is on one hand due to higher nighttime traffic emissions and on the other hand due to the influence of vegetation uptake during the day which definitely has an effect on the reduced daytime fluxes during west wind situations. The area west of the site consists of a lot of green backyards and smaller, less frequented roads. ST $\tilde{x}_{h\min}$ on Saturdays and Sundays is therefore reached in the afternoon while all other minima of $F_{C(39)}$ happen to be between 3 and 6 CET in the early morning. The WT reduction of west wind affected $F_{C(39)}$ is generally lower for all days of the week because plant respiration is reduced and additional contribution of $CO_2$ emissions from heating takes place.

A wind direction dependent analysis of $F_C$ can be derived from Fig. 10. Here, the relative sectoral contribution is compared to the relative sectoral frequency of winds. For 39 m it depicts that there is a disproportionately high $F_{C(39)}$ from a broad easterly sector and lower $F_{C(39)}$ from western to northern directions. This underlines the relative importance of the Klingelbergstrasse as a $CO_2$ source and the comparatively lower emissions from the buildings, backyards and smaller streets in the west. At the top of the canyon it could be expected that the wind sectors contribute in equal measure to $F_{C(19)}$ as the only relevant underlying source is the traffic on the street. This assumption is true for the east hemicycle where relative $F_{C(19)}$ and wind direction frequencies are generally of the same size for each bin but not for fluxes falling together with winds from the western hemicycle. For wind directions from 220 to 270° relative $F_{C(19)}$ is comparatively higher and for 270–340° it is comparatively lower than would be expected when considering the frequency of those wind directions. This shift from perpendicular to the canyon axis (290°) toward a more oblique angle (20–70° instead of 90°) implies that the exchange of $CO_2$ from the street layer to the RSL is not only dependent on the general wind direction (e.g. from which hemicycle in relation to the canyon axis the wind is blowing). It can also be influenced to a great extent by only a few degrees of wind direction differences from perpendicular and exchange-restricting directions toward directions that obviously enhance vertical $F_C$ (For the influence of wind direction on vertical $CO_2$ distribution see Fig. 7 and description).

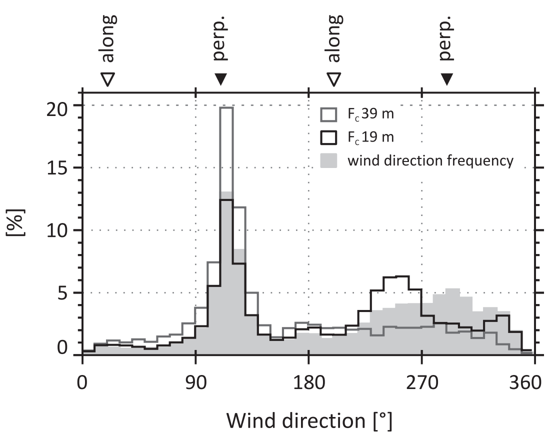


**Fig. 10.** Relative contribution of each 10° wind sector bin to total $F_{C(39)}$ (gray line) and $F_{C(19)}$ (black line) compared to the relative frequency of winds from each sector (gray shaded area). Wind direction is taken from 39 m for all cases. Perpendicular and along canyon directions are marked on top of the plot.

The explanation for this fact is not straightforward and is filled with some assumptions. Consulting Fig. 2 for this issue, it can be seen that different approaching angles of ISL winds generally classified as westerly lead to diametrically opposite directed in-canyon flows. 220–270° result in a northward turning 'corkscrew' flow inside the canyon and 270–340° in a southward turning one. One assumption is that for some reason the second case results in restricted vertical exchange rates due to the already mentioned lid-effect of the wind while in the first case, this lid-effect is not that strongly developed. On the other hand, the advective part of the vertical transport is probably bigger in the second case due to larger vertical inclination angles of the average wind vector (Figs. 3 and 4). Assuming that the total transport of $CO_2$ out of the canyon is more or less constant, a higher advective fraction may result in a reduced turbulent fraction and thus reduced $F_{C(19)}$. Additionally, the differences of the source areas inside the canyon may be of importance. The discharged air from the relatively close entrance to the large underground parking garage may be an additional $CO_2$ source during south wind cases. However, this contribution can not be quantified as it was not measured separately.

If the values for average $F_C$ for the year 2010 are compared to results from other urban studies that have been published, the 11.15 µmol $m^{-2}$ $s^{-1}$measured at 39 m rank among the first third and lie halfway between the maximum reported by Nemitz et al. (2002) and the minimum reported by Ramamurthy and Pardyjak (2011). Vogt et al. (2006) report 9.90 µmol $m^{-2}$ $s^{-1}$ for another site in Basel. This data was collected in June 2002 in a more densely built up area with less vegetation but also with less traffic. Yet this value is in accordance with the average ST $F_{C(39)}$of 9.85 µmol $m^{-2}$ $s^{-1}$ at the present site.

## 4. Summary and conclusions

The aim of this study was to gain more insight into the causes of the variability of $CO_2$ fluxes and concentrations within the roughness sublayer of an urban area and to link the data to processes associated with the diverse urban structure. For this purpose, field research was conducted in Basel, Switzerland, where processes in and above a street canyon were studied in detail.

The street canyon orientation (20°) is approximately perpendicular to the main wind directions. As a result, in-canyon air flow forms a vortex that shows a corkscrew-like lateral motion, the direction of which is dependent on the direction of the wind above. Eastern (90–130°) and western winds from less than 270° lead to northward flowing air masses inside the canyon whereas western winds from directions greater than 270° result in a southwards directed flow.

Daytime in-canyon distribution of *$CO_2$ concentration* depends heavily on this vortex structure. Western winds act as a lid on top of the canyon and lead to a vertically homogeneous distribution in the canyon center and an accumulation at the leeward wall with maximum concentrations at the upper half of that wall. For east wind situations, the vertical exchange from the canyon to the air above is unhindered, the concentrations at the center decrease with height and lower values are observed at the lower part of the upwind wall. Building heights and street canyon orientation relative to the dominating wind directions for a city thus play an important role in the removal process of $CO_2$ and pollutants from street level and are a determining factor for their in-canyon distribution.

Mean diurnal courses of $CO_2$ concentrations are comparable to that of other cities but spatial differences reveal some interesting patterns. Basically, the concentration level is coupled to the height of the urban boundary layer. Traffic as the dominant $CO_2$ source in the street canyon has only a relatively minor influence on absolute concentrations at all heights. However, traffic emissions result in a superimposed effect that is generally stronger closer to the ground. This fact is represented by the vertical differences between the bottom or top of the canyon and 39 m. They reflect the diurnal course of traffic density well and also allow for a clear distinction between working day and weekend courses.

In the case of *$CO_2$ fluxes* ($F_C$), traffic is the determining factor. Mean diurnal courses of traffic density and $F_{C(19)}$ have almost identical characteristics. In accordance with traffic density, $F_{C(19)}$ shows distinct working day/weekend differences and also the one hour shift in morning traffic increase between the Central European Summer- and Wintertime periods is clearly visible. Strong linear correlations support the assumption of a distinct relationship. We are well aware that $F_{C(19)}$ is measured in the RSL and the influence of individual roughness elements can not be avoided. A height dependency of turbulent fluxes in the UCL (Rotach, 2001) was expected and the sensor at 19 m was intended to capture the influence of the traffic of this busy street and to see how far up this influence reaches. The excellent qualitative agreement of the $F_{C(19)}$ flux patterns with the diurnal patterns of traffic confirms this approach and demonstrates the applicability of the EC method for such a specific purpose. Obviously sufficient mixing blends the traffic emissions to a representative flux.

Even at 39 m some parts of the diurnal pattern of $F_{C(39)}$ can be directly related to traffic density on the road below. At this height, the diurnal course strongly depends on wind direction and the related changes in source areas. Under east wind conditions, $F_{C(39)}$ shows a clear relationship to traffic density while under west wind conditions, it is comparatively reduced and influenced more by the source areas west of the site where less $CO_2$ emissions seem to be generated. Such an obvious determination through a directly underlying source was not expected as the source area for east wind conditions is supposed to extend a lot farther and to include a variety of other contributing sources. Investigations toward reliable source area determination in this heterogeneous urban area are thus a strong focus of the upcoming part in this project.

As a first consequence, it can be argued that urban $CO_2$ fluxes at a height of approximately $2z_h$ are extremely sensitive to the placement of the tower. A few tens of meters of horizontal displacement may lead to totally different diurnal regimes depending on prevailing wind directions combined with the given road and building orientation and configuration. For example, measurements on the other side of the road would probably have resulted in diurnal flux patterns with different traffic dependencies, i.e. lower nighttime and higher daytime fluxes, in relation to the observed wind direction dependencies.

The findings of this paper are derived from one of only a few direct and simultaneous long-term measurements in and above a real urban street canyon and may thus be of interest to other studies dealing with urban air quality. Also, the shown processes of venting or accumulation of $CO_2$ (as a representative for other, presumably more harmful substances) dependent on ambient wind direction and building configuration can probably meet different concerns of city planners on local air quality enhancements.

## Acknowledgments

This study was conducted in the framework of the EU FP7 Project BRIDGE (SustainaBle uRban plannIng Decision support accountinG for urban mEtabolism) and was partially funded through the CAPAC project of the MCR Lab of the University of Basel. Thanks go to the Basel City authorities for providing the year-long traffic record of Johanniterbrücke.

## References

Balczó, M., Gromke, C., Ruck, B., 2009. Numerical modeling of flow and pollutant dispersion in street canyons with tree planting. Meteorologische Zeitschrift 18, 197–206.

Baldocchi, 2008. "Breathing" of the terrestrial biosphere: lessons learned from a global network of carbon dioxide flux measurement systems. Australian Journal of Botany 56, 1–26.

Barlow, J.F., Harman, I.N., Belcher, S.E., 2004. Scalar fluxes from urban street canyons. Part I: laboratory simulation. Boundary-Layer Meteorology 113, 369–385.

Bergeron, O., Strachan, I.B., 2011. $CO_2$ sources and sinks in urban and suburban areas of a northern mid-latitude city. Atmospheric Environment 45, 1564–1573.

Burba, G., McDermitt, D.K., Grelle, A., Anderson, D.J., Xu, L., 2008. Addressing the influence of instrument surface heat exchange on the measurements of $CO_2$ flux from open-path gas analyzers. Global Change Biology 14, 1854–1876.

Burri, S., Frey, C., Parlow, E., Vogt, R., 2009. $CO_2$ fluxes and concentrations over an urban surface in Cairo/Egypt. In: The seventh International Conference on Urban Climate, 29 June–3 July 2009, Yokohama, Japan.

Caton, F., Britter, R.E., Dalziel, S., 2003. Dispersion mechanisms in a street canyon. Atmospheric Environment 37, 693–702.

Christen, A., Coops, N., Crawford, B., Kellett, R., Liss, K., Olchovski, I., Tooke, T., van der Laan, M., Voogt, J., 2011. Validation of modeled carbon-dioxide emissions from an urban neighborhood with direct eddy-covariance measurements. Atmospheric Environment 45, 6057–6069.

Coutts, A., Beringer, J., Tapper, N., 2007. Characteristics influencing the variability of urban $CO_2$ fluxes in Melbourne, Australia. Atmospheric Environment 41, 51–62.

Crawford, B., Grimmond, C., Christen, A., 2011. Five years of carbon dioxide fluxes measurements in a highly vegetated suburban area. Atmospheric Environment 45, 896–905.

DePaul, F.T., Sheih, C.M., 1985. A tracer study of dispersion in an urban street canyon. Atmospheric Environment 19, 555–559.

Feigenwinter, C., Vogt, R., Christen, A., 2012. Eddy covariance measurements over urban areas. In: Aubinet, M., Vesala, T., Papale, D. (Eds.), Eddy Covariance – a Practical Guide to Measurement and Data Analysis. Springer Atmospheric Sciences, p. 430.

Foken, T., Wichura, B., 1996. Tools for quality assessment of surface-based flux measurements. Agricultural and Forest Meteorology 78, 83–105.

Gartmann, A., Müller, M., Parlow, E., Vogt, R., 2011. Evaluation of numerical simulations of $CO_2$ transport in a city block with field measurements. Environmental Fluid Mechanics, 1–16.

George, K., Ziska, L., Bunce, J., Quebedeaux, B., 2007. Elevated atmospheric $CO_2$ concentration and temperature across an urban–rural transect. Atmospheric Environment 41, 7654–7665.

Grimmond, C., King, T., Cropley, F., Nowak, D., Souch, C., 2002. Local-scale fluxes of carbon dioxide in urban environments: methodological challenges and results from Chicago. Environmental Pollution 116, 243–254.

Grimmond, C., Oke, T., 1999. Aerodynamic properties of urban areas derived from analysis of surface form. Journal of Applied Meteorology 38, 1262–1292.

Grimmond, C.S.B., Salmond, J.A., Oke, T.R., Offerle, B., Lemonsu, A., 2004. Flux and turbulence measurements at a densely built-up site in Marseille: heat, mass (water and carbon dioxide), and momentum. Journal of Geophysical Research 109.

Gromke, C., Ruck, B., 2009. On the impact of trees on dispersion processes of traffic emissions in street canyons. Boundary-Layer Meteorology 131, 19–34.

Harman, I.N., Barlow, J.F., Belcher, S.E., 2004. Scalar fluxes from urban street canyons part II: model. Boundary-Layer Meteorology 113, 387–410.

Helfter, C., Famulari, D., Philipps, G., Barlow, J., Wood, C., Grimmond, C., Nemitz, E., 2011. Controls of carbon dioxide concentrations and fluxes above central London. Atmospheric Chemistry and Physics 11, 1913–1928.

Henninger, S., 2008. Analysis of near surface $CO_2$ variability within the urban area of Essen, Germany. Meteorologische Zeitschrift 17, 19–27.

Hoydysh, W., Dabberdt, W., 1988. Kinematics and dispersion characteristics of flows in asymmetric street canyons. Atmospheric Environment 22, 2677–2689.

Järvi, L., Nordbo, A., Junninen, H., Riikonen, A., Moilanen, J., Nikinmaa, E., Vesala, T., 2012. Seasonal and annual variation of carbon dioxide surface fluxes in Helsinki, Finland, in 2006–2010. Atmospheric Chemistry and Physics Discussions 12, 8355–8396.

Kanton Basel-Stadt, 2010. Zukunft Basel konkret – Bericht zur nachhaltigen Entwicklung Basel-Stadt 2010. Regierungsrat des Kantons Basel-Stadt.

Kastner-Klein, P., Plate, E.J., 1999. Wind-tunnel study of concentration fields in street canyons. Atmospheric Environment 33, 3973–3979.

Kordowski, K., Kuttler, W., 2010. Carbon dioxide fluxes over an urban park area. Atmospheric Environment 44, 2722–2730.

Matese, A., Gioli, B., Vaccari, P., Zaldei, A., Miglietta, F., 2009. Carbon dioxide emissions of the city center of Firenze, Italy: measurement, evaluation, and source partitioning. Journal of Applied Meteorology and Climatology 48, 1940–1947.

Moriwaki, R., Kanda, M., 2004. Seasonal and diurnal fluxes of radiation, heat, water vapor, and carbon dioxide over a suburban area. Journal of Applied Meteorology 43, 1700–1710.

Nemitz, E., Hargreaves, K., McDonald, A., Dorsey, J., Fowler, D., 2002. Micrometeorological measurements of the urban heat budget and $CO_2$ emissions on a city scale. Environmental Science & Technology 36, 3139–3146.

Oke, T.R., 1987. Boundary Layer Climates. Routledge, London.

Parshall, L., Gurney, K., Hammer, S., Mendoza, D., Zhou, Y., Geethakumar, S., 2010. Modeling energy consumption and $CO_2$ emissions at the urban scale: methodological challenges and insights from the United States. Energy Policy 38, 4765–4782.

Ramamurthy, P., Pardyjak, E., 2011. Toward understanding the behavior of carbon dioxide and surface energy fluxes in the urbanized semi-arid Salt Lake Valley, Utah, USA. Atmospheric Environment 45, 73–84.

Reid, K., Steyn, D., 1997. Diurnal variations of boundary-layer carbon dioxide in a coastal city – observations and comparison with model results. Atmospheric Environment 31, 3101–3114.

Rotach, M., 2001. Simulation of urban-scale dispersion using a lagrangian stochastic dispersion model. Boundary-Layer Meteorology 99, 379–410.

Rotach, M.W., 1995. Profiles of turbulence statistics in and above an urban street canyon. Atmospheric Environment 29, 1473–1486.

Salizzoni, P., Soulhac, L., Mejean, P., 2009. Street canyon ventilation and atmospheric turbulence. Atmospheric Environment 43, 5056–5067.

Salmond, J.A., Oke, T.R., Grimmond, C.S.B., Roberts, S., Offerle, B., 2005. Venting of heat and carbon dioxide from urban canyons at night. Journal of Applied Meteorology 44, 1180–1194.

Schotanus, P., Nieuwstadt, F.T.M., De Bruin, H.A.R., 1983. Temperature measurements with a sonic anemometer and its application to heat and moisture fluxes. Boundary-Layer Meteorology 26, 81–93.

Strong, C., Stwertka, C., Bowling, D.R., Stephens, B.B., Ehleringer, J.R., 2011. Urban carbon dioxide cycles within the Salt Lake Valley: a multiple-box model validated by observations. Journal of Geophysical Research 116.

Tanner, C.B., Thurtell, G.W., 1969. Anemoclinometer Measurements of Reynolds Stress and Heat Transport in the Atmospheric Surface Layer. University of Wisconsin Tech, p. 82. Rep. ECOM-66-G22-F.

UBA, 2012. Luftmessnetz des Umweltbundesamtes, Messstation Schauinsland. WMO Global Atmosphere Watch – World Data Centre for Greenhouse Gases. Federal Environment Agency Germany. Available at: http://ds.data.jma.go.jp/gmd/wdcgg/.

Vardoulakis, S., Fisher, B., Pericleous, K., Gonzalez-Flesca, N., 2003. Modelling air quality in street canyons: a review. Atmospheric Environment 37, 155–182.

Velasco, E., 2005. Measurements of $CO_2$ fluxes from the Mexico City urban landscape. Atmospheric Environment 39, 7433–7446.

Vogt, R., Christen, A., Rotach, M.W., Roth, M., Satyanarayana, A.N.V., 2006. Temporal dynamics of $CO_2$ fluxes and profiles over a Central European city. Theoretical and Applied Climatology 84, 117–126.

Webb, E.K., Pearman, G.I., Leuning, R., 1980. Correction of flux measurements for density effects due to heat and water vapour transfer. Quarterly Journal of the Royal Meteorological Society 106, 85–100.

Wilczak, J., Oncley, S., Stage, S., 2001. Sonic anemometer tilt correction algorithms. Boundary-Layer Meteorology 99, 127–150.

# P3 On the controlling factors for the variability of carbon dioxide flux in a heterogeneous urban environment

**Lietzke, B.**, Vogt, R., Feigenwinter, C. and Parlow, E. (2015):
On the controlling factors for the variability of carbon dioxide flux in a heterogeneous urban environment. *International Journal of Climatology*,
Article published online: 24 JAN 2015.

Available at http://dx.doi.org/10.1002/joc.4255

INTERNATIONAL JOURNAL OF CLIMATOLOGY
*Int. J. Climatol.* (2015)
Published online in Wiley Online Library
(wileyonlinelibrary.com) DOI: 10.1002/joc.4255

# On the controlling factors for the variability of carbon dioxide flux in a heterogeneous urban environment

Björn Lietzke,* Roland Vogt, Christian Feigenwinter and Eberhard Parlow

*MCR Lab, Department of Environmental Sciences, University of Basel, Switzerland*

**ABSTRACT:** Local heterogeneity of $CO_2$ sources and sinks is a key factor for the variability of carbon dioxide flux ($F_C$) in urban areas. Information on the urban structure around a site, especially the related emission characteristics, is thus of great importance to the understanding of observed $F_C$. Strong spatially confined sources like major roads inhibit a direct correlation of $F_C$ to area-averaged features of the urban structure and may lead to a heavily biased signal.

Four years of $F_C$ measured at Basel Aeschenplatz, Switzerland, are analysed with respect to the controlling factors and the cause for variability on different time scales. The source area is segregated into equal sectors to address heterogeneous emission patterns. Residential areas to the east are bordered by business areas and major roads to the west, which leads to a fundamental dependence of $F_C$ on wind direction. Besides, its diurnal course is explainable with traffic emissions while its annual course follows heating-related combustion emissions. Vegetation fraction is rather considered to be an indicator for urban land use types (residential/business) and the attributable emission characteristics than to be a measure for biological sink effects. Inter-annual variability occurs as a result of anomalies in wind direction patterns or air temperature. Average yearly $F_C$ is 16.4 μmol $m^{-2}s^{-1}$ with slight variations (±0.55 μmol $m^{-2}s^{-1}$) over the 4 years. It likely originates from an average of 70% traffic and 30% heating-related emissions with significant sectoral differences.

As a continuous measure for the emissions of each sector, the expected $CO_2$ flux ($eF_C$) per sector is introduced, leading to an enhanced comparability. Relating sectoral $eF_C$ instead of $F_C$ to urban surface fractions of buildings and vegetation results in a better agreement (also with data from other studies).

KEY WORDS carbon dioxide; long term flux measurements; eddy-covariance; urban; flux variability; controlling factors; gap filling; expected flux

*Received 19 December 2013; Revised 27 October 2014; Accepted 16 December 2014*

## 1. Introduction

### 1.1. Focus of the study

Recently an increasing amount of urban carbon dioxide flux measurements worldwide has contributed to the understanding of the role of cities in the global carbon cycle – with a broad range of findings (Table 1). The comparability between cities remains limited as the diversity of the sites is high: different climates, unequal site configurations and measurement periods and – probably most important – an innumerable variety of urban structures are only some of many factors that distinguish sites from each other. Attempts to standardize urban structure descriptions definitely enhance the comparability [e.g. classifications like Urban Climate Zones (UCZ, Oke, 2004) or Local Climate Zones (LCZ, Stewart and Oke, 2012)] but are often developed with a focus on a specific scope (e.g. temperature) and cannot account for all urban surface types and the differences in the resulting flux patterns. In this study, $CO_2$ flux ($F_C$) at a central urban flux station is analysed for its temporal behaviour and in relation to the varying urban structure and surface cover characteristics around the site. The focus is on identifying the controlling factors and source characteristics that determine the magnitude and the diurnal to yearly patterns of $F_C$.

Major $CO_2$ sources in cities are the different types of fossil fuel burning. The relative importance of soil and plant respiration as additional sources and photosynthesis as the only sink of $CO_2$ depends on the vegetation density, which is usually low in urban areas. The 'vegetation signal' is often heavily superimposed by anthropogenic emissions. The emitters are not homogeneously distributed in space and the temporal variation is high, thus the question as to where to place the measuring instruments to capture the representative carbon flux of a certain urban area is crucial. It is important to know the potential emission characteristics of the surroundings of the site, for example the locations of business districts, industrial areas, urban parks, residential areas or major roads. Spatially confined but strong and highly variable sources as the latter can have a decent influence on close-by measurements as Lietzke and Vogt (2013) show. Only with comprehensive information on the urban structure and urban land use/land cover (LULC) will an attribution of measured emissions to a certain area be defensible.

* Correspondence to: B. Lietzke, MCR Lab, Department of Environmental Sciences, University of Basel, Klingelbergstrasse 27, 4056, Basel, Switzerland. E-mail: bjoern.lietzke@unibas.ch

Table 1. Overview of different recent studies on urban $CO_2$ fluxes, sorted by averaged $F_C$ and showing site characteristics that influence $F_C$. An asterisk indicates that the $F_C$ data coverage was at least a whole year. Plan area fractions are $\lambda_b$ for buildings, $\lambda_g$ for ground (pervious and/or impervious) and $\lambda_v$ for vegetation. Traffic density $\upsilon$ is generally reported for one major road only and not an area average, except where noted.

| City | Code | Site/sector | Meas. height [m] ($z/z_h$) | Meas. period [MM/YY] | $\lambda_b$ [%] | $\lambda_g$ [%] | $\lambda_v$ [%] | $F_C$ [μmol $CO_2$ $m^{-2}s^{-1}$] | $\upsilon$ [veh $d^{-1}$] | Pop. density [inh. $km^{-2}$] | References |
|---|---|---|---|---|---|---|---|---|---|---|---|
| Edinburgh, Scotland | Ed00 | Calton Hill | 65 (6) | 11/00 | | | 20 | 26 | | 1724 | Nemitz *et al.* (2002) |
| Florence, Italy | Fl05 | Ximeniano | 33 (1.3) | 09–12/05 | 68.5[a] | 29.1 | 2.4 | 25.8 | 28300[b] | 3561[a] | Matese *et al.* (2009) |
| London, UK | Lo08 | BT Tower | 190 (22) | 10/06–05/08 | | | 8 | 25.58* | 76500[b] | 10000 | Helfter *et al.* (2011) |
| Florence, Italy | Fl11 | Ximeniano | 33 (1.7) | 03/05–06/11 | 68.5[a] | 29.1 | 2.4 | 21.83 | | 3561[a] | Gioli *et al.* (2012) |
| Basel, Switzerland | | Klingelbergstr. UCL | 19 (1) | 2010 | | | | 21.58* | 15000 | | Lietzke and Vogt (2013) |
| Marseille, France | Ma01 | Cour d'appel admin. | 43.9 (2.8) | 06–07/01 | 59.5[a] | 26.9 | 13.6 | 18.61 | | | Crawford *et al.* (2011); Grimmond *et al.* (2004) |
| Vancouver, Canada | Va10 | Sunset | 28.8 (5.3[a]) | 05/08–04/10 | 29 | 35 | 35 | 17.73* | 87000 | 4700 | Christen *et al.* (2011) |
| Basel, Switzerland | Ba13 | Aeschenplatz | 41 (2.5) | 06/09–06/13 | 35 | 38 | 27 | 16.35* | 30500 | 4300–8500 | this study |
| Bejing, China | Be08 | Urban Site | 47 (2.35) | 2008 | 65 | 12 | 23 | 14.85* | | 6533 | Song and Wang (2012) |
| Montreal, Canada | Mo09u | Urban site | 25 (3.2) | 11/07–10/09 | 27 | 44 | 29 | 14.7* | | 8400 | Bergeron and Strachan (2011) |
| Mexico City, Mexico | Mx06 | Escandon | 42 (3.5) | 03/06 | 57 | 37 | 6 | 13.41 | 41523[f] | 7412[a] | Velasco *et al.* (2009) |
| Beijing, China | Be09 | Urban Site | 47 (2.8) | 2006–2009 | | | 15 | 12.95* | | 1309 | Liu *et al.* (2012) |
| Helsinki, Finland | He11 | Hotel Torni | 60 (2.5) | 10/10–09/11 | 55 | 42 | 3 | 12.53* | 22000 | | Nordbo *et al.* (2012, 2013) |
| Basel, Switzerland | Ba10 | Klingelbergstr. ISL | 39 (2.3) | 2010 | 38.3 | 37.9 | 23.8 | 11.15* | 15000 | | Lietzke and Vogt (2013) |
| Basel, Switzerland | Ba02 | Sperrstrasse | 31 (2.2) | 06/02 | 54 | 30 | 16 | 9.9 | 2000 | | Christen (2005); Vogt *et al.* (2006) |
| Mexico City, Mexico | Mx03 | Iztapalapa | 37 (3.1) | 04/03 | 50[a] | 38 | 12 | 9.22 | 77490 | 12800 | Velasco *et al.* (2005) |
| Copenhagen, Denmark | | Whole city[c] | | 2001 | | | | 9.21* | | | Soegaard and Möller-Jensen (2003) |
| Tokyo, Japan | To02 | Kugahara | 29 (4) | 05/01–04/02 | 32.6 | 38.3 | 20.6 | 8.87* | 1.75[d] | 11800 | Moriwaki and Kanda (2004) |
| Lodz, Poland | Lo08 | Lipowa | 37 (3.4) | 07/06–08/08 | 30 | 40 | 30 | 7.78* | | | Offerle *et al.* (2005); Pawlak *et al.* (2011) |
| Helsinki, Finland | He08 | Kumpula | 31 | 07/07–06/08 | 14 | 40 | 46 | 6.95* | 50000 | | Järvi *et al.* (2009a, 2009b) |
| Cairo, Egypt | Ca08 | All Sectors | 35 (1.6) | 11/07–02/08 | 17 | 24.3 | 58.7 | 6.18 | | | Burri *et al.* (2009); Frey and Parlow (2010) |
| Melbourne, Australia | Me05 | Preston | 40 (6.3) | 02/04–06/05 | 45 | 17 | 38 | 6.12* | 29404 | 2940 | Coutts *et al.* (2007a, 2007b) |
| Münster, Germany | Mü06 | All Sectors | 65 (2.6) | 08–09/06 | 40[a] | 25 | 35 | 5.92 | | 926 | Schmidt *et al.* (2008) |
| Helsinki, Finland | He10r | Kumpula | 31 | 2006–2010 | 34 | 22 | 44 | 4.65* | 44000 | | Järvi *et al.* (2012) |
| Essen, Germany | Es07u | All Sectors | 26 (2.2) | 09/06–10/07 | 33 | 43 | 24 | 4.35* | | | Kordowski and Kuttler (2010) |
| Münster, Germany | Mü09 | All Sectors | 65 (2.6) | 07–09/09 | 40[a] | 25 | 35 | 4.2[b] | 0.62[b,e] | 926 | Dahlkötter *et al.* (2010) |
| Montreal, Canada | Mo09s | Suburban site | 25 (3.9) | 11/07–10/09 | 12 | 37 | 50 | 3.75* | | 2400 | Bergeron and Strachan (2011) |
| Chicago, USA | Ch95 | Suburban | 27 (4.3) | 06–08/95 | 36 | 25 | 39 | 3.67 | | | Grimmond *et al.* (2002) |
| Melbourne, Australia | Me04 | Surrey Hills | 38 (5.3) | 02–07/04 | 39 | 14 | 47 | 3.21 | 36993 | 2748 | Coutts *et al.* (2007a, 2007b) |
| Baltimore, USA | Ba06 | Club Hill | 41.2 (7.4) | 2002–2006 | 16 | 17 | 67 | 0.95* | | 1500 | Crawford *et al.* (2011) |
| Salt Lake Valley, USA | Sa05 | Murray | 35.9 (8.2) | 06–09/05 | 17 | 16 | 67 | 0.92 | | | Ramamurthy and Pardyjak (2011) |

Table 1. Continued

| City | Code | Site/sector | Meas. height [m] ($z/z_h$) | Meas. period [MM/YY] | $\lambda_b$ [%] | $\lambda_g$ [%] | $\lambda_v$ [%] | $F_C$ [μmol $CO_2$ $m^{-2}s^{-1}$] | $\upsilon$ [veh $d^{-1}$] | Pop. density [inh. $km^{-2}$] | References |
|---|---|---|---|---|---|---|---|---|---|---|---|
| Forests | | | | | | | 100 | −4.41 to −17.70* | | | Curtis *et al.* (2002); Valentini *et al.* (2000) |
| *Sites where sectoral data was published* | | | | | | | | | | | |
| Vancouver, Canada | Va10ne | Sunset, NE sector | 28.8 (5.3[a]) | 05/08–04/10 | 34.2 | 34.2 | 31.6 | 17.36* | | 4700 | Christen *et al.* (2010, 2011) |
| Vancouver, Canada | Va10se | Sunset, SE sector | 28.8 (5.3[a]) | 05/08–04/10 | 32.2 | 32.2 | 35.7 | 34.78* | 87000 | 4700 | Christen *et al.* (2010, 2011) |
| Vancouver, Canada | Va10sw | Sunset, SW sector | 28.8 (5.3[a]) | 05/08–04/10 | 34 | 34 | 32 | 11.39* | | 4700 | Christen *et al.* (2010, 2011) |
| Vancouver, Canada | Va10nw | Sunset, NW sector | 28.8 (5.3[a]) | 05/08–04/10 | 28.4 | 28.4 | 43.2 | 7.43* | | 4700 | Christen *et al.* (2010, 2011) |
| Helsinki, Finland | He10r | Kumpula, road sector | 31 | 2006–2010 | 29 | 30 | 41 | 9.25* | 44000 | | Järvi *et al.* (2012) |
| Helsinki, Finland | He10v | Kumpula, veg. sector | 31 | 2006–2010 | 35 | 15 | 50 | 2.3* | | | Järvi *et al.* (2012) |
| Helsinki, Finland | He06u | Kumpula, urban sector | 31 (1.6) | 12/05–08/06 | 42 | 51 | 7 | 6.11 | | | Vesala *et al.* (2008) |
| Essen, Germany | Es07v | Park Sector | 26 (2.2) | 09/06–10/07 | 14 | 36 | 52 | 0.8* | 6650 | | Kordowski and Kuttler (2010) |
| Essen, Germany | Es07u | Urban Sector | 26 (1.7) | 09/06–10/07 | 59 | 19 | 22 | 9.3* | 8600 | | Kordowski and Kuttler (2010) |
| Cairo, Egypt | | Urban Sector | 35 (1.6) | 11/07–02/08 | | | | 7.62 | | | Burri (2009) |
| Münster, Germany | | Urban Sector | 65 (2.6) | 07–09/09 | | | | 6.58[b] | 0.78[b,e] | 926 | Dahlkötter *et al.* (2010) |

[a]Source: Urban Flux Network (http://www.geog.ubc.ca/urbanflux/; accessed 14 October 2013). [b]Value estimated from figures or other information in the respective publication. [c]Calculated by assigning fluxes to land use types. [d]$10^6$ veh km $d^{-1}$. [e]$10^{-6}$ veh km $m^{-2}s^{-1}$. [f]Average of reported values.

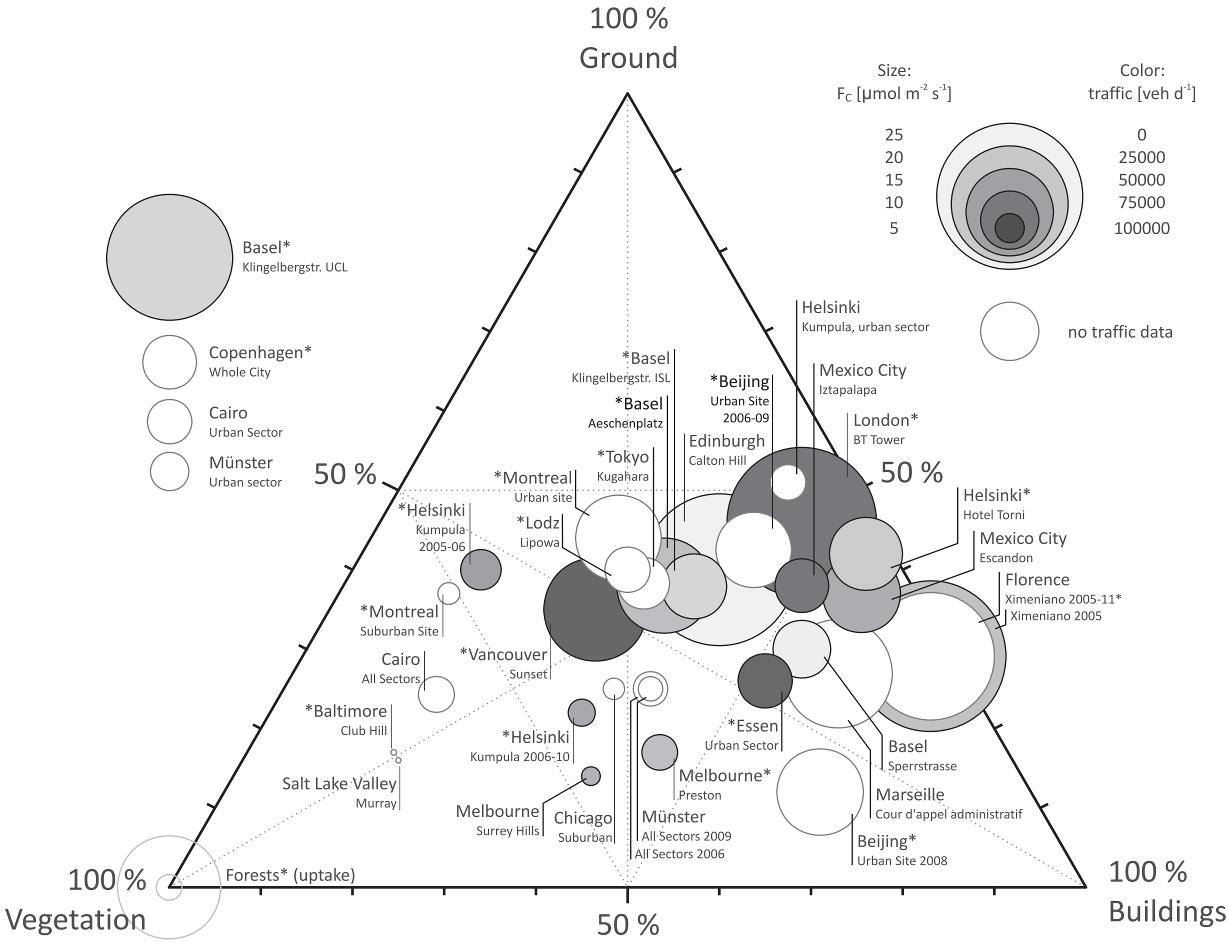


Figure 1. Results from the studies listed in Table 1 in a ternary plot. The centre point of each circle gives the plan area fractions. The size represents $F_C$ and the gray tone represents the reported traffic density $\upsilon$, if available in veh d$^{-1}$ (see legend). An asterisk indicates that the $F_C$ data coverage was at least a whole year. Where only vegetation cover was listed, the remaining fraction was assumed to be equally split between buildings and ground. For circles outside the plot no plan area fractions were reported.

## 1.2. Review of methods to determine urban sources of $F_C$

Carbon dioxide flux studies in cities are diverse as can be seen in Table 1. They range from suburban areas with high vegetation fractions ($\lambda_v$) and near zero average $F_C$ to central urban sites with high building fractions ($\lambda_b$) and small $\lambda_v$ where fluxes can exceed 20 µmol m$^{-2}$s$^{-1}$. Not even the greenest suburban areas in this world have revealed a negative $CO_2$ budget on average thus far. Even if some of the studies only cover a few weeks and not a whole year or more, long-time $F_C$ measurements (marked with an asterisk in Table 1) confirm this range. The surface fractions of an area definitely represent a basic indicator for the expected size of $F_C$ but only a weak dependency emerges when looking at the ternary plot in Figure 1. Fossil fuel emissions seem to have a strong influence (Christen *et al.*, 2011; Lietzke and Vogt, 2013). By comparing these studies one has to keep in mind that measurement procedures (e.g. measurement heights, tower locations, data processing) as well as determination and classification methods of surface characteristics have yet to be fully standardized and the methodological framework requires further development. Without standardized approaches, cross comparisons include a lot of uncertainties.

Investigations concerning the influence of different types of urban surface, especially vegetation, on $F_C$ at a certain site may, for example, be done by dividing the investigated area into land use sectors according to their vegetation fraction. Vesala *et al.* (2008) distinguish between a road ($\lambda_v = 30\,\%$), vegetation (85%), and urban (7%) sector in suburban Helsinki where road sector emissions are, on average, four times higher than vegetation sector emissions. But the urban sector does not show typical urban emission characteristics. Rather uncommon for urbanized areas, $F_C$ in winter is only slightly higher than for the vegetation sector and tends in summer, after a morning peak, to be zero or below.

Another approach to determine the influence of plant respiration on $F_C$ can be the use of proxy data, for example particle number flux (Nemitz *et al.*, 2008; Järvi *et al.*, 2009c; Dahlkötter *et al.*, 2010). Dahlkötter *et al.* (2010) quantify the contribution of vegetation for the city of Münster, Germany, by relating $F_C$ to particle number flux. Both are emitted through fossil fuel combustion but the latter is not affected by sink effects through photosynthesis. At night, $F_C$ is found to be a function of particle flux whereas during daytime $F_C$ is comparatively reduced due to vegetation activity.

Establishing relationships between inventory data and $F_C$ is generally a useful method to verify measurements and to identify sources. A fairly good agreement between inventory based flux calculations and measurements is found for Florence, Italy (Matese *et al.*, 2009). Based on observed traffic density, hourly gas consumption and estimated human respiration emissions, a period without domestic heating is compared to one with heating. For both periods the difference between estimated and measured fluxes is within 10%. A similar agreement is found by Christen *et al.* (2011) between source area weighted modelled emissions and measured $F_C$. At their suburban site (Vancouver, Canada) close to an intersection of major roads, transportation emissions accounted for 70%, building emissions for 27%, human respiration for 5%, and vegetation and soil activities accounted for an uptake of −2% of the measured flux.

Even higher values for traffic contribution are reported by Koerner and Klopatek (2002) and Vesala *et al.* (2008). With the help of GIS calculations based on inventory data, vehicle emissions were estimated by the first to account for 80% of the $CO_2$ input in the urban environment of Phoenix, USA. The latter concluded from a linear regression function between vehicle number and $F_C$ that the contribution of non-vehicle sources was only 5.5% for their traffic sector (where roads were clearly more dominant than at other urban sites).

The shares of different emitters of $CO_2$ on $F_C$ were estimated by several other measurement studies. For Edinburgh, Scotland, Nemitz *et al.* (2002) found a near linear relationship with a high correlation between traffic and $F_C$. They estimated traffic emissions to account for 41% of $F_C$. This is in relation to 52% for natural gas combustion, 7% for human exhalation, and only 1% for vegetation. Measurements were carried out in November so plant activity was low and domestic heating was higher than the yearly average. Winter fluxes that were, due to domestic heating, around two third higher than in summer were reported by Kordowski and Kuttler (2010) for Essen, Germany. For Copenhagen, Denmark, Soegaard and Möller-Jensen (2003) attribute summer to winter changes in traffic contribution (51%–39%) to increased heating. Dahlkötter *et al.* (2010) found the average contribution of traffic emissions in summer to be in a similar range as for winter in Edinburgh or Copenhagen, with 40% on weekdays and 28% on weekends. This in turn agrees well with the 39.5% during summer found by Helfter *et al.* (2011) during daytime in London, UK. Natural gas contribution in summer, spring (both 59%), and winter (71.1%) was higher than Nemitz *et al.* (2002) reported for winter, and only in fall was the share of natural gas about equal to traffic with 48.9%–47.8%.

While inventory based calculations of flux contributions rely on indirect approaches, direct insights in the sources of measured atmospheric $CO_2$ can be gained by analyses of its carbon isotope ratio (Clark-Thorne and Yapp, 2003). For Salt Lake City, a distinct annual cycle of approximately 60% natural gas combustion contributions in winter (at night-time) and negligible contribution in mid-summer was found (Pataki *et al.*, 2003). Because of higher biogenic respiration in summer, the proportional contribution of traffic emissions remained relatively constant throughout the year (Pataki *et al.*, 2007). Wintertime diurnal patterns varied from 60 to 70% of total anthropogenic $CO_2$ during evening rush hours to 30%–40% before dawn (Pataki *et al.*, 2006).

The spectrum of all these results reflects the variety of urban areas with respect to carbon dioxide exchanges. This variety and the different methods for the identification of $F_C$ sources again underline the difficulties of comparisons between cities and sites. As briefly discussed in Lietzke and Vogt (2013), methodical issues generated by the roughness of the structures also contribute to the uncertainties in urban flux experiments (Feigenwinter *et al.*, 2012). Surface cover, source characteristics, and the three dimensional and heterogeneous structures of urban areas affect vertical exchange processes of $CO_2$ between the urban surface and the urban boundary layer. The presence of a roughness sublayer (Oke, 2004) and the often reduced extent of the inertial sublayer (Rotach, 1999) lead to restrictions for the height of the sampling and in turn influences the spatial extent to which a measurement is representative (Raupach *et al.*, 1991; Grimmond and Oke, 1999).

The current study continues the tradition of urban climate studies at the Meteorology, Climatology and Remote Sensing Lab (MCR Lab) of the University of Basel. Preceding papers on the sites 'Basel Sperrstrasse' (Vogt *et al.*, 2006) and 'Basel Klingelbergstrasse' (Lietzke and Vogt, 2013) focused primarily on $CO_2$ exchange processes in and above a street canyon over periods of 1 month and 1 year, respectively. The latter revealed high variability of $CO_2$ fluxes, which raised questions concerning the representativeness of the flux for the surrounding urbanized area and the linking to the controlling factors for this variability. In respect to this, comprehensive analyses of 10 years of flux data are planned. The aim of the current study is to identify the controlling factors for the variability of $F_C$ at a second long term site with comparable characteristics of the surrounding urban structure (e.g. similar building heights and density). One of the main differences to the Klingelbergstrasse is that there is no single street canyon next to the site but rather an open place with twice as much traffic. This study will show that the spatial and temporal distribution of traffic and heating emissions, in combination with typical prevailing wind directions, result in typical site-specific patterns of $F_C$ that are different from what was found at the Klingelbergstrasse (Lietzke and Vogt, 2013). Another focus of this study is on data quality tests (Section 2.2) and statistical gap-filling (Section 2.2.3) which form the basis for the comprehensive analyses and lead to high data availability. Gap-filled data allows for estimating net ecosystem exchange values

 


Figure 2. Surface cover data for buildings (derived from a digital elevation model (DEM) provided by Basel city authorities) and vegetation [trees and lawns, derived from hyper-spectral data provided through the Hyper-Swiss-Net project (Koetz *et al.*, 2009)] for a radius of 1000 m around the site. Represented as an overlay is the average $F_C$ source area estimation for the whole data period. Contour lines give the areas of relative flux contribution to the measurement. The dotted raster has 100 m resolution centred on the site and the solid raster is the Swiss National Coordinate System. The nine wind direction sectors as addressed in the text are marked.

over the four investigated years and also for calculating equally weighted sectoral fluxes (Section 2.3) which help in estimating the total $CO_2$ emissions of the surrounding urban area and identifying the influence of the controlling factors.

## 2. Methods

### 2.1. Site and surroundings

#### *2.1.1. Site*

The urban flux site at Basel Aeschenplatz (7°35′44.17″E/ 47°33′4.42″N, 270.6 m a.s.l., see Figure 2 for a map of the surroundings) has been in operation since June 2009. It is the second long term flux station in Basel besides the site at the Klingelbergstrasse (Lietzke and Vogt, 2013) which is located about 1.6 km to the northwest. Measurements take part on top of the 'Turmhaus', Basel's first so called high-rise building built of concrete, constructed in 1930 right on eastern border of the Aeschenplatz.

Basel is a central European city located in the northwestern corner of Switzerland at the border to Germany and France. The administrative unit of the City of Basel covers an area of 23.9 km$^2$ and has an average population density of 7140 inhabitants km$^{-2}$. The area of the Canton of Basel is 37.0 km$^2$, which is 1.5 times the size of the city.

According to the city authorities (Lufthygieneamt beider Basel, personal communication) the $CO_2$ emissions within the area of the Canton of Basel were estimated to be 0.9 Mio tons per year in 2010. 58.5% resulted from stationary fossil fuel combustion (27.6% households, businesses, and services; 12.5% industry; 18.5% district heating), 22.0% from traffic and 19.3% from waste disposal (primarily incineration). Emissions by industry, district heating, and waste incineration are of no relevance in the vicinity of the measurement site.

Table 2. Average building heights ($z_h$ and $z_{h(t)}$) and surface fractions ($\lambda_v$: vegetated surface; $\lambda_b$: buildings; $\lambda_g$: impervious ground) within a radius of 500 m for nine different wind sectors (see Figure 2).

| Sector | $z_h$ | $z_{h(t)}$ | $\lambda_v$ | $\lambda_b$ | $\lambda_g$ | NEE [kgC m$^{-2}$y$^{-1}$] | | | | eNEE [kgC m$^{-2}$y$^{-1}$] | | | |
|---|---|---|---|---|---|---|---|---|---|---|---|---|---|
| | | | | | | 09/10 | 10/11 | 11/12 | 12/13 | 09/10 | 10/11 | 11/12 | 12/13 |
| 10°–50° | 14.7 | 13.2 | 32 | 32 | 36 | 0.17 | 0.22 | 0.20 | 0.14 | 4.73 | 4.77 | 4.70 | 4.72 |
| 50°–90° | 16.4 | 15.9 | 38 | 28 | 34 | 0.30 | 0.27 | 0.18 | 0.23 | 5.22 | 5.24 | 5.20 | 5.20 |
| 90°–130° | 13.9 | 13.9 | 39 | 28 | 33 | 1.51 | 1.43 | 1.21 | 1.40 | 4.15 | 4.15 | 4.06 | 4.10 |
| 130°–170° | 16.2 | 18.0 | 39 | 23 | 39 | 0.28 | 0.23 | 0.37 | 0.26 | 4.67 | 4.72 | 4.66 | 4.64 |
| 170°–210° | 14.1 | 18.8 | 35 | 33 | 32 | 0.23 | 0.16 | 0.21 | 0.21 | 5.24 | 5.26 | 5.20 | 5.21 |
| 210°–250° | 19.1 | 23.6 | 26 | 32 | 43 | 0.58 | 0.55 | 0.53 | 0.65 | 4.72 | 4.76 | 4.68 | 4.69 |
| 250°–290° | 15.8 | 15.4 | 11 | 52 | 37 | 1.20 | 1.30 | 1.46 | 1.32 | 7.37 | 7.43 | 7.29 | 7.29 |
| 290°–330° | 17.9 | 15.6 | 8 | 50 | 42 | 1.09 | 1.29 | 1.11 | 1.13 | 8.99 | 9.05 | 8.93 | 8.94 |
| 330°–10° | 15.7 | 14.4 | 19 | 39 | 42 | 0.96 | 0.95 | 0.78 | 0.61 | 7.27 | 7.30 | 7.22 | 7.23 |
| All sectors | 16.0 | 16.5 | 27.3 | 35.2 | 37.6 | 6.31 | 6.40 | 6.05 | 5.96 | | | | |
| Average $F_C$ [μmol m$^{-2}$s$^{-1}$] | | | | | | 16.67 | 16.91 | 15.95 | 15.76 | | | | |

NEE and eNEE are calculated from June to May of each year.

### 2.1.2. *Instrumentation*

The tower like Turmhaus building is oriented 20° to the west, with its 'northward wall' facing toward the Aeschenplatz at 340°. It has a rooftop terrace of 9.4 × 9.4 m 30 m above street level. At the centre, a smaller structure of four massive pillars supports a second terrace of 3.5 × 3.5 m at 35.5 m, with a flagpole on top. Almost at the top of this flagpole at 41 m above street level, a 3 m horizontal boom holds an Eddy Covariance (EC) system consisting of a LI-7500 open path gas analyzer and a CSAT3 ultrasonic anemometer on one side (340° orientation) and a CNR1 net radiometer on the other side (160°), each instrument at a distance of approximately 1.5 m to the flagpole. The LI-7500 is tilted 30° vertically to avoid the accumulation of droplets on its window and is mounted at a horizontal distance of 0.5 m from the CSAT3. Both measure at 20 Hz. Data is sampled with a CR1000 Campbell Scientific data logger and stored as raw data and as preliminary online calculated fluxes. Instruments are controlled and cleaned at least every second week.

### 2.1.3. *Structure and surface cover of the surroundings*

The Aeschenplatz is dominated by traffic: Individual motorized traffic, public transport trams and buses, pedestrians and cyclists have their interlaced pathways across the place. During rush hours (see Section 3.5.2. for diurnal traffic characteristics), stop and go traffic is common on the place and its six major access roads. Two of those roads (toward northeast and southwest) were built at the location of a former mediaeval city wall and are thus wider and have a park-like green space with mature trees in the middle (Figure 2).

The farther surroundings of the site consist of basically two different types of urban structures: First, to the west and north, it is densely built (LCZ compact midrise) with little vegetation and the area serves as the main business district for the city of Basel (4300 inhabitants km$^{-2}$). Behind the business district, starting at a distance of about 500 m to the northwest (330°), the old core of the city is also densely built with old and generally narrow buildings as well as newer business buildings (5530 inhabitants km$^{-2}$). The functional use of this central part of the city is a mix of business and residential, with shopping streets, museums, churches, and public open places. Second, to the east is a former middle to upper class housing area (LCZ open midrise to low-rise) with a lot of green backyards and gardens that extend for about 1 km (8490 inhabitants km$^{-2}$). About 500 m to the north the river Rhine flows through the city and 550 m SSW, the railway station 'Basel SBB' borders both the business and the housing area.

To allow for differentiated spatial analyses of $F_C$, the surroundings of the site were partitioned into nine sectors (Figure 2). Nine is a compromise between high spatial resolution and enough flux data from each sector. Table 2 shows the average sectoral building heights $z_h$ and $z_{h(t)}$ for each sector as well as the surface fractions of vegetated surface ($\lambda_v$), buildings ($\lambda_b$), and sealed ground surface or water ($\lambda_g$). $z_{h(t)}$ is $z_h$ relative to the base height of the Turmhaus, that is corrected for topography which varies approximately ±10 m within 400 m around the site. The gauge of the river Rhine, the lowest point, is 25 m below the base height.

Values in Table 2 are derived for a radius $r = 500$ m around the site from the data in Figure 2. The radius of 500 m is considered to give a solid representation of the area that is contributing to the flux measurements as sectoral $\lambda_v$ does not change considerably between 500 m and the 90%-contour line of the average flux source area (Figure 2, see Section 3.4). Additionally, the correlation between sectoral $\lambda_v$ and the 'expected NEE' (See Section 3.6) is found to be the best for this radius. The average corrected building height over all sectors is $z_{h(t)} = 16.5$ m and decreases with increasing radius ($z_{h(t)} = 13.7$ m for $r =$ 1000 m, Figure 3(a)). This indicates that the measurements at $z = 41$ m can presumably be considered to take place above the influence of the individual roughness elements ($> 2z_{h(t)}$). The few higher buildings (30–45 m) in the vicinity are located to the south and north of the site and affect the measurements only marginally as wind only occasionally blows from these directions (Figure 4). Average surface fractions are: $\lambda_v = 27$ %; $\lambda_b = 35$ %; $\lambda_g = 38$ %.

 

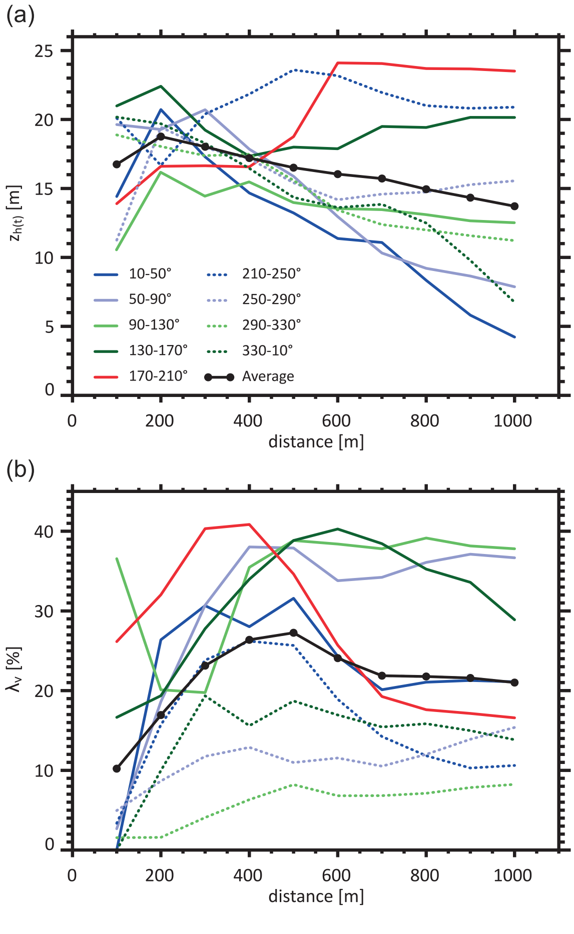


Figure 3. (a) Building heights ($z_{h(t)}$) and (b) surface fraction covered by vegetation ($\lambda_v$) as sectoral cumulative averages for radial 100 m distance intervals around Basel Aeschenplatz. The nine 40° sectors are marked on the map in Figure 2.

Highest $\lambda_v$ values are found between 50 and 210°, the lowest are between 250 and 10° with a minimum of only 8% for 190°–330°. With an increasing radius, average $\lambda_v$ slightly decreases toward 20% for $r$ = 1200 m (Figure 3(b)).

No clear relation has been found between surface cover and $F_C$ observed in various cities (Section 1.2, Figure 1). Nordbo *et al.* (2012) show an exponential dependence of $F_C$ on vegetation cover for a selection of the cities listed in Table 1. They also compare $F_C$ derived from GHG inventories to $F_C$ parameterized on the basis of vegetation cover derived from satellite measurements. Both relationships were found to be reasonable within uncertainty that can be expected due to the diversity of sites and methods (Nordbo *et al.*, 2012). Nevertheless, strong local sources in cities often do better explaining dynamics in carbon fluxes than vegetation cover fractions, as shown by Christen *et al.* (2011) or Lietzke and Vogt (2013).

An advantage of the present site is that it is, on the one hand, completely surrounded by 'average urban areas' and not affected by 'urban anomalies' like for example large open water areas, green spaces, or industrial areas. On the other hand, the differences in urban structure and surface fraction between the individual sectors (Figures 2 and 3) are distinct enough to allow for a spatially differentiated analysis with one single measurement system.

### *2.1.4. Wind patterns*

A narrow, predominantly nocturnal east–south–east sector and a broader western sector represent the dominant wind directions over the city of Basel [Figure 4, see also Lietzke and Vogt (2013) for a detailed description]. In a heterogeneous urban environment wind direction is a major determining factor for observed $F_C$. As the main wind sectors in Figure 4 can be clearly separated from each other we can roughly classify wind directions in an eastern (0°–180°) and western (180°–360°) hemicycle. The average diurnal course typically consists of nocturnal drainage flows from the Rhine valley in the east and west winds as the counterpart of the regional mountain-valley wind system during daytime [see Christen and Vogt (2004) for a topographic map]. This basic pattern occurs throughout the year and is generally better developed during summer than winter. As Basel lies in the mid-latitude west wind zone, synoptically induced winds contribute to the western sector.

### *2.1.5. Traffic density*

Unfortunately, no directly measured traffic data exists in the vicinity of the site, only modelled average daily vehicle totals for all main roads in Basel were available from the city authorities (Gesamtverkehrsmodell Basel, Hochbau- und Planungsamt Basel-Stadt [personal communication]). Thus, traffic density ($v_K$) from a parallel experiment (Lietzke and Vogt, 2013) 1.6 km away at the Klingelbergstrasse is taken as a rough indicative value and is scaled with a factor (the ratio of the average daily vehicle sums of the two roads, taken from the city authorities model) to represent traffic density at the Aeschenplatz ($v_A = 2.03 v_K$). The characteristics of the average diurnal courses are presumably similar, but at the Aeschenplatz more frequent traffic jams and stop-and-go traffic occur, especially during morning and evening rush hours. While, on average, a simple linear relationship between the amount of passing vehicles and the measured $CO_2$ flux is assumed, slower traffic may increase the emissions per vehicle. Even though on a cantonal basis stationary fossil fuel combustion has the highest share on $CO_2$ emissions (Section 2.1.1.), traffic is considered to be the dominant local short-term contributor to the $CO_2$ flux measurements at the Aeschenplatz site due to the high amount of passing vehicles, their proximity to the measurement site and the strong influence already found at the Klingelbergstrasse-site (Lietzke and Vogt, 2013).

### *2.1.6. Heating related combustion*

Due to the lack of adequate inventory data, the diurnal cycle of local heating-related combustion emissions and their contribution to measured $F_C$ cannot be estimated directly. Rather, Heating Degree Days [HDD, see e.g. Soegaard and Möller-Jensen (2003)] are analysed as a first

 

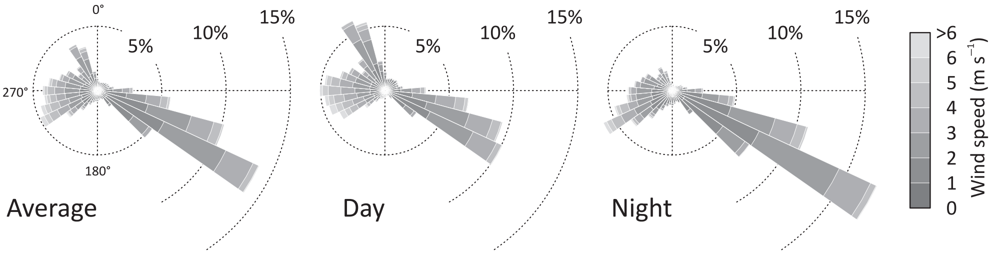


Figure 4. Wind direction frequencies and velocities at Basel Aeschenplatz for (a) all cases, (b) day-, and (c) night-time. Data is binned into 36 10°-classes.

order indicator, for example per month. HDD are simply calculated as the total of the differences between a desired room temperature $T_r = 20\,^\circ\mathrm{C}$ and the average daily air temperature $T_d$ for days where $T_d$ is less than 15°C. For the monthly sums, only days where HDD > 0 are included and only months with a total of HDD > 180 (in all years September to March plus April in 2010/13) are considered as heating months.

## 2.2. Data processing

The data presented in this paper covers four years from June 2009 to May 2013, with one larger data gap between November 2011 and March 2012 and another from November to December 2012 due to power problems at the site. Raw data are processed as blocks of 30 min. First Quality Control (QC) steps consist of the exclusion of instrument maintenance periods from raw data processing and the application of a physically reasonable range filter to each variable. $CO_2$ concentrations are excluded if the internal data quality control value (Automatic Gain Control) of the LI-7500 shows an obstruction of the path (precipitation, droplets, dust). No gap-filling is applied on raw data that is only considered for further processing if at least 75% of each half hourly data set are available.

An iterative despiking procedure is applied where 30 min blocks are temporarily detrended and spikes are removed until all values are within a range of $6\sigma$ (standard deviation). This is followed by a streamline rotation correction of the wind vectors (Section 2.2.1.) and subsequently the vertical wind component $w$ and the $CO_2$ concentration $c$ are detrended. Reynolds averaging is applied to calculate the covariances $\overline{w'c'}$ and they are then tested for stationarity (Section 2.2.2.). Sensible heat flux is corrected according to Schotanus *et al.* (1983) and then used to correct $F_C$ according to Webb *et al.* (1980) (WPL-correction). Data gaps in $F_C$ are finally filled as described in Section 2.2.3.

QC procedures can have strong effects on $F_C$ and have to be adapted to the specific data sets, the measurement location and conditions. They are thus not necessarily standardized between different research groups.

### 2.2.1. *Streamline rotation*

A basic requirement for the EC method is a horizontal wind field. As a consequence of non-zero vertical inclination angles of the 3D wind vector to the horizontal plane (represented through $\gamma = \arctan\left(w/\sqrt{u^2+v^2}\right)$, Figure 5(a)), the wind vector coordinate system is rotated to the average wind direction [2D streamline rotation, e.g. Tanner and Thurtell (1969)] for each half hour. This has the effect of setting the average lateral and vertical wind velocity, $\overline{v}$ and $\overline{w}$ respectively, to zero. In a homogeneous measurement environment $\gamma$ can be expected to show no dependence on wind direction – or a sinusoidal dependence if the sensor is not perfectly aligned with the horizontal wind field.

### 2.2.2. *Stationarity test*

It can be expected that non-stationary conditions occur more often over rough urban surfaces, where thermal convection is also increased, than over comparatively flat and more homogeneous surfaces. Carbon dioxide flux is tested for stationarity according to Foken and Wichura (1996) with the assumption that non-stationarity is given if the average of six consecutive 5 min covariance $(\overline{w'c'})$ estimates depart by more than 30% from the 30 min covariance of the same period. These data were removed.

### 2.2.3. *Gap-filling procedure*

For comprehensive analyses of $F_C$, especially to calculate annual carbon exchange rates, it is inevitable to fill gaps in 30 min $F_C$ data. Järvi *et al.* (2012) compare artificial neural networks (ANN, e.g. Schmidt *et al.* 2008) and median diurnal cycles (MDC), two typical methods for $F_C$ gap filling in urban areas, and found only small differences in the results. Similar to the MDC method tested by Järvi *et al.* (2012), missing $F_C$ data are replaced based on a set of MDC for the existing data where each cycle accounts for different conditions. MDC are calculated separately for: (1) working days and weekends; (2) each season (spring (MAM), summer (JJA), fall (SON), and winter (DJF)); and (3) nine wind sectors of 40° each (starting with 10°, see Figure 2). Cases where wind data is missing (15.3% in total, 8.5% and 3.2% caused by data gaps in winter 2011/12 and 2012/13, respectively) are replaced with data from the nearby site Basel Klingelbergstrasse. A running mean filter of ±3 adjacent values (including 7 values or 3.5 h) is applied to smooth the MDC. Finally, 72 individual MDC consisting of 48 values each are used as an inventory to replace missing $F_C$ data (44.2% after QC). Benefiting from the wind data from the Klingelbergstrasse, all gaps could be filled with the appropriate MDC values.

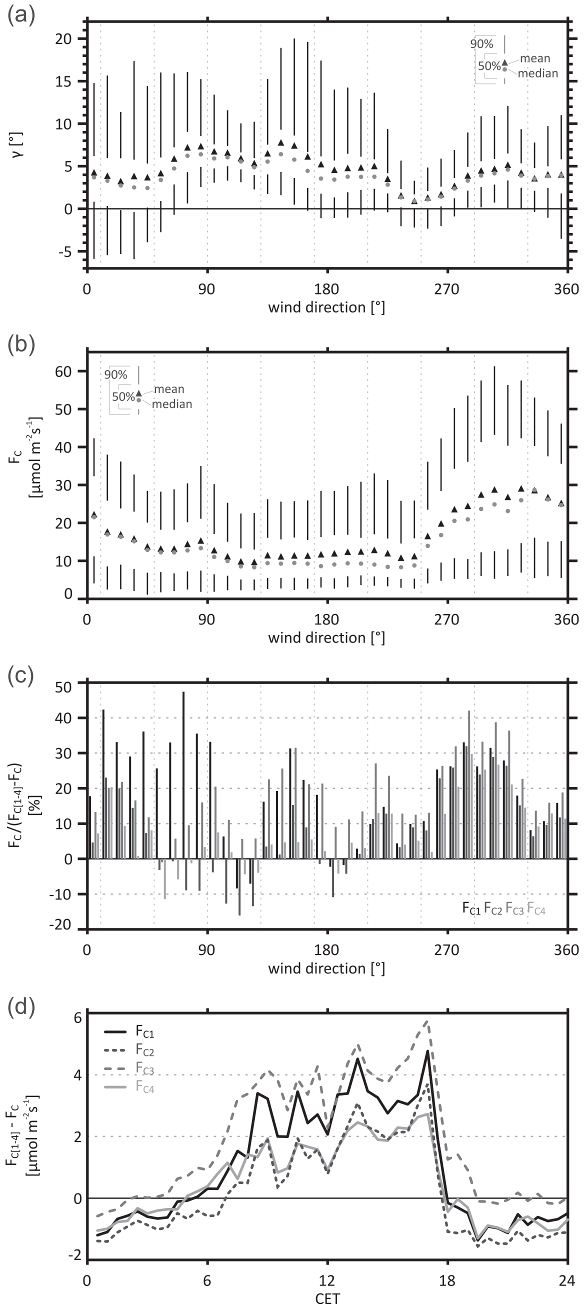


Figure 5. The effect of the individual QC procedures on $F_C$. In dependence of the ambient wind direction (10° bins) are shown: (a) the vertical streamline inclination angle $\gamma$, (b) final $F_C$, and (c) the relative difference of $F_C$ to the QC-steps ($F_{C1}-F_{C4}$) as referred to in the text. Dotted vertical lines mark the nine wind sectors (see Figure 2). (d) Shows the average diurnal course of the differences of the QC-steps to final $F_C$.

### 2.3. NEE and up-scaled sectoral $F_C$

Sectoral analyses of the carbon exchange rate require as much data as possible from each sector and ideally an equal representation of each sector in the overall data set. Wind direction frequencies are very different for the individual sectors (Figure 4), thus as an up-scaling method, sectoral data is temporally extended by the use of MDC. Similar to the calculation of the net ecosystem exchange rate (NEE), the up-scaled theoretically 'expected NEE' per sector (eNEE) is calculated. eNEE is thought to be a measure for the annual emission characteristics of a sector, that is what is expected to be measured if wind would constantly blow from that direction. It is derived by splitting $F_C$ into nine sectoral data sets and filling the missing values with MDC data for the respective sectors. This results in $eF_C$, the expected average $F_C$ for each sector and leads to the respective eNEE, both of them continuously available for the whole period. The average of all sectoral $eF_C$ is the average expected flux and the sum of all sectoral eNEE is the average expected eNEE, respectively.

$eF_C$ as an up-scaled measure is expected to give a more accurate average representation of the heterogeneous surroundings than $F_C$ as the latter represents only a patchwork of single, temporally restricted and wind direction dependent images of the surroundings. Nevertheless, relying on the MDC for calculating $eF_C$ for nine sectors implies that 8/9th of all $eF_C$ values are solely based on the MDC. Thus, an accurate determination of MDC is inevitable. Using the median instead of the mean might lead to an estimate of $eF_C$ that is too conservative.

### 2.4. Turbulent source area

$F_C$ at 41 m above street level depends to a great extent on direction and velocity of the wind, which, together with atmospheric stability, can give an impression of the source area or footprint of the measured signal. In an environment like a city, emission sources are not evenly distributed and can be considered as points (e.g. chimneys) or lines (e.g. roads) in space. These spatially confined sources have an extremely high share in urban $CO_2$ emissions compared to the actual area they cover. Thus it is important to know whether a certain, strong $CO_2$ source like for example a major road does or does not affect the measurements. Flux footprint calculations in urban areas may help in identifying important contributors and distinguishing between contributing surfaces types with different emission characteristics.

The applied source area model in this study is that of Kormann and Meixner (2001), a 2D gradient diffusion model accounting for crosswind dispersion, which was preferred to other models [see e.g. Vesala *et al.* (2008) for a recent review of footprint models] due to its relatively simple implementation (e.g. no mixing layer height needed) and the fact that it has been successfully used by other studies before (e.g. Christen *et al.*, 2011; Liu *et al.*, 2012; Salmond *et al.*, 2012). The model input parameters displacement height $z_d$ and roughness length $z_0$ were derived from the average building height $z_h$ within a radius of 500 m around the site ($z_d = 2/3z_h = 10.7$ m; $z_0 = 0.1z_h = 1.6$ m).

Individual source area calculations are run for each 30 min period by calculating the relative flux contribution on the basis of a 5 m grid over a domain of 2000 by 2000 m. $F_C$ is then weighted by the individual half-hourly source areas and aggregated to seasonal or annual average source areas. The four year average source area is shown in Figure 2.

## 3. Results

### 3.1. Data quality

To test the effects of the different QC procedures (Section 2.2) on $F_C$, intermediate $F_C$ versions (all including the WPL-correction and stationarity filter) are considered: before QC ($F_{C1}$), after despiking ($F_{C2}$), after streamline rotation ($F_{C3}$), after detrending ($F_{C4}$) and including gap-filling (final $F_C$). The relative effects in dependence on the ambient wind direction and the absolute effects on the diurnal course of $F_C$ are shown in Figure 5(c) and (d).

The streamline rotation correction (Section 2.2.1.) delivers the vertical inclination angle $\gamma$ (Figure 5(a)) that is neither uniform over all wind directions nor sinusoidally dependent. Thus, the flow field around the Turmhaus is – despite $z > 2z_{h(t)}$ – apparently influenced by individual surface roughness elements, for example by surrounding buildings or by the structure of the Turmhaus itself. Each 10° sector shows positive values for mean and median $\gamma$ which indicates that streamlines are, on average, directed upwards. The largest values are observed with wind blowing from 60 to 170°, lowest with wind from 230 to 270°. A dependence on the average building heights by sectors was not detected (Table 2). The minimum of $\gamma$ at 240°–250° (parallel to the northern wall) can be explained with the fact that the EC-System is not mounted exactly at the centre of the Turmhaus but almost above the northern wall where for these wind directions the wake effect of the western wall (resp. the vertical deviation of the streamlines) is supposedly less strong.

After applying previous QC procedures, non-stationary conditions (Section 2.2.2.) were found for 15.3% of $F_C$ (Table 3). Excluding them from further analyses leads to a reduction in $F_C$ availability from 71.1% to 55.8%. Table 3 shows the counts of non-stationary values for each year and for two other arbitrarily chosen levels of differences (60% and 90%).

While despiking reduces $F_{C2}$ on average to 95% of $F_{C1}$, the additional streamline correction again increases $F_{C3}$ to 105% of $F_{C1}$. The size of the corrections, however, is to a great part dependent on the ambient wind direction (Figure 5(c)). The relative influence of despiking ($F_{C1}$ to $F_{C2}$) is low for the western hemicycle and higher for the eastern with the greatest influence being between 60 and 100° and a ‘peak’ of more than 50% between 70 and 80°. Adding the streamline correction ($F_{C2}$) reduces the strength of this effect in this sector. Detrending ($F_{C3}$, 95% of $F_{C1}$) and gap-filling ($F_{C4}$, 88% of $F_{C1}$) both lead to a further reduction of average $F_C$.

Table 3. Frequency of $F_C$ (after QC, relative to the whole period) classified as non-stationary for the stationarity levels of 30%, 60%, and 90%.

| Year | Level of stationarity | | | Available $F_C$ | |
|---|---|---|---|---|---|
| | 30% | 60% | 90% | Before | After |
| 2009/10 | 15.5% | 6.0% | 3.6% | 77.9% | 62.4% |
| 2010/11 | 18.5% | 7.5% | 4.4% | 84.9% | 66.4% |
| 2011/12 | 12.8% | 5.6% | 3.6% | 54.4% | 41.6% |
| 2012/13 | 14.2% | 6.0% | 3.8% | 67.1% | 52.9% |
| Total | 15.3% | 6.3% | 3.8% | 71.1% | 55.8% |

Available $F_C$ gives the amount of available data before and after the applied 30%-stationarity-filter. Years are from June to May.

Figure 5(d) shows the diurnal course of the absolute differences of the separate QC steps $F_{C1-4}$ to final $F_C$. Despiking leads to a constant reduction, the streamline rotation augments the diurnal course over $F_{C1}$ and detrending results in a course that is, at night, similar in size to $F_{C1}$ and at daytime similar to $F_{C2}$. Gap-filling augments night-time flux and reduces average afternoon $F_{C4}$ by 2 μmol m$^{-2}$s$^{-1}$ or more. The maximum overall correction effect ($F_C$-$F_{C1}$) in the diurnal course is 4.8 μmol m$^{-2}$s$^{-1}$. Basic diurnal patterns are not changed by any of the corrections but the total effect on average fluxes or NEE values is distinct.

### 3.2. Diurnal courses of carbon dioxide flux

The average yearly $F_C$ of 16.4 μmol m$^{-2}$s$^{-1}$ is of similar size to what was measured at suburban Vancouver (Christen *et al.*, 2011), urban Beijing (Liu *et al.*, 2012) and urban Montreal (Bergeron and Strachan, 2011) and lies in the upper range of the published studies (Table 1). Other $F_C$ data for Basel are 11.15 μmol m$^{-2}$s$^{-1}$ for the Klingelbergstrasse in 2010 (Lietzke and Vogt, 2013) and 9.9 μmol m$^{-2}$s$^{-1}$ for the Sperrstrasse in June 2002 (Vogt *et al.*, 2006).

Typically, $F_C$ in urban areas shows cyclical variations at two different timescales: annual and diurnal. Both are driven by source and sink dynamics of combustion (stationary and mobile sources) and biological activity (respiration and photosynthesis). A good approach to assess exchange characteristics of the surroundings of the site is the examination of average diurnal cycles and their controlling factors. Annual and inter-annual variations can be analysed based on monthly averages. Average monthly diurnal cycles may provide further detail. In figures showing the diurnal courses of $F_C$, a general distinction between working days and weekends is made due to significantly different diurnal flux characteristics. Public holidays are also treated as weekend days (as in Lietzke and Vogt, 2013).

The basic characteristics of average diurnal $F_C$ at this site can be seen in Figure 6, where diurnal working day courses for Central European summertime (ST, CET + 1, last Sunday in March until last Sunday in October) and wintertime (WT, CET) are depicted. Similarities between the two courses are the low values during the night, a rapid increase in the morning, high values during daytime with a maximum in the late afternoon and a rapid decrease in the evening. No negative fluxes are observed in these average courses, which implies that the underlying urban surface is generally a constant net source of $CO_2$.

The mean diurnal patterns reveal a clear dependence on human activities (i.e. traffic) given the morning increase

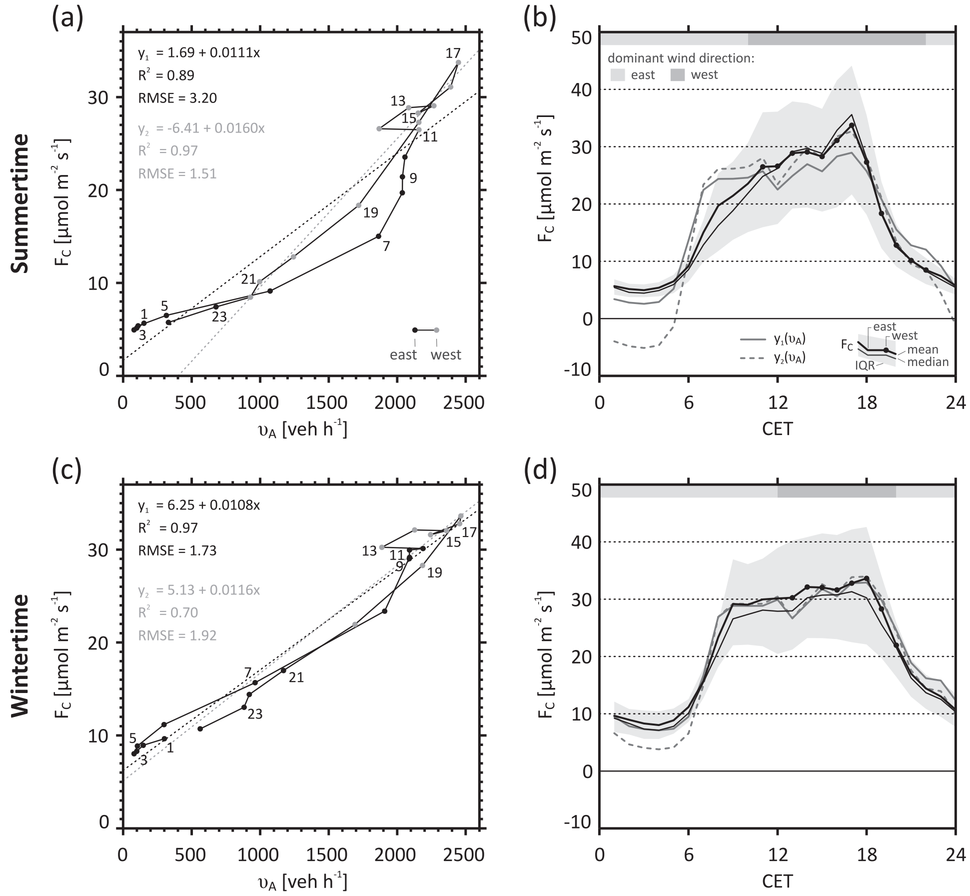


Figure 6. Average diurnal data (hourly mean) of $F_C$ and $\upsilon_A$ (vehicles per hour, data: 2010) for working days. (a,b) Summertime. (c,d) Wintertime. Left: $F_C$ as a function of $\upsilon_A$. The black line is the regression for all data points, the gray line is the regression for those times of the day where >50% of the wind originates from eastern directions. For the sake of clarity, only the odd hours of $F_C$ are labelled next to the data points. Right: Average diurnal courses of $F_C$ and of the functions $y_1$ and $y_2$ of $\upsilon_A$ (scaled traffic). The light gray bar at the top of each plot denotes >50% winds from eastern directions, the dark gray >50% from western directions. $F_C$ values measured under west wind influence are marked with black circles.

of $F_C$ shifts with changes from winter- to summertime. In ST (Figure 6(b)), night-time fluxes are lower, the morning increase is less rapid but the afternoon maximum is higher. WT $F_C$ (Figure 6(d)) has a steeper morning increase until 8 CET, followed by slightly increasing values until the afternoon maximum and the decrease in the evening. These differences are supposedly caused by seasonal source dynamics in the urban environment but also by variances of the local (diurnal) wind pattern (the dominant wind directions are depicted by the gray shaded bars), which will be analysed in the following sections.

### 3.3. Monthly diurnal courses and inter-annual variability

A more detailed image of the variability of $F_C$ evolves from Figure 7. Here, the average diurnal working day and weekend courses for each single month over the whole measurement period are shown. This allows not only for monthly comparisons but also for analyses of inter-annual variability. The already mentioned general characteristics for summer and winter months can be seen in most of the monthly courses. April to September and, to a certain degree, March show typical ST characteristics with a slow but steady increase toward a distinct maximum in the late afternoon. The lowest maxima of all summer months are often found in July due to lower traffic emissions during school holidays. Typical WT patterns such as a faster morning increase and a relatively constant $F_C$ throughout the daytime are visible in most of the courses from October to February.

Inter-annual variability over the considered years is low – in July for example, diurnal courses are almost congruent – but exceptions do occur. At night, when $F_C$ is at a low level, inter-annual differences are usually lowest. Higher variability is often observed during daytime. In November and December 2010 $F_C$ is at a remarkably higher level than for the other years. December has values that are up to 10–15 µmol m$^{-2}$s$^{-1}$ higher. The reason for these high fluxes and peculiarities of other months (e.g. the afternoon differences of more than 10 µmol m$^{-2}$s$^{-1}$ between August 2009/12 and 2010/11) are typically found in the diurnal course of the west to east wind ratio discussed in Section 3.5.

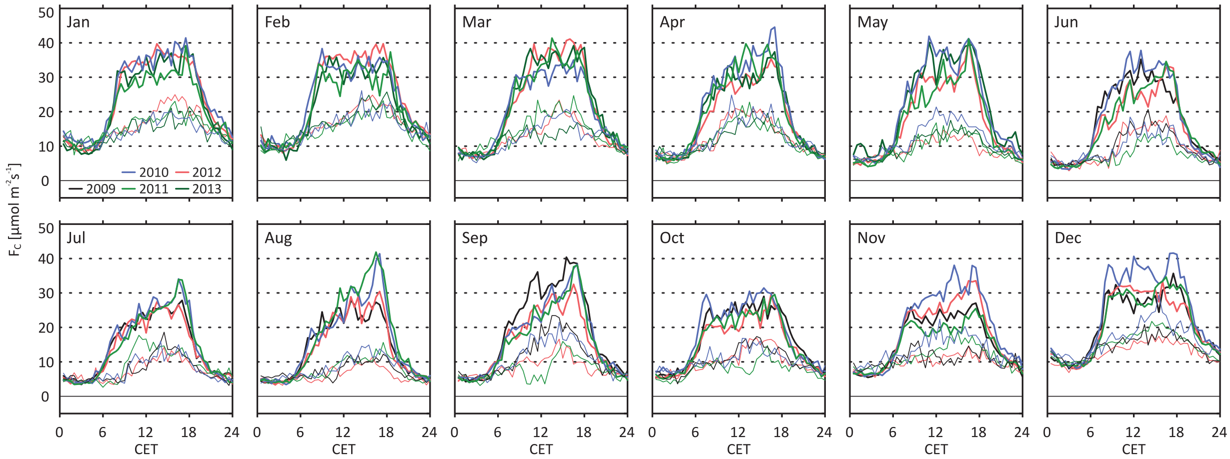


Figure 7. Monthly average diurnal courses of $F_C$ for the separate years. Thick lines are for working days, thin lines are for weekends.

## 3.4. Source area estimation

A calculation of the average source area of $F_C$ (Section 2.4) is shown in Figure 2. The shape of the contour lines reflects the average wind direction distribution (Figure 4) with the narrow ESE-sector and the broader western sector. In combination with the underlying map, it also gives an impression of how ideal the measurement site is to capture traffic emissions from the Aeschenplatz (to the west) and to distinguish between this sparsely vegetated (see $\lambda_v$ in Table 2) and extremely traffic dominated business area and a more densely vegetated residential area without major roads in the east where heating-related combustion is supposedly a more important $CO_2$ source than traffic.

In each direction, 50% of the flux originates within a distance of about 300 m or less. Enclosed by the western bulge of the 50% line lies the whole Aeschenplatz and about the first 100 m of its arterial roads to the west and north. The rest is covered by buildings and vegetation is restricted to some street trees. To the east, the bulge of the 50% line lies between the two eastern arterial roads and is only intersected by two barely frequented side streets (the closer one according to the 'Gesamtverkehrsmodell Basel' by 4800 veh d$^{-1}$, the second probably has less). Buildings are less dense and with distance from the site the vegetation fraction increases (Figure 3).

With the eastern source area sector often relevant during the night and the western during the day, combined with low $\upsilon_A$ at night and high $\upsilon_A$ during daytime, the source area calculations support the typical diurnal course of $F_C$ as for example depicted in Figure 6.

## 3.5. Controlling factors

### 3.5.1. *Wind*

The average diurnal course of the east to west wind ratio for each month is shown in Figure 8. While a good inter-annual persistence can be seen for most months, exceptions do occur which may have a remarkable influence on $F_C$ due to related source area variations. A good example is given by the month of August, which has the strongest diurnal amplitude in 2011 with less than 20% west wind cases in the early morning and up to more than 90% in the afternoon. August 2010 has a similar afternoon ratio but in 2009 and 2012 it is remarkably reduced. This unusually frequent east winds coincide with that time of the day when traffic emissions on the Aeschenplatz are highest (see Figure 6) and lead to decreased afternoon $F_C$ in 2009/12.

The contrary effect was detected in November and December 2010. Higher frequency of west wind throughout the whole day results in a stronger representation of the emissions from the Aeschenplatz in the $F_C$ signal, with the greatest influence at the time when $\upsilon_A$ is also high (Figure 6). Similar effects of the wind direction ratio can be seen in May (2010 and 2013) and September (2009). In both cases, more frequent west winds during the night and the morning result in temporarily higher $F_C$.

Substantial night-time differences in wind direction frequencies (Figure 8) between the years are observed in several months, for example from November to January and in May, June, and September. These differences have only a small effect on absolute $F_C$ as night-time $CO_2$ emissions are usually at a low level. Highest inter-annual variability and least pronounced diurnal changes are observed in the winter months, leading to high daytime differences in $F_C$ (e.g. in November where each year has a unique course).

### 3.5.2. *Traffic*

Figure 6(b) and (d) show the scaled average diurnal courses of working day $\upsilon_A$ for ST and WT. To make it comparable to $F_C$ it is plotted as a function of the regression equations derived from the respective scatter plots to the left. As a stronger dependence of $F_C$ on $\upsilon_A$ is expected for western wind directions, not only the overall regression $y_1$ but also the equation for west wind situations $y_2$ is used as a scaling function.

In ST (Figure 6(a)), the linear fit for west wind conditions $y_2$ shows a high correlation ($R^2 = 0.97$, RMSE = 1.51 µmol m$^{-2}$s$^{-1}$), while the overall fit is slightly worse ($R^2 = 0.89$, RMSE = 3.20 µmol m$^{-2}$s$^{-1}$).

 

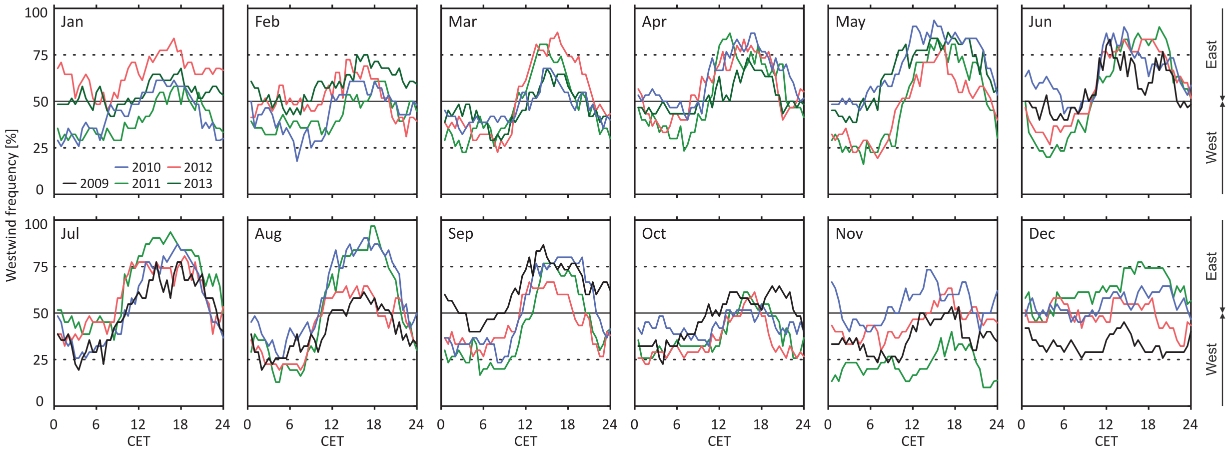


Figure 8. Relative frequency of west wind (180°–360°) as monthly average diurnal courses for the separate years. The area below a line represents west wind cases, the area above represents east wind cases. Missing cases were replaced with data from the Klingelbergstrasse.

Looking at the diurnal course, a general dependence of $F_C$ on $\upsilon_A$ (Figure 6(b)) is given, with a decent relationship under west wind dominance opposed by a more decoupled course under east wind situations. ST $F_C$ does not reflect the quick traffic increase in the morning due to higher east wind frequency.

The fit over all WT situations ($y_1$ in Figure 6(c)) is of similar statistical quality as for ST west wind situations ($R^2 = 0.97$, RMSE = 1.73 μmol m$^{-2}$s$^{-1}$). The whole diurnal course for $y_1(\upsilon_A)$ (Figure 6(d)) is therefore more or less congruent with $F_C$. At first this is surprising because east wind is more frequent in WT and traffic emissions to the east of the site are expected to be much lower than to the west. The reason for the congruency is that in WT (Nov–Mar), diurnal wind direction frequencies are more equally distributed than in ST (Apr–Oct) (Figure 8). In December for example, diurnal variations are small so the measured signal is assumed to be almost equally influenced by both wind direction sectors, hence a constant contribution of traffic emissions can be assumed. The almost similar regression equations for $y_1$ and $y_2$ are another indicator of weak diurnal wind direction changes.

The slope of the regression equations represents the average contribution of a vehicle to $F_C$ while the $y$-axis intercept can be interpreted as the summarized contribution of other, diurnally constant sources and sinks (e.g. Nemitz *et al.*, 2002; Soegaard and Möller-Jensen, 2003; Järvi *et al.*, 2012; Lietzke and Vogt, 2013). Consequently, the average share of $\upsilon_A$ on $F_C$ would be given by the average $F_C$ minus the $y$-axis intercept. In WT, the intercept ($y_1$: 6.25 μmol m$^{-2}$s$^{-1}$) can be clearly attributed to heating-related combustion emissions. In ST the night-time contribution (east wind) of $\upsilon_A$ and stationary combustion (no heating) is almost negligible, hence a great part of the night-time flux – at least the value of the intercept of $y_1$, as Figure 6(a) suggests – probably originates from sources like human or other biological respiration. Given the non-linearity of the function described by the points, this value might instead be closer to the lowest $F_C$ value shown in Figure 6(a). On the other hand, the regression $y_2$ for west wind dominated situations suggests a daytime sink effect through photosynthesis. $y_2$ gives a negative offset of −6.41 μmol m$^{-2}$s$^{-1}$ but is assumed to be an estimate that is too low as vegetation is rare to the west of the site ($\lambda_v$ less than 20%, compared to almost 40% to the east. See Table 2).

Measured $F_C$ is 1.4 to 1.5 times higher than at Basel Klingelbergstrasse. At both sites the diurnal course is primarily dependent on traffic emissions from close-by major roads, but, as opposed to the Aeschenplatz site, the Klingelbergstrasse lies to the east of the measurement site. In combination with the typical diurnal wind direction pattern for Basel, this often leads to remarkably lower afternoon $F_C$ (west wind) at the latter.

It can be summarized that on a diurnal basis, $\upsilon_A$ is clearly the dominant controlling factor for local $F_C$ and that this dependence is best expressed for persistent westerly winds in WT.

### 3.5.3. Heating-related combustion

In Figure 9(a), a good dependence of average monthly $F_C$ on HDD ($R^2 = 0.58$; RMSE = 1.51 μmol m$^{-2}$s$^{-1}$) is shown. To reduce the influence of $\upsilon_A$, cases are selected where its contribution to $F_C$ is considered to be low. By selecting a wind sector that does not include any major road and that is thus expected to have the lowest $\upsilon_A$ (90°–130°, Figure 9(b)), plus, assuming that photosynthesis effects can be ignored in the colder months, an indicative value for the influence of heating-related combustion activity from the respective sector on $F_C$ can be derived – on a monthly averaged basis. In Figure 9(b), one HDD (i.e. each degree that $T_d$ is below 15°C) results in an average increase of 0.019 μmol m$^{-2}$s$^{-1}$. The agreement is similar and leads, as could be expected due to lower $\upsilon_A$, to a smaller offset of 7.41 instead of 12.52 μmol m$^{-2}$s$^{-1}$ in Figure 9(a). Comparing only night-time cases (usually the lowest $\upsilon_A$ of the day, Figure 9(a)) shows a clear improvement of the fit ($R^2$ = 0.81; RMSE = 0.66 μmol m$^{-2}$s$^{-1}$) and an offset through other sources, supposedly traffic, of

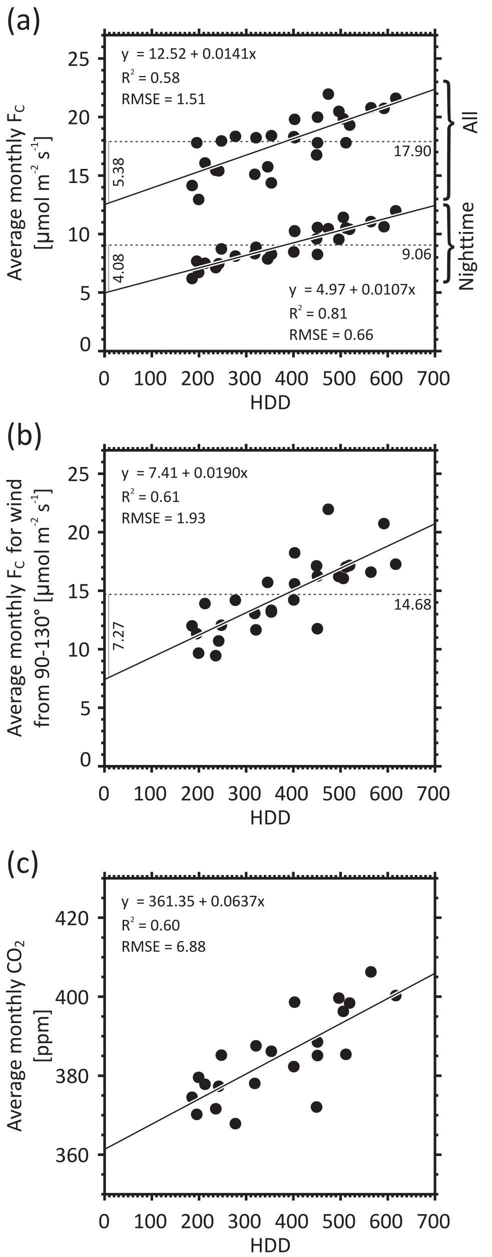


Figure 9. Average monthly $F_C$ (a,b) and $CO_2$ (c) in relation to total monthly HDD. Only heating months are depicted. Average $F_C$ is marked as a dotted line and the difference of the average to the *y*-axis intercept is depicted by the thin vertical line. Both are labelled with their value in μmol m$^{-2}$s$^{-1}$. Lower dots in (a) are night-time cases (ST 24–5 CET and WT 1–6 CET) when $\upsilon_A$ is less than 400 veh. h$^{-1}$ (Figure 6(a) and (c)). Figure (b) is for the 90°–130° sector where traffic emissions are supposedly lower.

4.97 μmol m$^{-2}$s$^{-1}$. Thus, neither for this sector with lowest traffic counts nor for night-time cases with overall reduced emissions from transport does the impact of traffic density on $F_C$ vanish.

The good agreement of monthly average $CO_2$ concentrations (Figure 9(c)) with HDD depicts a clear dependence. In Figure 10 the seasonality of $F_C$, $CO_2$, HDD, air temperature $(1 - T_A)$ and $\upsilon_A$ is compared over four years. Monthly average background $CO_2$ concentrations, measured at the Global Atmosphere Watch (GAW) regional station Schauinsland, Germany [a rural station about 46 km to the north at 7.92°E, 47.90°N, 1205 m a.s.l; data provided by UBA (2012)], exhibit a slightly delayed course compared to concentrations measured at the Aeschenplatz. Annual minima and maxima are generally shifted by about one month at the GAW station due to the higher altitude and remoteness of the station.

The scaled courses of the monthly averages of $F_C$, $CO_2$, HDD, and $1 - T_A$ are relatively smooth and congruent and depict clear annual cycles that are related to each other. December 2010 and February 2012 are cold months with high HDD, $CO_2$, and $F_C$, December 2011 and March 2012 have relatively warm periods with lower HDD, $CO_2$, and $F_C$. The deviations observed for $F_C$ are a result of unusual wind direction distributions in the respective months, resulting in comparatively higher or lower fluxes as shown by the monthly average diurnal courses (Section 3.3). Peaks occur in September 2009 and August 2011 and lower values in October and November 2011. Average $F_C$ in January 2010 and 2012 is higher than in 2011/13, the first as a result of colder temperatures and thus in agreement with the other courses, the latter due to more frequent west wind, hence standing out from the others.

$\upsilon_A$ follows no regular seasonal pattern but shows a slightly overall declining trend. It contributes a constant basic share to $F_C$ on this time scale. Thus, HDD – or combustion due to space heating, respectively – is considered to be the main controlling factor for the seasonality of $F_C$ (as e.g. in Matese *et al.*, 2009; Bergeron and Strachan, 2011; Helfter *et al.*, 2011), superimposed by occasional anomalies due to exceptional wind direction frequencies.

### *3.5.4. Vegetation*

The sector-averaged eNEE (Figure 11) correlates well with $\lambda_v$, but its dependence on $\lambda_b$ has similar correlation values. It is therefore not evident if it is either the relative presence of vegetation or the relative absence of buildings that has a reducing effect on observed $F_C$, and vice versa. Photosynthesis is expected to have a distinct effect, primarily in the vegetated period (approximately Mar/Apr–Sep/Oct) during daytime. However, the observations show particularly high fluxes during this time (except in July, when traffic is reduced due to school holidays) with average diurnal $F_C$ maxima (Figure 7) even exceeding those during most winter months. This can be explained by wind direction dependence detected in August 2009 (Section 3.5.1., Figure 8). Daytime wind from areas with a higher $\lambda_v$ (east) are simply too rare in summer to let vegetation have a noticeable reducing influence on $F_C$. This is supported by the analyses in Section 3.6.

## 3.6. NEE and up-scaled sectoral $F_C$

Table 2 lists the yearlong sums of NEE from June to May, while the temporal evolution over these periods is shown in Figure 12(a). 2010/11 is the year with the highest NEE, mainly caused by higher $F_C$ during Nov/Dec. NEE

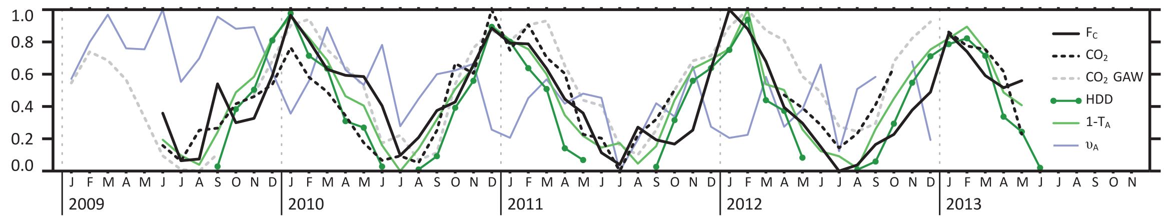


Figure 10. The seasonality of the monthly averages of $F_C$, $CO_2$ concentration, HDD, air temperature ($1-T_A$), and $\upsilon_A$, all normalized by their maximum and minimum value (set to 1 and 0, respectively). Atmospheric background $CO_2$ concentration ($CO_2$ GAW) is given as a reference. Data gaps in $T_A$ were filled with values from the Klingelbergstrasse [see Lietzke and Vogt (2013) for a site description].

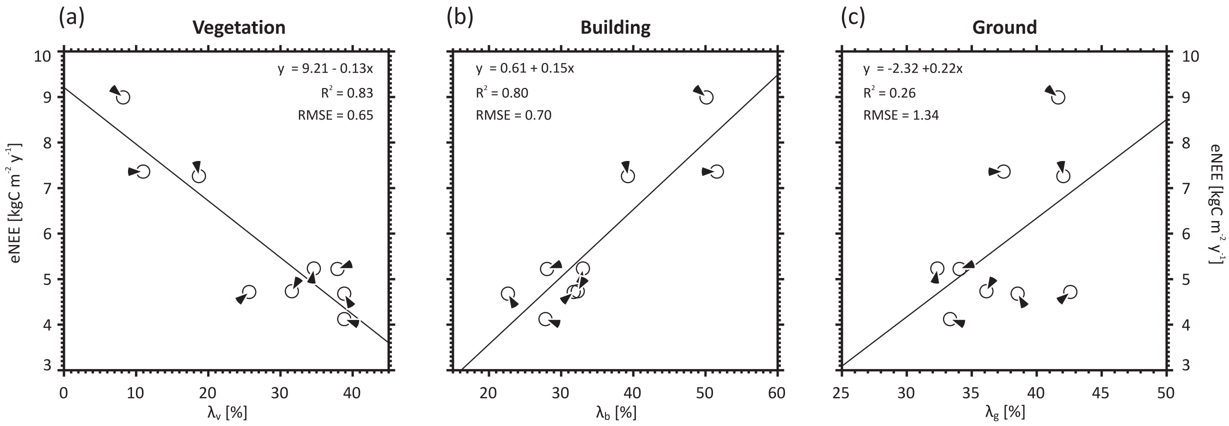


Figure 11. Yearly average eNEE as a function of sectoral surface cover fractions (500 m radius) for (a) $\lambda_v$, (b) $\lambda_b$, and (c) $\lambda_g$. Sectors are depicted as part of the markers.

differences between the sectors and the years (Table 2) can be greatly attributed to the frequency of wind from the sectors, thus eNEE enhances the comparability of the sectors.

As already mentioned (Section 2.3), using median instead of mean diurnal cycles might lead to a much too conservative estimate of $eF_C$ (and eNEE, consequently) which is with 10.9 μmol m$^{-2}$s$^{-1}$ on average 5.5 μmol m$^{-2}$s$^{-1}$ lower than $F_C$.

The patterns shown in Figure 12(b) are sectoral eNEE rates minus the average NEE rate from Figure 12(a). We can assume comparatively small annual $\upsilon_A$ variations within a sector and thus a constant contribution to eNEE. Combustion activity due to space heating leads to a stronger increase during winter and plant activity to a reduced increase in the summer months. A relatively constant course (e.g. for 330°–10°) can consequently be interpreted as being dominated by traffic emissions while a more undulated course (e.g. for 50°–90°) represents a sector where traffic emissions are less dominant and/or overprinted by seasonally variable sink and source effects due to vegetation activity and other combustion emissions, respectively. It is thus not surprising that Table 2 shows high eNEE for sectors with low $\lambda_v$ and vice versa.

It is not primarily the biological activity expressed through $\lambda_v$ that is crucial for NEE but the characteristics of $CO_2$ emissions that are coupled to $\lambda_v$ through the presence or absence of other urban structures. $\lambda_v$ can be taken as an indicator for local urban land cover and the attributable emission characteristics and may have indirect links to other factors determining $CO_2$ release (Nordbo *et al.*, 2012). In this study, higher $\lambda_v$ represent residential areas (low $\upsilon_A$, higher heating-related combustion activities, more plant activity) and lower $\lambda_v$ represent business areas (higher $\upsilon_A$, lower heating-related combustion, less plant activity).

Combining $F_C$ and $\lambda_v$ data from this study (Figure 12(b)) with data from literature (Table 1) to Figure 13 shows that average $F_C$ and its sectoral components are among the higher values. All sectoral $F_C$ data of the Aeschenplatz lie above the regression through literature studies of one year or longer ($y_1$) whereas sectoral $eF_C$ values agree with $y_1$. There is also a good agreement of sectoral $eF_C$ with $\lambda_v$ (expressed by $R^2$ for the regression $y_3$). The extreme biassing influence that strong local point or line sources may have can be seen in the sectoral data for Vancouver, Canada (Va10). This site was heavily influenced by traffic emissions from the SE sector. The influence of single sectors is also distinct for Essen, Germany (Es07), or Helsinki, Finland (He10), where strongly vegetated areas reduce the ‘urban character’ of the sites.

Similar to sectoral data, studies that are restricted to time scales of less than a year provide only a temporally limited image of their source area and thus have restricted comparability. When looking at the open symbols in Figure 13 and assuming that $F_C$ is usually highest in winter and lowest in summer, yearlong measurements for sites where now only temporally limited data are

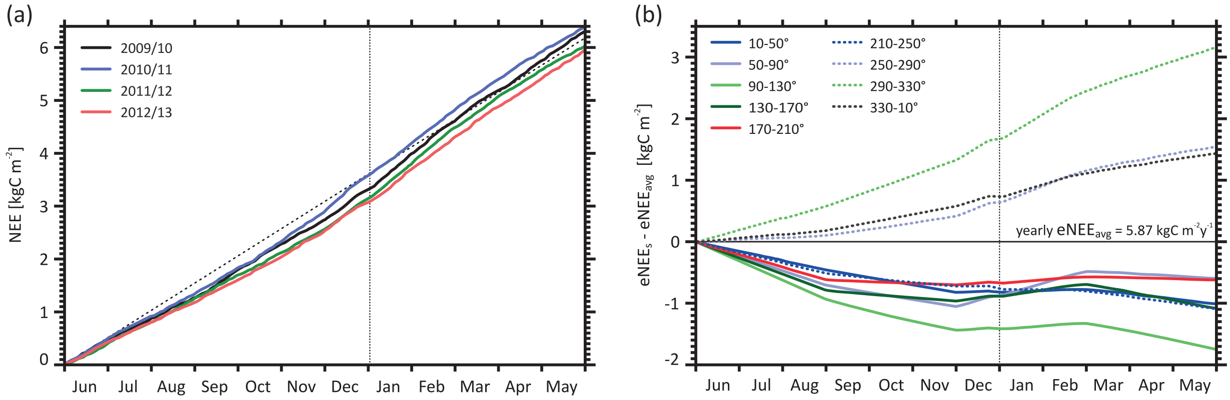


Figure 12. Temporal evolution of (a) NEE for the separate years and (b) the difference of average sectoral eNEE (eNEE$_s$) to a constant overall average eNEE increase (eNEE$_{avg}$). The dotted line is New Year's Day, the dashed line (a) and the 0-line (b) represent NEE$_{avg}$ and eNEE$_{avg}$, respectively.

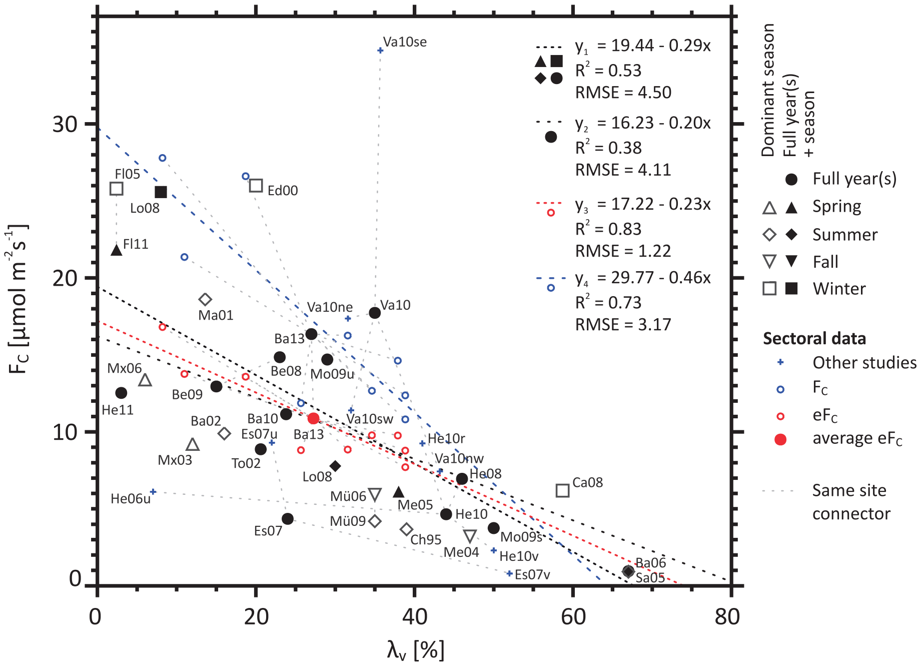


Figure 13. Average $F_C$ as a function of $\lambda_v$ for international studies (see Table 1 for abbreviations). Open symbols are according to the season the data was measured. Filled circles represent measurements of one or more full years, all other filled symbols stand for full years plus an additional part of the respective season. Sectoral average $F_C$ and $eF_C$ (derived from eNEE, same data as in Figure 11(a)) of this study are denoted by the small open circles. Regression equations ($y_1$-$y_4$) are for the respective groups of data as labelled. Other dashed lines connect different results from one single site (e.g. for sectors or years) and show site-specific variability.

available would probably move most of them closer to the regression line $y_1$ (as shown by Fl05 and Fl11).

## 3.7. Flux composition

As described in Section 3.5.2., a statistical fit of $F_C$ to an environmental driver or its indicator allows for splitting of the latter into a driver determined part and an offset through other sources. Doing this for different subsets (ST/WT, working days/weekends) of $\upsilon_A$ and HDD results in the values given in Table 4.

The most useful and reliable period for the comparison are working days (higher data availability than for weekends) during WT (heating-related combustion negligible in ST). The fitted traffic and HDD data both lead to a $F_C(\upsilon_A)/F_C(HDD)$ ratio of 70/30, suggesting that 100% of $F_C$ is explainable with the two contributors. For WT weekends the ratios are not in accordance, but $F_C(\upsilon_A)$ is definitely lower than for working days and $F_C(HDD)$ might be higher due to increased heating. The effects of photosynthesis, biological respiration, and other emissions have individual temporal characteristics and interfere with $F_C(\upsilon_A)$. This makes the ST ratios less reliable but $F_C(\upsilon_A)$ is comparable to WT for working days and weekends, which can be expected since $\upsilon_A$ is, on average, merely constant throughout the year.

 

Table 4. The contribution of traffic density ($\upsilon_A$) and heating-related combustion (HDD) to $F_C$ separated by ST/WT and working days (WD)/weekends (WE).

| Period | | $\overline{F_C}$ | Contributor | Regression intercept results for | | Difference |
|---|---|---|---|---|---|---|
| | | | | $\upsilon_A$ vs. $F_C$ | HDD vs. $F_C$ | |
| WT | WD | 21.2 | $F_C(\upsilon_A)$<br>$F_C(HDD)$ | 15.0 (70.6)<br>6.2 (29.4)<br>*0.97, 1.73* | 14.7 (69.2)<br>6.6 (30.8)<br>*0.20, 4.81* | 0.31 (1.4) |
| | WE | 13.9 | $F_C(\upsilon_A)$<br>$F_C(HDD)$ | 6.2 (44.7)<br>7.7 (55.3)<br>*0.90, 1.06* | 3.8 (27.3)<br>10.1 (72.7)<br>*0.20, 2.66* | 2.42 (17.4) |
| ST | WD | 17.1 | $F_C(\upsilon_A)$<br>other | 15.4 (90.1)<br>1.7 (9.9)<br>*0.89, 3.2* | | |
| | WE | 9.5 | $F_C(\upsilon_A)$<br>other | 6.1 (64.8)<br>3.3 (35.2)<br>*0.90, 1.04* | | |

$\overline{F_C}$ is the average $F_C$ for each period. The size of the contributions is calculated with the regression intercept method as described in Section 3.5.2. HDD regression values are calculated from daily values (no figure). $\upsilon_A$ regressions for WD are derived from Figure 6, whereas WE cases are not shown. $F_C$ unit is μmol m$^{-2}$s$^{-1}$, values in brackets are relative to $\overline{F_C}$ and numbers in italics are $R^2$ and RMSE. Differences in the results of the two comparisons are given absolute and relative to $\overline{F_C}$.

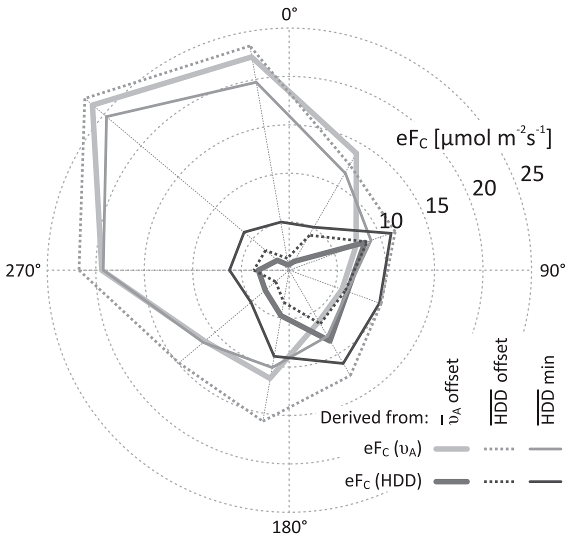


Figure 14. Contribution of $\upsilon_A$ and HDD to sectoral $eF_C$ (for working days), derived from linear regressions for each sector between both parameters and $F_C$ as described in Section 3.6.

A spatially differentiated image is achieved by expanding this method to sectoral $eF_C$ (not shown). In these comparisons $\upsilon_A$ is not valid for all sectors but its diurnal course serves as a good qualitative indicator. For HDD the *y*-axis intercept (HDD offset) as well as the summer month with the lowest $F_C$ (HDD min) are used. The resulting shares on $eF_C$ (Figure 14) exhibit a clear domination of $eF_C(\upsilon_A)$ for west and north sectors (Aeschenplatz) with a maximum from the northwest. The pattern changes for east to south sectors (residential area) where minimum $eF_C(\upsilon_A)$ is found and – dependent on the method – $eF_C(HDD)$ is of similar magnitude or slightly higher.

Averaging the results of all three methods shown in Figure 14 – $\upsilon_A$ offset, HDD offset, and HDD min – leads to shares of 73% for $eF_C(\upsilon_A)$ and 27% for $eF_C(HDD)$ which agrees with the shares for WT working days in Table 4. The discrepancy to the inventory data for the whole canton (Section 2.1.1.), where the share of combustion by households, businesses, and services is 27.6% and of traffic 22%, shows that at the local scale traffic emissions are comparatively important.

The 70/30% ratio coincides with the 70/27% ratio found by Christen *et al.* (2011) for Vancouver, Canada, whereas they also mention 5% human respiration and −2% plant and soil activity contribution. Traffic contributions of 80% published for Phoenix, USA were even higher (Koerner and Klopatek, 2002) whereas for Münster, Germany (Dahlkötter *et al.*, 2010), London, UK (Helfter *et al.*, 2011), Copenhagen, Denmark (Soegaard and Möller-Jensen, 2003) and Edinburgh, Scotland (Nemitz *et al.*, 2002) values were around 40%–50% – a ratio of the size suggested by the 55/45% inventory-ratio of household combustion to traffic for the whole canton of Basel.

## 4. Conclusions

Four years (June 2009–May 2013) of carbon dioxide flux data at the urban site Basel Aeschenplatz are analysed for the controlling factors. The source area calculation shows that measured $F_C$ originates from a composition of individual types of urban structures to the east and west of the site, which makes it ideal to observe differences between a heavily urbanized and traffic dominated business district and a residential area. This local heterogeneity around the site also allows for spatially differentiated analyses on the basis of sectoral data. Nine sectors with individual surface fractions and wind direction frequencies were compared in this study.

Average yearly $F_C$ is 16.4 μmol $m^{-2}s^{-1}$ which is in the upper range of the studies published so far (Table 1). Compared to the yearlong record from the Klingelbergstrasse site (1.6 km away), $F_C$ at Basel Aeschenplatz is 1.4 to 1.5 times higher. This is an evident sign that single measurements are not representative for a whole city.

$F_C$ shows typical cyclic variations on the diurnal and the yearly scale. The first is clearly driven by traffic emissions from the Aeschenplatz, especially during wintertime and under west wind conditions during summertime. The latter depends primarily on heating-related combustion emissions. Both are a result of the heterogeneous source area, also strongly dependent on the prevailing wind direction and thus also occasionally affected by its variability.

Monthly average diurnal courses show that inter-annual variability is usually low but exceptions due to changes in the average wind direction frequency or air temperature (in winter) can lead to higher or lower $F_C$. Greatest deviations of $F_C$ are observed if wind direction exceptions happen to coincide with high traffic densities in the daytime. In the winter months, for example November, the inter-annual wind direction variability is highest and the diurnal amplitude of the generalized east to west wind ratio is small. This leads to higher inter-annual differences in monthly $F_C$.

Partitioning of the flux results in an estimated average local contribution ratio of 70/30% by traffic and heating-related combustion, respectively, with a distinct dependence on sectoral emission characteristics. To the north and west traffic emissions are substantially higher than combustion emissions due to space heating while to the east they are estimated to be of similar size. In the vicinity of the Aeschenplatz, the overall reducing effect of the urban vegetation on $F_C$ is supposedly low, particularly because the greatest influence could be expected under daytime east wind conditions in summer. Such situations are rarely observed because at daytime in summer, the more frequent wind direction is west.

In a heterogeneous environment, measured $F_C$ represents the part of the total surrounding area – the instantaneous source area – where the wind is actually coming from. Thus, average fluxes can only account for a kind of mixed pattern where certain areas or situations might be overrepresented, others almost neglected. This results in a biassed representation, depending on the grade of spatial and temporal heterogeneity of $CO_2$ emissions. Deriving spatially referenced and continuous $eF_C$ data for individual sectors gives the opportunity to derive more realistic emission characteristics of the entire surrounding area. These result in a potentially more representative average flux of 10.9 μmol $m^{-2}s^{-1}$ which is substantially lower than average $F_C$.

Provided sufficient data availability (EC fluxes, LULC, morphology, urban form, etc.) the concept of $eF_C$ and eNEE may be of help for the interpretation of measured carbon fluxes at other urban sites, especially those surrounded by areas with different emission characteristics and unequally distributed wind directions. As $eF_C$ relies on statistical up-scaling, its application is restricted to long-term measurement sites. An interesting option for future applications would be the combination with LCZ classification (Stewart and Oke, 2012) which could lead to a more standardised implementation.

It can be assumed that in an urbanized area observed $F_C$ is far more dependent on the variability of strong anthropogenic sources than on relatively weak biological sink effects of street trees, parks, or green backyards. Surface fractions of vegetation, buildings, or impervious ground thus have a limited explanatory power for the expected size of $CO_2$ emissions. In this study, it is primarily the absence of major roads in the residential areas to the east that leads to reduced $F_C$, not the presence of vegetation. Nevertheless, surface fractions can be taken as indicators for typical emission characteristics.

Though sectoral $F_C$ fits well into the image that evolves from literature it is obvious that further comprehensive long-time studies are needed to complete the image and enhance the comparability between sites and cities. Special attention should thereby be paid to the local heterogeneity of the urban structure and the reasons for variability on different timescales in order to adequately address the controlling factors for $F_C$. The differences to the Klingelbergstrasse-site and between the sectors show that variations within a city or even only around a site may be of greater order than the differences between cities. Interpretation and comparisons of globally observed urban carbon fluxes could thus benefit from detailed site-specific information. If the origin of fluxes, that is the source areas, could be attributed to standardized land use/land cover classes or for example distinct LCZ, results may become more comparable.

## Acknowledgements

Research leading to this paper received funding from the EU FP7 (European Community's Seventh Framework Programme) project BRIDGE (grant agreement no. 211345). Special thanks go to Turmhaus Consulting and Basler Versicherungen for granting access to the Turmhaus and allowing the installation and maintenance of the instruments. The Basel city authorities provided data on traffic density, the traffic model data, and the building model and the Umweltbundesamt Germany provided the GAW data. Personal thanks to A. Christen (University of British Columbia) for providing the source area model implementation.

## References

Bergeron O, Strachan IB. 2011. $CO_2$ sources and sinks in urban and suburban areas of a northern mid-latitude city. *Atmos. Environ.* **45**: 1564–1573, doi: 10.1016/j.atmosenv.2010.12.043.

Burri S. 2009. *$CO_2$ Fluxes and Concentrations over an Urban Surface in Cairo/Egypt*, Master's thesis, University of Basel, Basel, Switzerland.

Burri S, Frey C, Parlow E, Vogt R. 2009. $CO_2$ fluxes and concentrations over an urban surface in Cairo/Egypt. In *The Seventh International*

 

*Conference on Urban Climate*, Yokohama, Japan, 29 June–3 July 2009.
Christen A. 2005. *Atmospheric Turbulence and Surface Energy Exchange in Urban Environments*. PhD thesis, University of Basel, Basel, Switzerland.
Christen A, Vogt R. 2004. Energy and radiation balance of a central European city. *Int. J. Climatol.* **24**: 1395–1421.
Christen A, Coops N, Kellett R, Crawford B, Heyman E, Olchovski I, Tooke R, van der Laan M. 2010. A LiDAR-based urban metabolism approach to neighbourhood scale energy and carbon emission modelling. Research Report, University of British Columbia, Vancouver, BC, Canada.
Christen A, Coops NC, Crawford BR, Kellett R, Liss KN, Olchovski I, Tooke TR, van der Laan M, Voogt JA. 2011. Validation of modeled carbon-dioxide emissions from an urban neighborhood with direct eddy-covariance measurements. *Atmos. Environ.* **450**(33): 6057–6069, doi: 10.1016/j.atmosenv.2011.07.040.
Clark-Thorne ST, Yapp CJ. 2003. Stable carbon isotope constraints on mixing and mass balance of $CO_2$ in an urban atmosphere: Dallas metropolitan area, Texas, USA. *Appl. Geochem.* **18**: 75–95.
Coutts AM, Beringer J, Tapper NJ. 2007a. Characteristics influencing the variability of urban $CO_2$ fluxes in Melbourne, Australia. *Atmos. Environ.* **41**: 51–62.
Coutts AM, Beringer J, Tapper NJ. 2007b. Impact of increasing urban density on local climate: spatial and temporal variations in the surface energy balance in Melbourne, Australia. *J. Appl. Meteorol. Climatol.* **460**(4): 477–493.
Crawford B, Grimmond CSB, Christen A. 2011. Five years of carbon dioxide fluxes measurements in a highly vegetated suburban area. *Atmos. Environ.* **45**: 896–905.
Curtis PS, Hanson PJ, Bolstad P, Barford C, Randolph JC, Schmid HP, Wilson KB. 2002. Biometric and Eddy-covariance based estimates of annual carbon storage in five eastern North American deciduous forests. *Agric. For. Meteorol.* **1130**(1–4): 3–19, doi: 10.1016/S0168-1923(02)00099-0.
Dahlkötter F, Griessbaum F, Schmidt A, Klemm O. 2010. Direct measurement of $CO_2$ and particle emissions from an urban area. *Meteorol. Z.* **190**(6): 565–575, doi: 10.1127/0941-2948/2010/0492.
Feigenwinter C, Vogt R, Christen A. 2012. Eddy covariance measurements over urban areas. In *Eddy Covariance – A Practical Guide to Measurement and Data Analysis*. Springer Atmospheric Sciences, Aubinet M, Vesala T, Papale D (eds). Springer: Dordrecht, the Netherlands, 377–397.
Foken T, Wichura B. 1996. Tools for quality assessment of surface-based flux measurements. *Agric. For. Meteorol.* **78**: 83–105.
Frey C, Parlow E. 2010. Determination of the aerodynamic resistance to heat using morphometric methods. *EARSeL eProc.* **90**(2): 52–63.
Gioli B, Toscano P, Lugato E, Matese A, Miglietta F, Zaldei A, Vaccari FP. 2012. Methane and carbon dioxide fluxes and source partitioning in urban areas: the case study of Florence, Italy. *Environ. Pollut.* **164**: 125–131, doi: 10.1016/j.envpol.2012.01.019.
Grimmond CSB, Oke T. 1999. Aerodynamic properties of urban areas derived from analysis of surface form. *J. Appl. Meteorol.* **38**: 1262–1292.
Grimmond CSB, King TS, Cropley FD, Nowak DJ, Souch C. 2002. Local-scale fluxes of carbon dioxide in urban environments: methodological challenges and results from Chicago. *Environ. Pollut.* **116**: 243–254.
Grimmond CSB, Salmond JA, Oke TR, Offerle B, Lemonsu A. 2004. Flux and turbulence measurements at a densely built-up site in Marseille: heat, mass (water and carbon dioxide), and momentum. *J. Geophys. Res.* **109**: 1–19, doi: 10.1029/2004JD004936.
Helfter C, Famulari D, Philipps GJ, Barlow JF, Wood CR, Grimmond CSB, Nemitz E. 2011. Controls of carbon dioxide concentrations and fluxes above central London. *Atmos. Chem. Phys.* **11**: 1913–1928, doi: 10.5194/acp-11-1913-2011.
Järvi L, Hannuniemi H, Hussein T, Junninen H, Aalto PP, Hillamo R, Mäkelä T, Keronen P, Siivola E, Vesala T, Kulmala M. 2009a. The urban measurement station SMEAR III: continuous monitoring of air pollution and surface-atmosphere interactions in Helsinki, Finland. *Boreal Environ. Res.* **14**: 86–109.
Järvi L, Mammarella I, Eugster W, Ibrom A, Siivola E, Dellwik E, Keronen P, Burba G, Vesala T. 2009b. Comparison of net $CO^2$ fluxes measured with open- and closed-path infrared gas analyzers in an urban complex environment. *Boreal Environ. Res.* **14**: 499–514.
Järvi L, Ranik Ü, Mammarella I, Sogachev A, Aalto PP, Keronen P, Siivola E, Kulmala M, Vesala T. 2009c. Annual particle flux observations over a heterogeneous urban area. *Atmos. Chem. Phys.* **9**: 7847–7856.
Järvi L, Nordbo A, Junninen H, Riikonen A, Moilanen J, Nikinmaa E, Vesala T. 2012. Seasonal and annual variation of carbon dioxide surface fluxes in Helsinki, Finland, in 2006–2010. *Atmos. Chem. Phys.* **120**(3): 8355–8396, doi: 10.5194/acpd-12-8355-2012.
Koerner B, Klopatek J. 2002. Anthropogenic and natural $CO_2$ emission sources in an arid urban environment. *Environ. Pollut.* **116**: 45–51.
Koetz B, Itten KI, Borgeaud M, Brunner D, Buchmann B, Feigenwinter Ch, Hüsler F, Kneubühler M, Parlow E, Psomas A, Wunderle S, Zimmermann NE. 2009. Fostering the Swiss research community in the field of imaging spectroscopy. In *Proceedings of the 6th EARSeL Workshop on Imaging Spectroscopy*, Tel Aviv, Israel, 16–18 March 2009.
Kordowski K, Kuttler W. 2010. Carbon dioxide fluxes over an urban park area. *Atmos. Environ.* **44**: 2722–2730.
Kormann R, Meixner FX. 2001. An analytical footprint model for non-neutral stratification. *Bound.-Layer Meteorol.* **99**: 207–224.
Lietzke B, Vogt R. 2013. Variability of $CO_2$ concentrations and fluxes in and above an urban street canyon. *Atmos. Environ.* **74**: 60–72.
Liu HZ, Feng JW, Järvi L, Vesala T. 2012. Four-year (2006–2009) Eddy covariance measurements of $CO_2$ flux over an urban area in Beijing. *Atmos. Chem. Phys.* **12**: 7881–7892.
Matese A, Gioli B, Vaccari P, Zaldei A, Miglietta F. 2009. Carbon dioxide emissions of the city center of Firenze, Italy: measurement, evaluation, and source partitioning. *J. Appl. Meteorol. Climatol.* **48**: 1940–1947.
Moriwaki R, Kanda M. 2004. Seasonal and diurnal fluxes of radiation, heat, water vapor, and carbon dioxide over a suburban area. *J. Appl. Meteorol.* **43**: 1700–1710.
Nemitz E, Hargreaves KJ, McDonald AG, Dorsey JR, Fowler D. 2002. Micrometeorological measurements of the urban heat budget and $CO_2$ emissions on a city scale. *Environ. Sci. Technol.* **360**(14): 3139–3146.
Nemitz E, Jimenez JL, Huffman JA, Ulbrich IM, Canagaratna MR, Worsnop DR, Guenther AB. 2008. An Eddy covariance system for the measurement of surface/atmosphere exchange fluxes of submicron aerosol chemical species – first application above an urban area. *Aerosol Sci. Technol.* **42**: 636–657.
Nordbo A, Järvi L, Haapanala S, Wood CR, Vesala T. 2012. Fraction of natural area as main predictor of net $CO_2$ emissions from cities. *Geophys. Res. Lett.* **39**: 1–5, doi: 10.1029/2012GL053087.
Nordbo A, Järvi L, Haapanala S, Moilanen J, Vesala T. 2013. Intra-city variation in urban morphology and turbulence structure in Helsinki, Finland. *Bound.-Layer Meteorol.* **146**: 469–496.
Offerle B, Grimmond CSB, Fortuniak K. 2005. Heat storage and anthropogenic heat flux in relation to the energy balance of a Central European city centre. *Int. J. Climatol.* **250**(10): 1405–1419, doi: 10.1002/joc.1198.
Oke TR. 2004. Initial guidance to obtain representative meteorological observations at urban sites. Instruments and Observing Methods Report 81, WMO, Geneva, Switzerland.
Pataki DE, Bowling DR, Ehleringer JR. 2003. Seasonal cycle of carbon dioxide and its isotopic composition in an urban atmosphere: anthropogenic and biogenic effects. *J. Geophys. Res.* **1080**(D23): 4735–4742, doi: 10.1029/2003JD003865.
Pataki DE, Bowling DR, Ehleringer JR, Zobitz JM. 2006. High resolution atmospheric monitoring of urban carbon dioxide sources. *Geophys. Res. Lett.* **33**: 1–5, doi: 10.1029/2005GL024822.
Pataki DE, Xu T, Luo YQ, Ehleringer JR. 2007. Inferring biogenic and anthropogenic carbon dioxide sources across an urban to rural gradient. *Oecologia* **152**: 307–322, doi: 10.1007/s00442-006-0656-0.
Pawlak W, Fortuniak K, Siedlecki M. 2011. Carbon dioxide flux in the centre of Lodz, Poland – analysis of a 2-year Eddy covariance measurement data set. *Int. J. Climatol.* **310**(2): 232–243, doi: 10.1002/joc.2247.
Ramamurthy P, Pardyjak ER. 2011. Toward understanding the behavior of carbon dioxide and surface energy fluxes in the urbanized semi-arid Salt Lake Valley, Utah, USA. *Atmos. Environ.* **45**: 73–84.
Raupach MR, Antonia RA, Rajagopalan S. 1991. Rough-wall turbulent boundary layers. *Appl. Mech. Rev.* **44**: 1–25.
Rotach MW. 1999. On the influence of the urban roughness sublayer on turbulence and dispersion. *Atmos. Environ.* **33**: 4001–4008.
Salmond JA, Roth M, Oke TR, Christen A, Voogt JA. 2012. Can surface cover tiles be summed to give neighbourhood fluxes in cities. *J. Appl. Meteorol. Climatol.* **51**: 133–149, doi: 10.1175/JAMC-D-11-078.1.
Schmidt A, Wrzesinsky T, Klemm O. 2008. Gap filling and quality assessment of $CO_2$ and water vapour fluxes above an urban area with

radial basis function neural networks. *Bound.-Layer Meteorol.* **126**: 389–413, doi: 10.1007/s10546-007-9249-7.

Schotanus P, Nieuwstadt FTM, De Bruin HAR. 1983. Temperature measurements with a sonic anemometer and its application to heat and moisture fluxes. *Bound.-Layer Meteorol.* **26**: 81–93.

Soegaard H, Möller-Jensen L. 2003. Towards a spatial $CO_2$ budget of a metropolitan region based on textural image classification and flux measurements. *Remote Sens. Environ.* **870**(2–3): 283–294, doi: 10.1016/S0034-4257(03)00185-8.

Song T, Wang Y. 2012. Carbon dioxide fluxes from an urban area in Beijing. *Atmos. Res.* **106**: 139–149.

Stewart ID, Oke TR. 2012. Local climate zones for urban temperature studies. *Bull. Am. Meteorol. Soc.* **93**: 1879–1900.

Tanner CB, Thurtell GW. 1969. Anemoclinometer measurements of Reynolds stress and heat transport in the atmospheric surface layer. Technical Report ECOM-66-G22-F, University of Wisconsin, Madison, WI, 82 pp.

UBA. 2012. *Luftmessnetz des Umweltbundesamtes, Messstation Schauinsland*. WMO Global Atmosphere Watch – World Data Centre for Greenhouse Gases, Federal Environment Agency, Germany. http://ds.data.jma.go.jp/gmd/wdcgg/ (accessed 8 July 2013).

Valentini R, Matteucci G, Dolman AJ, Schulze E-D, Rebmann C, Moors EJ, Granier A, Gross P, Jensen NO, Pilegaard K, Lindroth A, Grelle A, Bernhofer C, Grunwald T, Aubinet M, Ceulemans R, Kowalski AS, Vesala T, Rannik U, Berbigier P, Loustau D, Gúmundsson J, Thorgeirsson H, Ibrom A, Morgenstern K, Clement R, Moncrieff J, Montagnani L, Minerbi S, Jarvis PG. 2000. Respiration as the main determinant of carbon balance in European forests. *Nature* **404**: 861–865, doi: 10.1038/35009084.

Velasco E, Pressley S, Allwine E, Westberg H, Lamb B. 2005. Measurements of $CO_2$ fluxes from the Mexico City urban landscape. *Atmos. Environ.* **39**: 7433–7446.

Velasco E, Pressley S, Grivicke R, Allwine E, Coons T, Foster W, Jobson T, Westberg H, Ramos R, Hernández F, Molina LT, Lamb B. 2009. Eddy covariance flux measurements of pollutant gases in urban Mexico City. *Atmos. Chem. Phys.* **9**: 7325–7342, doi: 10.5194/acp-9-7325-2009.

Vesala T, Järvi L, Launiainen S, Sogachev A, Rannik Ü, Mammarella I, Siivola E, Keronen P, Rinne J, Riikonen A, Nikinmaa E. 2008. Surface-atmosphere interactions over complex urban terrain in Helsinki, Finland. *Tellus* **60B**: 188–199, doi: 10.1111/j.1600-0889.2007.00312.x.

Vogt R, Christen A, Rotach MW, Roth M, Satyanarayana ANV. 2006. Temporal dynamics of $CO_2$ fluxes and profiles over a Central European city. *Theor. Appl. Climatol.* **84**: 117–126.

Webb EK, Pearman GI, Leuning R. 1980. Correction of flux measurements for density effects due to heat and water vapour transfer. *Q. J. R. Meteorol. Soc.* **106**: 85–100.

 

# 5 Conclusions

This thesis presents one of the first experiments analyzing $CO_2$ fluxes and concentrations at two central urban long term sites within one city. The main aim was to identify the factors that are responsible for the variability of the concentrations and fluxes on different spatial and temporal scales. For this purpose, the experiment consisted of three parts, each adding additional information on specific scales:

i The measurements at Basel Klingelbergstrasse that account for local scale exchange processes and give information on long term scales of up to ten years,

ii the street canyon tower which assessed micro scale processes in the urban canopy layer during one year and

iii the second site Basel Aeschenplatz that focuses also on local scale fluxes and long term patterns and introduces the city scale into the experiment. Site specific conclusions are presented in the respective publications, included in this thesis as Section P2-4 and Section P3-4.

Summarizing the results from the two sites shows that the flux patterns are similar in the way they depend on local source characteristics, but show also distinct differences that are attributable to the spatial distribution of strong sources in the closer part of the source areas of the measurements. This emphasizes that – assuming that precautions considering the usual methodological and technical challenges are accounted for – the following four points are crucial criteria when planning or analyzing $CO_2$ flux measurements in urban areas: (i) the location of the sensor, respectively the site, (ii) the prevailing typical wind directions and their variability, (iii) the general grade of heterogeneity and variability in the spatio-temporal source and sink distribution and (iv) specifically the distance (and direction) to and the extent of $CO_2$ sources that are comparatively stronger than the average source strength of the footprint area.

Combined, these points account for typical and atypical features in measured $F_C$ and lead to the following set of general conclusions derived from the presented results:

**In terms of temporal variability, long-term data sets are important in urban areas.** They give representative average flux values and urban ecosystem exchange rates. The more heterogeneous the source area is in regard to its urban structure and related $CO_2$ emissions, the longer data sets are needed to represent as many possible cases of combinations and interplays between the various controlling factors for $F_C$. Short- and long term variability (up to inter-annual) depend heavily on these interplays and exceptions from common cyclical patterns.

**In terms of spatial variability, fluxes on coarser scales are strongly linked to the processes and the urban structure on finer scales.** In the urban canopy layer, micro scale $CO_2$ distribution and exchange processes with the layers above show a strong dependence on the urban structure and the wind direction and can thus strongly affect close-by local scale measurements. City scale differences are directly related to urban structure and $CO_2$ source location differences on the local scale. Wind direction, traffic density and heating activity as the main controlling factors for $F_C$ are in their typical temporal patterns valid at city scale: Higher traffic or heating emissions at the local scale would result in a constant offset or a deviating amplitude of the course of $F_C$ but the typical cycles remain usually the same. Apart from such constant offsets, differences in diurnal, monthly, seasonal or annual courses are typically related to the spatial distribution of (comparatively strong) $CO_2$ sources.

**Non-homogeneous terrain requires spatially segregated footprint analyses.** When measuring $CO_2$ flux in urban areas with a heterogeneous source distribution, results have to be related to spatially separated parts (e.g. sectors) of the total flux footprint to account for the differences in the source/sink characteristic. These separate sub-footprints ideally incorporate a more homogeneous spatial distribution of sources and sinks than the total footprint. To allow for reliable comparisons, the temporal share and representation of the sub-footprints must be equal or has to be made equal through adequate up-scaling resp. gapfilling. Otherwise, statistical representation in the average signal is low for specific sub-footprints or situations. Up-scaled fluxes give a more representative image of the spatial average $F_C$ for the whole footprint area. This underlines the need for long term data sets that give a statistically reliable representation of the daily, seasonal and inter-annual courses for the total spatial extent of the source area of a site.

In these terms, the applied gapfilling method could surely be enhanced to account for the short-term variance of $F_C$ on scales of hours or less. Further, the method is influenced by the controlling factors for $F_C$ and introduces these dependencies into the filled data set which can lead to autocorrelations. For the temporal scope of the presented experiment, the gapfilling method is considered to be a reliable approach, but avoiding gaps in the sampled data should be a major concern throughout experiments.

**Neither one nor two sites represent a whole city.** Identification of the controlling factors for $F_C$ and their often complex interplay on different temporal and spatial scales enhances the interpretability of measured fluxes. Spatial segregation of fluxes accounts for the heterogeneity of the urban structure and the source distribution and can be taken as a flux inventory for characteristic urban areas. Spatial averaging through up-scaling leads to a more comprehensive information on the total carbon exchange rate of the source area and an extended spatial information. But neither one nor two sites are able to represent a whole city, to account for the enormous variability of the urban structure and the controlling factors for $F_C$.

# 6 Review of contributions

This thesis consist of this summary part, two research articles and a book chapter. The articles analyze the controlling factors for the high spatial and temporal variability of $CO_2$ concentrations and fluxes in urban areas, based on micrometeorological observations in the city of Basel, Switzerland. The book chapter (Lietzke et al. (2015b), Section P1) presents an introduction to the physical flows of energy, water and carbon in cities.

I bear sole responsibility for the summary part of this thesis. All data processing leading to the presented results in Lietzke and Vogt (2013) (Section P2) and Lietzke et al. (2015a) (Section P3) was in my responsibility and both papers were completely written by myself. Dr. Roland Vogt contributed trough thorough review work, especially during the work on Lietzke and Vogt (2013). At BKLI I was benefiting from the existing measurements at the rooftop tower, whereas the street canyon tower and the measurements at BAES were organized, planned, installed and maintained by myself with the support of Roland Vogt and team members from the MCR Lab.

The book chapter is a condensed and simplified version of the deliverable D2.1 of the BRIDGE project which consists of three parts written by the respective authors (see below for my work in WP2). As in D2.1, I am responsible for all the writing in the energy chapter. For the chapter on water I mostly summarized the D2.1 part on water, written originally by the respective authors. The carbon chapter is only to a small part relying on D2.1 and was, to keep its structure consistent with that of the other chapters, rewritten.

As one out of four persons from the MCR Lab that where involved in the BRIDGE project, my direct contribution consisted of the following work:

WP2: Responsible for writing 'Part I: Energy in the urban system' with the support of Roland Vogt. The other authors and contributors, mainly Sue Grimmond (book captain, King's College London, UK), acted as reviewers for Part I and vice versa. Participation in the 1st progress meeting in Helsinki (06/2009).

WP3: Least contribution of all WPs. Presentation of first measurement results from Gliwice at the 3rd progress meeting in Athens (05/2010).

WP8: Supporting the project partner ALTERRA (University of Wageningen, The Netherlands) in the preparation of the first umbrella CoP in Athens (May 5, 2010) through a two week stay at the Wageningen University. Monitoring end user experiences with the DSS prototype in the try-out session during the umbrella CoP. Analyzing the reports from the 10 local CoP meetings for shared issues and preparing and writing the synthesis for D8.1 'DSS demonstration report' (Chapter 2), supported by Judith Klostermann (book captain, ALTERRA) and reviewed by the other authors of D.8.1 (and vice versa). In cooperation with ALTERRA responsible for the organization (planning, invitation of participants, venue, infrastructure) of the final (2nd) umbrella CoP meeting, the so called demonstration event, in Brussels, Belgium on October 26, 2011.

# Bibliography


Aubinet, M., Vesala, T. and Papale, D., eds (2012), *Eddy Covariance - a Practical Guide to Measurement and Data Analysis*, Springer Atmospheric Sciences.

Baldocchi (2008), '"Breathing" of the terrestrial biosphere: Lessons learned from a global network of carbon dioxide flux measurement systems', *Australian Journal of Botany* **56**, 1–26.

Bergeron, O. and Strachan, I. B. (2011), '$CO_2$ sources and sinks in urban and suburban areas of a northern mid-latitude city', *Atmospheric Environment* **45**, 1564–1573.

Boyden, S., Millar, S., Newcombe, K. and O'Neill, B. (1981), 'The ecology of a city and its people', *ANU Press, Canberra.* .

Britter, R. E. and Hanna, S. R. (2003), 'Flow and dispersion in urban areas', *Annual Review of Fluid Mechanics* **35**, 469–496.

Christen, A. (2005), Atmospheric turbulence and surface energy exchange in urban environments, PhD thesis, University of Basel, Stratus. ISBN 3-85977-266.X.

Christen, A., Coops, N., Crawford, B., Kellett, R., Liss, K., Olchovski, I., Tooke, T., van der Laan, M. and Voogt, J. (2011), 'Validation of modeled carbon-dioxide emissions from an urban neighborhood with direct eddy-covariance measurements', *Atmospheric Environment* **45**(33), 6057–6069.

Chrysoulakis, N., Anselmo de Castro, E. and Moors, E., eds (2015), *Understanding Urban Metabolism: A Tool for Urban Planning*, Routledge Oxford.

Chrysoulakis, N., Lopes, M., San José, R., Grimmond, C., Jones, M. B., Magliulo, V., Klostermann, J., Synnefa, A., Mitraka, Z., Castro, E., González, A., Vogt, R., Vesala, T., Spano, D., Pigeon, G., Freer-Smith, P., Staszewski, T., Hodges, N., Mills, G. and Cartalis, C. (2013), 'Sustainable urban metabolism as a link between bio-physical sciences and urban planning: The BRIDGE project', *Landscape and Urban Planning* **112**, 100–117.

Crawford, B., Grimmond, C. and Christen, A. (2011), 'Five years of carbon dioxide fluxes measurements in a highly vegetated suburban area', *Atmospheric Environment* **45**, 896–905.

Dahlkötter, F., Griessbaum, F., Schmidt, A. and Klemm, O. (2010), 'Direct measurement of $CO_2$ and particle emissions from an urban area', *Meteorologische Zeitschrift* **19**(6), 565–575.

Diethelm, S. (2011), Open- or closed-path gas analyzer: which one delivers the 'better' $CO_2$ fluxes?, Master thesis, University of Basel.

Feigenwinter, C., Vogt, R. and Christen, A. (2012), Eddy covariance measurements over urban areas, *in* M. Aubinet, T. Vesala and D. Papale, eds, 'Eddy Covariance - A Practical Guide to Measurement and Data Analysis', Springer Atmospheric Sciences, p. 430.

Foken, T., Leuning, R., Oncley, S. R., Mauder, M. and Aubinet, M. (2012), Corrections and data quality control, *in* M. Aubinet, T. Vesala and D. Papale, eds, 'Eddy Covariance - A Practical Guide to Measurement and Data Analysis', Springer Atmospheric Sciences, p. 430.

Foken, T. and Wichura, B. (1996), 'Tools for quality assessment of surface-based flux measurements', *Agricultural and Forest Meteorology* **78**, 83–105.

Garratt, J. R. (1993), *The atmospheric boundary layer*, Cambridge University Press, Cambridge.

Gartmann, A., Müller, M., Parlow, E. and Vogt, R. (2011), 'Evaluation of numerical simulations of $CO_2$ transport in a city block with field measurements', *Environmental Fluid Mechanics* pp. 1–16.

Grimmond, C., King, T., Cropley, F., Nowak, D. and Souch, C. (2002), 'Local-scale fluxes of carbon dioxide in urban environments: methodological challenges and results from Chicago', *Environmental Pollution* **116**, 243–254.

Grimmond, C. and Oke, T. (1999), 'Aerodynamic properties of urban areas derived from analysis of surface form', *Journal of applied meteorology* **38**, 1262–1292.

Helfter, C., Famulari, D., Philipps, G., Barlow, J., Wood, C., Grimmond, C. and Nemitz, E. (2011), 'Controls of carbon dioxide concentrations and fluxes above central London', *Atmospheric Chemistry and Physics* **11**, 1913–1928.

Hsieh, C.-I., Katul, G. and Chi, T. (2000), 'An approximate analytical model for footprint estimation of scalar fluxes in thermally stratified atmospheric flows', *Advances in Water Resources* **23**, 765–772.

Järvi, L., Nordbo, A., Junninen, H., Riikonen, A., Moilanen, J., Nikinmaa, E. and Vesala, T. (2012), 'Seasonal and annual variation of carbon dioxide surface fluxes in Helsinki, Finland, in 2006 - 2010', *Atmospheric Chemistry and Physics Discussions* **12**(3), 8355–8396.

Kljun, N., Rotach, M. and Schmid, H. (2002), 'A three-dimensional backward lagrangian footprint model for a wide range of boundary-layer stratifications', *Boundary-Layer Meteorology* **103**, 205–226.

Koerner, B. and Klopatek, J. (2002), 'Anthropogenic and natural $CO_2$ emission sources in an arid urban environment', *Environmental Pollution* **116**, 45–51.

Koller, P. (2010), The calibration of an open path gas analyzer and its effects onto carbon dioxide and water vapor fluxes, measured using the eddy covariance method, Bachelor's thesis, University of Basel.

Kordowski, K. and Kuttler, W. (2010), 'Carbon dioxide fluxes over an urban park area', *Atmospheric Environment* **44**, 2722–2730.

Kormann, R. and Meixner, F. X. (2001), 'An analytical footprint model for non-neutral stratification', *Boundary-Layer Meteorology* **99**, 207–224.

Lee, X., Massman, W. and Law, B., eds (2004), *Handbook of Micrometeorology*, Kluwer Academic Publishers.

Lietzke, B. and Vogt, R. (2013), 'Variability of $CO_2$ concentrations and fluxes in and above an urban street canyon', *Atmospheric Environment* **74**, 60–72.

Lietzke, B., Vogt, R., Feigenwinter, C. and Parlow, E. (2015a), 'On the controlling factors for the variability of carbon dioxide flux in a heterogeneous urban environment', *International Journal of Climatology* .

Lietzke, B., Vogt, R., Young, D. and Grimmond, C. (2015b), Physical fluxes in the urban environment, *in* N. Chrysoulakis, E. Anselmo de Castro and E. Moors, eds, 'Understanding Urban Metabolism: A tool for Urban Planning', Routledge Oxford, pp. 29 – 44.

Mauder, M. and Foken, T. (2006), 'Impact of post-field data processing on eddy covariance flux estimates and energy balance closure', *Meteorologische Zeitschrift* **15**, 597–609.

Mauder, M., Foken, T., Clement, R., Elbers, J., Eugster, W., Grünwald, T., Heusinkveld, B. and Kolle, O. (2008), 'Quality control of CarboEurope flux data - Part 2: Inter-comparison of eddy-covariance software', *Biogeosciences* **5**, 451–462.

Moriwaki, R. and Kanda, M. (2004), 'Seasonal and diurnal fluxes of radiation, heat, water vapor, and carbon dioxide over a suburban area', *Journal of Applied Meteorology* **43**, 1700–1710.

Nemitz, E., Hargreaves, K., McDonald, A., Dorsey, J. and Fowler, D. (2002), 'Micrometeorological measurements of the urban heat budget and $CO_2$ emissions on a city scale', *Environmental Science & Technology* **36**(14), 3139–3146.

Newman, P. W. G. (1999), 'Sustainability and cities: Extending the metabolism model', *Landscape and Urban Planning* **44**, 219–226.

Nordbo, A., Järvi, L., Haapanala, S., Wood, C. R. and Vesala, T. (2012), 'Fraction of natural area as main predictor of net $CO_2$ emissions from cities', *Geophysical Research Letters* **39**.

Oke, T. (2006), 'Towards better scientific communication in urban climate', *Theoretical and Applied Climatology* **84**, 179–190.

Oke, T. R. (2004), Initial guidance to obtain representative meteorological observations at urban sites, Instruments and Observing Methods Report 81, WMO.

Ramamurthy, P. and Pardyjak, E. (2011), 'Toward understanding the behavior of carbon dioxide and surface energy fluxes in the urbanized semi-arid Salt Lake Valley, Utah, USA', *Atmospheric Environment* **45**, 73–84.

Raupach, M., Antonia, R. and Rajagopalan, S. (1991), 'Roughwall turbulent boundary layers', *Appl. Mechanics Reviews* **44**, 1–25.

Rebmann, C., Kolle, O., Heinesch, B., Queck, R., Ibrom, A. and Aubinet, M. (2012), Data acquisition and flux calculations, *in* M. Aubinet, T. Vesala and D. Papale, eds, 'Eddy Covariance - A Practical Guide to Measurement and Data Analysis', Springer Atmospheric Sciences, p. 430.

Rotach, M. (2001), 'Simulation of urban-scale dispersion using a lagrangian stochastic dispersion model', *Boundary-Layer Meteorology* **99**, 379–410.

Rotach, M., Vogt, R., Bernhofer, C., Batchvarova, E., Christen, A., Clappier, A., Feddersen, B., Gryning, S.-E., Martucci, G., Mayer, H., Mitev, V., Oke, T., Parlow, E., Richner, H., Roth, M., Roulet, Y., Ruffieux, D., Salmond, J., Schatzmann, M. and Voogt, J. (2005), 'BUBBLE - an urban boundary layer meteorology project', *Theoretical and Applied Climatology* **81 (3-4)**, 149–156.

Rotach, M. W. (1999), 'On the influence of the urban roughness sublayer on turbulence and dispersion', *Atmospheric Environment* **33**, 4001–4008.

Roth, M. (2000), 'Review of atmospheric turbulence over cities', *Quarterly Journal of the Royal Meteorological Society* **126**, 941–990.

Schmid, H. (1994), 'Source areas for scalars and scalar fluxes', *Boundary-Layer Meteorology* **67**, 293–318.

Schotanus, P., Nieuwstadt, F. T. M. and De Bruin, H. A. R. (1983), 'Temperature measurements with a sonic anemometer and its application to heat and moisture fluxes', *Boundary-Layer Meteorology* **26**, 81–93.

Soegaard, H. and Möller-Jensen, L. (2003), 'Towards a spatial $CO_2$ budget of a metropolitan region based on textural image classification and flux measurements', *Remote Sensing of Environment* **87**(2-3), 283–294.

Sogachev, A. and Lloyd, J. (2004), 'Using a one-and-a-half order closure model of the atmospheric boundary layer for surface flux footprint estimation', *Boundary-Layer Meteorology* **112**, 467–502.

Stewart, I. D. and Oke, T. R. (2012), 'Local climate zones for urban temperature studies', *Bulletin of the American Meteorological Society* **93**, 1879–1900.

UNEP (2012), *World Urbanization Prospects, the 2011 Revision: Highlights*, United Nations, Department of Economic and Social Affairs, Population Division. New York.

Vesala, T., Järvi, L., Launiainen, S., Sogachev, A., Rannik, Ü., Mammarella, I., Siivola, E., Keronen, P., Rinne, J., Riikonen, A. and Nikinmaa, E. (2008), 'Surface-atmosphere interactions over complex urban terrain in Helsinki, Finland', *Tellus* **60B**, 188–199.

Vogt, R., Christen, A., Rotach, M. W., Roth, M. and Satyanarayana, A. N. V. (2006), 'Temporal dynamics of $CO_2$ fluxes and profiles over a Central European city', *Theoretical and Applied Climatology* **84**, 117–126.

Webb, E. K., Pearman, G. I. and Leuning, R. (1980), 'Correction of flux measurements for density effects due to heat and water vapour transfer', *Quarterly Journal of the Royal Meteorological Society* **106**, 85–100.

Wolman, A. (1965), 'The metabolism of the city', *Scientific American* **213**(3), 179–190.